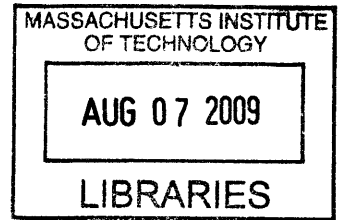# Study on Transformation-Based Invisibility Cloaks

by

Baile Zhang

B.S., Electrical Engineering,
Tsinghua University, China (2003)
M.S., Electrical Engineering,
Tsinghua University, China (2006)

Submitted to the Department of Electrical Engineering and Computer
Science
in partial fulfillment of the requirements for the degree of

Doctor of Philosophy

ARCHIVES

at the

MASSACHUSETTS INSTITUTE OF TECHNOLOGY

June 2009

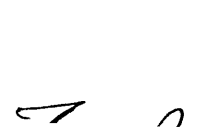© Massachusetts Institute of Technology 2009. All rights reserved.

Author . . . .
Department of Electrical Engineering and Computer Science
May 12, 2009

Certified by . . . .

David Staelin
Professor of Electrical Engineering
Thesis Supervisor

Certified by . . . .

Bae-Ian Wu
Research Scientist
Thesis Supervisor

Accepted by. . . . .

Terry Philip Orlando
Chairman, Department Committee on Graduate Students

Study on Transformation-Based Invisibility Cloaks

by

Baile Zhang

Abstract

The combination of the development of modern metamaterials, which are artificial materials whose constitutive parameters can be engineered to achieve special functions, and the coordinate transformation theory, has offered an unprecedented opportunity for realizing invisibility cloaking. Coordinate transformation theory predicts that by squeezing the space to form a "hole" in it, any object inside the "hole" becomes completely invisible from electromagnetic waves. A metamaterial shell can thus be designed to mimic this space squeezing and function as an invisibility cloak whose user cannot be seen by others. In this thesis, a systematic electromagnetic study of transformation-based invisibility cloaks is provided based on the macroscopic Maxwell equations.

Analytic scattering models are formulated for studying ideal and non-ideal invisibility cloaks. The physics behind perfect invisibility that the coordinate transformation theory did not show is explored by analytically calculating the spatial distribution of electromagnetic fields. Firstly, it is shown that an external electromagnetic wave illuminating a cylindrical cloak will induce electric and magnetic surface currents along the ϕ direction at the inner boundary of this cloak. These surface currents have no counterparts in the transformation theory because they do not exist before transformation. Secondly, the reciprocity of a spherical cloak is demonstrated by showing that radiation from an active device in the concealed region is confined in the concealed region. The mechanism is that the outgoing radiation will induce surface voltages at the inner boundary of the cloak that reflect all waves back. These physical surface voltages provides a set of mathematical boundary conditions requiring normal D and normal B to vanish on the interface. Finally, the mechanical response of the cloak to external electromagnetic waves is analyzed by calculating the Lorentz force distribution. It is shown that an incoming plane wave tends to expand the bulk of a cloak while squeezing the outer boundary of the cloak at the same time. The recoil forces of these forces provides an alternative explanation for the bending of rays or photons.

More realistic cases with perturbed constitutive parameters are analyzed. It is shown that under certain symmetric lossy conditions, the spherical cloak is still invisible for a back-scattering detector due to impedance matching, while a cylindrical cloak with the same lossy conditions is visible. More emphasis is laid on the effect of dispersion associated with metamaterials. By applying the Drude and Lorentz types of dispersion to the

3

radial permittivity and radial permeability of a spherical cloak, it is shown that electromagnetic waves with different frequencies have different depths of penetration and thus form a rainbow-like field distribution inside the cloak. A quasi-monochromatic wave will experience a blue-shift in the forward propagating direction. Transmission of a Gaussian pulse through this dispersive cloak is discussed. It is shown that group velocity and energy transport velocity are not well-defined when the wave is approaching the inner boundary because the wave is seriously distorted. However, when the frequency band is narrow enough, we are still able to define the time-delay of the signal arriving at a target plane behind the cloak. A counterintuitive volcano-shaped time-delay is demonstrated as a concrete example.

An electromagnetic detection method is introduced for detecting a perfect cloak. While photons can be guided by the cloak along curved trajectories within the cloak, a moving charged particle will still follow a straight trajectory due to its inertia and thus generate radiation. We extend the previous Frank and Tamm's theory of Cerenkov radiation in isotropic and homogeneous media to the case of a perfect spherical cloak that is both anisotropic and inhomogeneous. From the transformation viewpoint, the radiation is from the nonuniform motion of the charged particle along a bent curve in the virtual space. The transition radiations that occur at the incident point and emitting point when the particle enters and leaves the cloak in the physical space correspond to the abrupt velocity changes at the corresponding points in the virtual space. The transition radiation during the piercing process in the physical space corresponds to the deceleration and acceleration radiation (Bremsstrahlung) and synchrotron radiation in virtual space. In our demonstrated spherical cloak with inner radius of 1μm and outer radius of 2μm, it is obtained that within the frequency range from 500 THz to 501 THz, a charge package of 1000 electrons moving with $0.9c$ can generate radiation energy equivalent to about 78 photons.

The practical implementation is considered. For simplified cloaks that are often preferred in experiments, the influences of nonlinear transformation and incident angle are first studied. It is seen that a square root transformation which forces the waves to be guided close to the outer boundary is more invisible than those generated by either linear or quadratic transformation. Simplified cylindrical cloaks may produce a larger scattering at nonnormal incidences than that from an object without any cloak. In addition, we suggest using a small number of homogeneous and anisotropic metamaterial layers to construct a practical cloak with satisfying performance with normal incidence and oblique incidence. Genetic algorithm was used to optimize the practical multi-layer structures. It is shown that using an optimized 4-layer cloak, the normalized scattering cross section from a perfect electric conductor cylinder can be reduced from 2.19 to 0.0039 with normal incidence. Another optimized 4-layer cloak working for the incidence of 30° is shown able to reduce the scattering cross section from 1.175 to 0.013. The latter cloak exhibits reduce scattering over a large range of incidence angles.

Thesis Supervisor: David Staelin
Title: Professor of Electrical Engineering

Thesis Supervisor: Bae-Ian Wu
Title: Research Scientist

4

Acknowledgments

I would like to express my sincere thanks to my supervisor Professor David Staelin, who has given me a lot of help and guidance during the preparation and writing of this thesis. Without him it would not be possible to finish this thesis. Though I became his student only one year ago, his kindness and attitude toward work, have been impressing me since the very beginning when I came to MIT. His unique rhythmical pacing, deep in thought, in the corridor of Building 26, has been and will continue reminding me to keep on thinking and never stop. My habit of pacing in the corridor of Building 26 these years is directly from him. Most of the ideas in this thesis came out during this pacing process.

I am also indebted to my co-supervisor Dr. Bae-Ian Wu for his continuous support. It is him who taught me how to simplify a complicated problem, how to do the TA's work, how to make presentation, how to prepare the demos, almost everything from research, study, to life. I was always surprised that whenever I asked him for something, he would provide it to me immediately from his mystic drawer. He is an example for me of diligence, erudition, loyalty and scientific integrity. I feel very lucky that I have this tutor, who sometimes is more like my brother, during my life at MIT.

Special thanks to my thesis readers Professor Qing Hu and Professor Steven Johnson for their helpful suggestions. I am also appreciative of Professor Hu for serving on both my thesis and RQE committees and of Professor Markus Zahn for serving on my RQE committee.

Thank you to all the graduate students I have met in CETA, Dr. Jie Lu, Dr. James Chen, Dr. Brandon Kemp, Dr. Beijia Zhang, Song Liang Chua, Micheal Yeung and Zhen Li. Thank you to all previous graduates in CETA who I have not met but heard of a lot. It is my honor to be a member of CETA and I will do my best to be worthy of being the last one who graduated from here. Thank you to all post-docs and visiting scholars as well as visiting students, among whom are Dr. Hongsheng Chen, Dr. Tomasz Grzegorczyk, Dr. Fanmin Kong, Dr. Hui Huang, Dr. Diren Liu, Dr. Zhaoyun Duan, Dr. Jiangtao Huangfu, Dr. Yang Du, Dongxing Wang, Jingjing Zhang, Sheng Xi, Cédric Blanchard, Peiheng Zhou and Shaoying Huang. Especially to Dr. Chen from whom I got a lot of care.

I would never forget my former research advisor, the former director of CETA, Professor Jin Au Kong. There has been a lot of words kept in my heart for a long time that I wanted to tell him but I will no longer have the chance. I always feel it's my fortune that I got the chance to be his student. Many times I questioned myself whether it was a mistake to come to MIT. His encouragement made me believe I can make it. During the time of being the TA in almost all his courses these years, I learned his passion in electromagnetics, and his kindness to his students. He is the greatest teacher I have ever seen in my life. I admire him not only because of his knowledge but also his personality. It is really sad that he passed away so quickly. However, his smiles, his stories, and his Maxwell equations, will remain in my deep heart for ever.

I also would like to thank my parents and my sister for everything they have done for me. Especially to Qingjiao, my wife, thank you. This accomplishment is as much yours as it is mine.

To Qingjiao

Contents

10

List of Figures

12

13

14

16

List of Tables

Chapter 1

Introduction and Motivation

From the Greek mythic hero Perseus to the most recent Harry Potter, the concept of invisibility cloaks whose user cannot be seen by others has been appearing frequently in legends and scientific fiction. Since 2005 the scientific study on invisibility has started in its true sense. It is the purpose of this thesis to provide a systematic electromagnetic study on the class of coordinate transformation-based invisibility cloaks.

Before our discussion, the scientific description of invisibility should be clarified . Figure 1-1 sketches the situation when an object is illuminated by an external electromagnetic wave. If the object is not identical with the background, it will produce reflection (backward scattering) and other scattering, which subsequently render the object visible or detectable. Therefore, the scattering in all different angles are the reasons of visibility of an object. If there is no absorption, no scattering, and the transmission is identical to the incidence, the object is completely invisible.

1.1 Historical efforts on invisibility cloaking

From Fig. 1-1, it is seen that the reflection and scattering are the main reasons of visibility and thus must be minimized to achieve invisibility. Historically, a lot of efforts has been made to reduce the reflection or scattering. Here we list several typical approaches before we introduce the transformation theory.

1. Radar absorbing materials
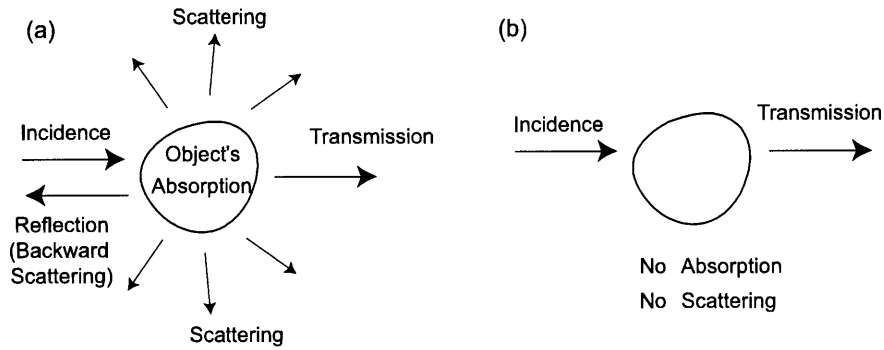
Figure 1-1: An external wave incident onto an object. (a) The object is visible due to reflection (backward scattering), other scattering, and absorption. (b) The object is invisible if the transmission is exactly the same as the incidence.

It is very intuitive that if all the incident waves are absorbed, at least the reflection can be very small. Since most radar systems are monostatic (the transmitter and receiver are at the same location) and detect objects by detecting the reflected waves, absorbing the incident wave is a good choice to be invisible from the monostatic radars. Due to this reason, radar absorbing materials (RAM) have been an important consideration in radar systems [7, 8]. However, this method in general does not work for bistatic radar systems (the transmitter and receiver are not at the same location).

2. Plasmonic cloaking of nanoparticles

In 2005, a new method was proposed to cloak nanoparticles by coating them with plasmonic materials whose permittivity is negative within the optical frequency region [9, 10]. Due to the negative value of the permittivity of the coat, the first order coefficient of Mie scattering, or the polarizability, is minimized. Given that in the quasi-static limit, only the first order scattering dominates, transparency can be achieved. This kind of cloaking is only valid for small particles. If the size of the particle is not small, even though the scattering of first order is minimized, the other orders of scattering are still nonzero.

3. Anomalous resonance

Another mechanism of cloaking relies on resonant interaction that can mask the

22

electromagnetic signature of the body to be cloaked [11]. Different from previous approaches, here the cloaking is achieved in a region external to the cloaking body. This cloaking is achievable for infinitely long polarizable line dipoles. The field from the polarizable line dipoles are canceled by anomalous resonance between the line dipoles and the cylindrical cloak with negative permittivity. However, the field inside this anomalous resonance region is divergent.

4. Non-local sensing

In this method [12], a lot of sensors are arranged in front of the object to be concealed. Active sources are also attached on the surface of the object. Once the sensors detect the incoming wave, they will send signals to the active sources which generate corresponding waves to cancel the incident wave in the concealed region. This way the object can be concealed from the incoming wave. However, this method requires the signals from the sensors propagate faster than the incident wave. Therefore, it will be difficult to be applied to electromagnetic waves.

From the above descriptions, we can see that these approaches are not ideal, each of which has significant limitations. For example, for the first approach, the invisibility is only in one direction. In the second and the third approaches, only small particles can be cloaked and the object being cloaked must has specified constitutive parameters. The last approach is not able to cloak object from electromagnetic waves.

In 2006, Pendry *et al.* [2] and Leonhardt [13] proposed a new cloaking method based on coordinate transformation, and this method is able to cloak a large object in all directions regardless of the object to be concealed. We will introduce the application of the coordinate transformation in electromagnetics in the following.

1.2 Transformation theory

Analogous to general relativity, where time and space are curved, transformation theory shows that the space of electromagnetics can also be bent in an almost arbitrary way. The relation between electromagnetic wave propagation and effective space-time geometries

was considered in early literatures [14], with the basics of transformation concepts established later [15]. However, these early literatures were almost forgotten. More recently, inspired by the transformation concepts and the assumption that metamaterial is able to realize arbitrary constitutive parameters, Pendry *et al.* [2] theoretically proposed a general recipe for designing an electromagnetic cloak in which the space from an original volume of free space is squeezed into a shell surrounding the object to be concealed and external waves which would have struck the object can effectively be guided by the "curved" space constructed by anisotropic and inhomogeneous metamaterials, as shown in Fig. 1-2. An arbitrary object can be hidden because it remains untouched from external radiation. At the same time, Leonhardt [13] described a method where the Helmholtz equation is transformed to produce similar effects in the geometrical optics limit but with a different opinion that "one can never completely hide from waves" due to "the wave nature of the light". Shortly after that, a simplified two-dimensional (2D) model based on Pendry *et al.*'s proposal was demonstrated experimentally to show the effectiveness of a transformation-based invisibility cloak [6]. However, due to its inherent scattering and other imperfections, this experiment did not answer the question whether perfect invisibility is achievable or not.

(a) Flat space   (b) Bent space
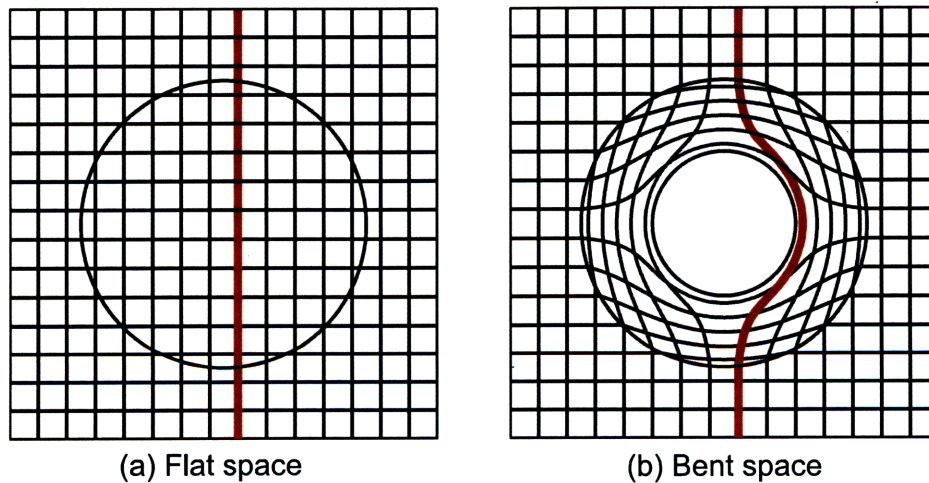
Figure 1-2: (a) A flat space in Cartesian coordinates. (b) A bent space generated by coordinate transformation from (a). A light trajectory (thick line) which is straight in (a) is guided around the central hole in (b).

In this section we will introduce the transformation properties of the constitutive rela-

tions of electromagnetic materials. We first start with the Minkowsky form of Maxwell's equations [16]

$$F_{\alpha\beta,\mu} + F_{\beta\mu,\alpha} + F_{\mu\alpha,\beta} = 0$$
$$G^{\alpha\beta}_{,\alpha} = J^\beta$$

(1.1)

which is form-invariant for general space-time transformations. The tensors in the above Minkowski form are

$$(F_{\alpha\beta}) = \begin{pmatrix} 0 & E_1 & E_2 & E_3 \\ -E_1 & 0 & -cB_3 & cB_2 \\ -E_2 & cB_3 & 0 & -cB_1 \\ -E_3 & -cB_2 & cB_1 & 0 \end{pmatrix}$$

(1.2)

$$(G^{\alpha\beta}) = \begin{pmatrix} 0 & -cD_1 & -cD_2 & -cD_3 \\ cD_1 & 0 & -H_3 & H_2 \\ cD_2 & H_3 & 0 & -H_1 \\ cD_3 & -H_2 & H_1 & 0 \end{pmatrix}$$

(1.3)

$$(J_\beta) = \begin{pmatrix} c\rho \\ J_1 \\ J_2 \\ J_3 \end{pmatrix}$$

(1.4)

The space-time coordinate vector is written as $(x^\alpha) = (ct, x, y, z)$. All the information regarding the topology of the space is contained in the constitutive relations

$$G^{\alpha\beta} = \frac{1}{2}C^{\alpha\beta\mu\nu}F_{\mu\nu}$$

(1.5)

where $C^{\alpha\beta\mu\nu}$ is the constitutive tensor representing the properties of the medium, including its permittivity, permeability and bianisotropic properties. $C^{\alpha\beta\mu\nu}$ is a tensor density of

weight +1, so it transforms as [15]

$$C^{\alpha'\beta'\mu'\nu'} = |\det(\Lambda_\alpha^{\alpha'})|^{-1} \Lambda_\alpha^{\alpha'} \Lambda_\beta^{\beta'} \Lambda_\mu^{\mu'} \Lambda_\nu^{\nu'} C^{\alpha\beta\mu\nu} \qquad (1.6)$$

where the Jacobian matrix is

$$\Lambda_\alpha^{\alpha'} = \frac{\partial x^{\alpha'}}{\partial x^\alpha} \qquad (1.7)$$

If we restrict ourselves to transformations that are time invariant, i.e., only the space is transformed, the permittivity and permeability are also tensors individually. Specifically, they are tensor densities of weight +1, which transforms as [15]

$$\epsilon^{i'j'} = |\det(\Lambda_i^{i'})|^{-1} \Lambda_i^{i'} \Lambda_j^{j'} \epsilon^{ij} \qquad (1.8)$$

$$\mu^{i'j'} = |\det(\Lambda_i^{i'})|^{-1} \Lambda_i^{i'} \Lambda_j^{j'} \mu^{ij} \qquad (1.9)$$

Now let us put these transformations to use. In Pendry *et al.*'s original paper [2], a simple transformation in spherical coordinates is applied by taking all fields in the region $r' < R_2$ in virtual space and compressing them into the region $R_1 < r < R_2$ in physical space, i.e.

$$\begin{cases} r = R_1 + r'(R_2 - R_1)/R_2 \\ \qquad \theta = \theta' \\ \qquad \phi = \phi' \end{cases} \qquad (1.10)$$

such that a "hole" in the region of $r < R_1$ is created. Utilizing Eqs. (1.8) and (1.9), a set of constitutive parameters can be obtained for a spherical invisibility cloak that mimics this space transformation: for $R_1 < r < R_2$,

$$\epsilon_r = \mu_r = \frac{R_2}{R_2 - R_1} \frac{(r - R_1)^2}{r^2} \qquad (1.11)$$

$$\epsilon_\theta = \mu_\theta = \frac{R_2}{R_2 - R_1} \qquad (1.12)$$

$$\epsilon_\phi = \mu_\phi = \frac{R_2}{R_2 - R_1} \qquad (1.13)$$

while for $r < R_1$, ϵ and μ are free to take any value and do not contribute to the electromagnetic scattering. In other words, any object inside the region $r < R_1$ is concealed perfectly from detection without distorting field outside. Any radiation tempting to penetrate into this region will be guided smoothly within the invisibility cloak [2].

We can also apply similar transformation in cylindrical coordinates from virtual space (ρ', ϕ', z') to physical space (ρ, ϕ, z) to create a cylindrical invisibility cloak. For example, cloaking a central cylindrical region of radius R_1 by a concentric cylindrical shell of outer radius R_2 can be achieved by the following transformation applied to the region $\rho' < R_2$ in virtual space

$$
\begin{cases}
\rho = R_1 + \rho'(R_2 - R_1)/R_2 \\
\phi = \phi' \\
z = z'
\end{cases}
\tag{1.14}
$$

which leads to the following constitutive parameters for a cylindrical invisibility cloak in physical space:

$$
\frac{\epsilon_\rho}{\epsilon_0} = \frac{\mu_\rho}{\mu_0} = \frac{\rho - R_1}{\rho}
\tag{1.15}
$$

$$
\frac{\epsilon_\phi}{\epsilon_0} = \frac{\mu_\phi}{\mu_0} = \frac{\rho}{\rho - R_1}
\tag{1.16}
$$

$$
\frac{\epsilon_z}{\epsilon_0} = \frac{\mu_z}{\mu_0} = \left(\frac{R_2}{R_2 - R_1}\right)^2 \frac{\rho - R_1}{\rho}
\tag{1.17}
$$

In most simulation studies and experiments, the cylindrical structure is commonly used due to its relative simplicity. When the normal incidence with only one polarization is considered, the requirements can be further relaxed by making one constitutive parameter a constant while maintaining the refractive index. For example, for a normally incident and vertically polarized (electric field parallel with z axis) wave, the requirements can be

$$
\epsilon_z = \epsilon_0 \left(\frac{R_2}{R_2 - R_1}\right)^2
\tag{1.18}
$$

$$
\mu_\phi = \mu_0
\tag{1.19}
$$

$$
\mu_\rho = \mu_0 \left(\frac{\rho - R_1}{\rho}\right)^2
\tag{1.20}
$$

27

This simplified cloak still has good performance within the limit of geometric optics since the k surface is kept the same as the original model.

1.3 Current state of research on invisibility cloaks

Theoretical part:

The theory of coordinate transformation was firstly applied by Pendry *et al* [2] and Leonhardt [13] to proposing an invisibility cloak model. In Pendry *et al*'s original work, the approach of ray tracing was adopted to demonstrate the cloaking phenomenon. The invisibility was explained by perfect guiding of light rays around the concealed region [2]. The ray's approach is an high-frequency approximation of Maxwell's equations, which intrinsically omits some properties of the wave nature of electromagnetic waves. For example, Pendry *et al* pointed out that there was a "critical ray" problem in their original model, i.e. the ray headed directly toward the center of sphere "does not know whether to be deviated up or down, left or right". After the computational confirmation on the effectiveness of a transformation-based cloak using the ray approach [2, 17], full-wave finite-element simulations were carried out [3, 18] which provided more information about invisibility cloaking. However, on the other hand, there were some concerns about the nonexistence of "finite energy solution" with active sources in the concealed region [19], the possible violation of causality [20] and energy bluing [21] of the invisibility cloak. Our group did the first analytic scattering formalism of invisibility cloaks, and used quantitative bistatic scattering data to evaluate ideal and nonideal cloaks [22, 23, 24]. This work is included in this thesis.

Practical part:

Most technical studies have been focused on the cylindrical (2D) cloaking. The first experimental demonstration of 2D cloaking was done with a simplified model where only the constitutive parameters lying in the 2D plane are varying [6]. It shows that "the cloak decreases scattering from the hidden object whilst at the same time reducing its shadow" in the microwave frequency range. The structure of the metamaterial utilized stacked split-ring resonators, each of which possesses a local resonance and behaves like an effective

28

atom composing the whole effective cloak. However, the scattering from the simplified model of cloak exists intrinsically even from a theoretical point of view [25], regardless of the practical deviations brought during the construction and experiment process. But this experiment demonstrated that metamaterials can be used to approximate the inhomogeneous and anisotropic medium and further suggested that invisibility cloaking created from coordinate transformation is potentially possible.

Subsequent studies aiming to realize cloaking can be divided into four aspects. The first involves possible structures of metamaterials. Some designs based on layered structures have been proposed. Homogeneous and isotropic layers can be stacked to approximate the required anisotropy of cloak [26]. Wires can be inserted in the radial direction to design a non-magnetic 2D cloak whose working frequency can be shifted to optical frequency range for horizontal polarization [27]. Similar structure can also be applied to vertical polarization [5]. Using concentric ring structure, cloaking in the visible frequency range has been demonstrated experimentally [28].

For the second aspect, efforts has been made to minimize the total scattering. A quadratic transformation was used and the impedance matching at the outer boundary was proposed to minimize the scattering [4]. However, this benefit is associated with some constraints on the size of the cloak. Other transformations and impedance matching approaches have been studied [29]. A gap is proposed to be added at the cloak's inner surface to eliminate the zeroth order scattering [30].

Thirdly, some efforts were carried out to extend the operating frequency range of cloaking. Due to the limitation imposed by causality, the perfect cloaks proposed in Ref. [2] can only exist at one single frequency. But for an imperfect model, the frequency band can be extended [31]. In addition, using active instead of passive metamaterials can possibly realize cloaking in multiple operating frequencies [32].

The last aspect is concerned with the cloaking in different background media and with different shapes. For example, the background can be multi-layered and gradually changing media [33], or bianisotropic media and moving media [34]. The cloak's shape can be adjusted according to different situations [35, 36, 37].

29

1.4 Organization of the thesis

Though the transformation theory is an elegant exhibition of invariance of Maxwell's equations, it does not provide a full physical picture of the phenomenon of transformation-based invisibility cloaking. For example, the original mathematical derivation of transformation theory is for nonsingular transformation, while a cloak is usually created from a singular transformation which needs careful examination. In addition, the properties of the transformed media, such as loss, dispersion and other electromagnetic conditions, must be taken into account. Only after all these situations are studied, can we understand the limitations and applicability of transformation theory.

The purpose of this thesis is to provide a systematic electromagnetic study of transformation-based invisibility cloaks. By establishing analytic scattering formalism of invisibility cloaks of canonical shapes, we are able to analyze both ideal and non-ideal cloaks by strictly calculating the instantaneous field over the entire physical space and providing quantitative bistatic scattering data. Some fundamental electromagnetic problems with invisibility cloaks, such as the boundary conditions, reciprocity, signal transport, are studied. The emphasis has been placed on the physical properties of cloaks and their interpretations. The results presented here solved some key problems in invisibility cloaking on both the theoretical and practical levels.

The basis of the theory in this thesis is macroscopic electromagnetic wave theory. The Chu formulation of electrodynamics [16] is used where magnetic charges and magnetic dipoles are treated as the sources of magnetization. Throughout this thesis, the materials considered are assumed to be linear and stationary. In addition, the complex notation is used to represent time harmonic waves. The time domain fields can be simply written as $\overline{E}(r,t) = \Re\{\overline{E}e^{-i\omega t}\}$, where ω is the angular frequency and $\Re$ means taking the real part.

The contents of each chapter are as follows.

Chapter 1 provides a general introduction of the background of this thesis work. Previous efforts on invisibility and the transformation theory are introduced. Current technical progress is summarized.

Chapter 2 is concerned with the basic physics behind the perfect invisibility cloaking.

The wave functions inside a spherical cloak and a cylindrical cloak are derived. Based on that, the interaction between a cloak and electromagnetic waves is explained in detail with some insights that the transformation theory did not show.

Chapter 3 extends the analysis of perfectly matched cloaks to realistic cases. Mismatches and losses are introduced as perturbations in the constitutive parameters. A multi-layer algorithm is developed to take into account the anisotropy, inhomogeneity, and the dispersion of materials. Some interesting phenomena, such as a rainbow-like field distribution caused by different penetrations of different frequency components and the blue-shift effect of a quasi-monochromatic wave, are studied. The signal transport is also studied. A volcano-shaped time-delay is demonstrated in a physical model.

Chapter 4 describes the radiation generated by a fast moving charged particle going through a cloak with uniform velocity. The dyadic Green function with an electric dipole within a spherical cloak is first derived by vector eigenwave expansion. Utilizing the dyadic Green function and other algebra, we demonstrate the complete time-domain radiation process. Total radiated power and the far-field radiation pattern at a particular frequency are calculated. This method can be utilized to detect a perfect cloak.

Chapter 5 deals with the implementation problems. The first part is about inhomogeneous cylindrical cloak with simplified parameters. The second part is concerned with multi-layered cylindrical cloak with anisotropic and homogeneous layers. Genetic algorithm is used to get optimized multi-layered structures that are closely invisible at normal incidence and oblique incidence.

Chapter 6 provides the conclusions of this thesis and suggests some potential future work.

In this thesis, the emphasis has been laid on the linearly transformed cloaks, except some parts in Chapter 5. For a general cloak created from an arbitrary transformation, the wave function can be found in Appendix A and Appendix B.

Chapter 2

Physics of Perfect Invisibility Cloaks

The invisibility cloaks are created from singular transformations that transform a point or a line into a surface and thus need careful examination. In this chapter, we will focus our discussion on the behavior of ideal cloaks being able to create perfect invisibility cloaking. The discussions are strictly based on the Maxwell equations without taking any approximation.

2.1 Scattering model of invisibility cloaks illuminated by external waves

In the following we will develop analytic full-wave scattering models for both spherical and cylindrical cloaks and provide strict analysis for each of them. The scattering models presented here are extensions of common Mie scattering models [1] that usually deal with isotropic and homogeneous objects to the cases of invisibility cloaks that are intrinsically anisotropic and inhomogeneous.

2.1.1 Spherical cloak and its critical ray problem

Figure 2-1 shows that an E_x polarized plane wave with unit amplitude, $E_i = \hat{x}e^{ik_0 z}$, is incident upon the coated sphere along the $\hat{z}$ direction, where $k_0 = \omega\sqrt{\mu_0\epsilon_0}$ is the wave number in air. The time dependence of $e^{-i\omega t}$ is suppressed. Without loss of generality, we
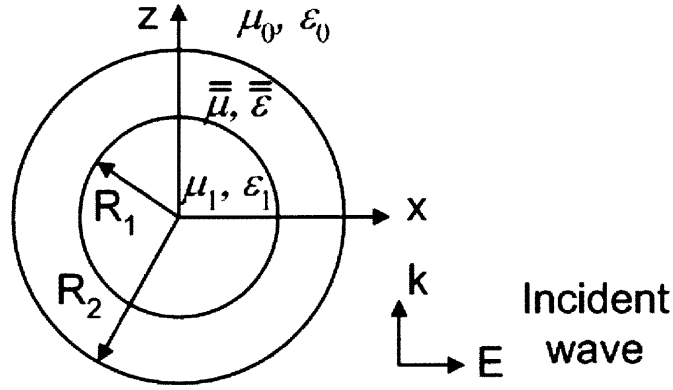
Figure 2-1: Configuration of scattering of a linearly polarized plane wave by a sphere coated with a spherical cloak. The inner and outer radii of the cloak are R_1 and R_2, respectively. The concealed sphere is assumed to be isotropic.

assume that the inner sphere $(r < R_1)$ has the permittivity of ϵ_1 and permeability of μ_1. The cloak $(R_1 < r < R_2)$ is a kind of spherically uniaxial media characterized by

$$\overline{\overline{\epsilon}} = (\epsilon_r(r) - \epsilon_t)\hat{r}\hat{r} + \epsilon_t\overline{\overline{I}}$$
$$\overline{\overline{\mu}} = (\mu_r(r) - \mu_t)\hat{r}\hat{r} + \mu_t\overline{\overline{I}}$$

(2.1)

where $\overline{\overline{I}} = \hat{r}\hat{r} + \hat{\theta}\hat{\theta} + \hat{\phi}\hat{\phi}$, ϵ_t and μ_t are the permittivity and permeability along the $\hat{\theta}$ and $\hat{\phi}$ direction, $\epsilon_r(r)$ and $\mu_r(r)$ are the permittivity and permeability along the $\hat{r}$ direction and both of them are functions of r. The field expressions for the wave propagation inside the cloak are first studied. For source free cases, we decompose the fields into TE/TM modes (with respect to $\hat{r}$) by introducing the scalar potentials, Ψ_{TM} and Ψ_{TE}:

$$\overline{B}_{TM} = \nabla \times (\hat{r}\Psi_{TM})$$
$$\overline{D}_{TM} = \frac{1}{-i\omega}[\nabla \times (\overline{\overline{\mu}}^{-1} \cdot \nabla \times (\hat{r}\Psi_{TM}))]$$
$$\overline{B}_{TE} = \frac{1}{-i\omega}[\nabla \times (\overline{\overline{\epsilon}}^{-1} \cdot \nabla \times (\hat{r}\Psi_{TE}))]$$
$$\overline{D}_{TE} = -\nabla \times (\hat{r}\Psi_{TE})$$

(2.2)

34

Using Eqs. (2.1)(2.2), and after some algebraic manipulations, we can obtain the wave equations for Ψ_{TM} and Ψ_{TE}:

$$\left\{ \frac{1}{AR}\frac{\partial^2}{\partial r^2} + \frac{1}{r^2 \sin\theta}\frac{\partial}{\partial\theta}(\sin\theta\frac{\partial}{\partial\theta}) + \frac{1}{r^2 \sin^2\theta}\frac{\partial^2}{\partial\phi^2} + \frac{1}{AR}k_t^2 \right\} \Psi = 0 \tag{2.3}$$

where $k_t = \omega\sqrt{\mu_t\epsilon_t}$; For TM wave, $AR = \epsilon_t/\epsilon_r$, and for TE wave, $AR = \mu_t/\mu_r$. Using the separation of variables method and assuming $\Psi = f(r)g(\theta)h(\phi)$, we get $h(\phi)$ as harmonic functions: $h(\phi) = e^{\pm im\phi}$, $g(\theta)$ as associated Legendre polynomials: $g(\theta) = P_n^m(\cos\theta)$, and $f(r)$ as the solution of the following equation:

$$\left[\frac{\partial^2}{\partial r^2} + (k_t^2 - AR\frac{n(n+1)}{r^2})\right] f(r) = 0 \tag{2.4}$$

If we take the parameters suggested in [2]: $\epsilon_t = \epsilon_0\frac{R_2}{R_2-R_1}$, $\epsilon_r = \epsilon_t\frac{(r-R_1)^2}{r^2}$, $\mu_t = \mu_0\frac{R_2}{R_2-R_1}$, and $\mu_r = \mu_t\frac{(r-R_1)^2}{r^2}$, then for both TE and TM modes, we get $AR = \frac{r^2}{(r-R_1)^2}$. Therefore, the solution of Eq. (2.4) is:

$$f(r) = k_t(r - R_1)b_n(k_t(r - R_1)) \tag{2.5}$$

where b_n is the spherical Bessel function. From the above analysis, we see that the solutions of Eq. (2.3) in the cloak layer are composed of a superposition of Bessel functions, associated Legendre polynomials, and harmonic functions.

In order to match the boundary conditions on the spherical surface, the incident fields are expanded in terms of spherical harmonics. With the solutions of Eq. (2.3) for the cloak layer, we can get the scalar potentials for the incident fields ($r > R_2$), the scattered fields ($r > R_2$), the internal fields ($r < R_1$), and the fields of the cloak layer ($R_1 < r < R_2$), respectively, to be of the form:

$$\Psi_{TM}^i = \frac{\cos\phi}{\omega}\sum_n a_n\psi_n(k_0r)P_n^1(\cos\theta)$$
$$\Psi_{TE}^i = \frac{\sin\phi}{\omega\eta_0}\sum_n a_n\psi_n(k_0r)P_n^1(\cos\theta) \tag{2.6}$$
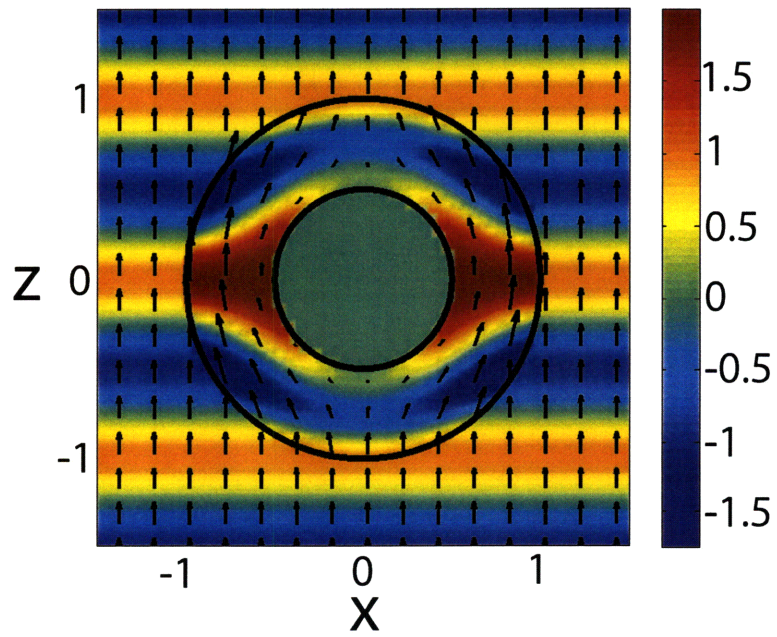
Figure 2-2: E_x field distribution and Poynting vectors due to an E_x polarized plane wave incident onto an ideal cloak with $R_1 = 0.5\lambda_0$ and $R_2 = \lambda_0$.

$$\Psi_{TM}^s = \frac{\cos\phi}{\omega}\sum_n a_n T_n^{(M)}\zeta_n(k_0 r)P_n^1(\cos\theta),$$

$$\Psi_{TE}^s = \frac{\sin\phi}{\omega\eta_0}\sum_n a_n T_n^{(N)}\zeta_n(k_0 r)P_n^1(\cos\theta), \tag{2.7}$$

$$\Psi_{TM}^{int} = \frac{\cos\phi}{\omega}\sum_n c_n^{(M)}\psi_n(k_1 r)P_n^1(\cos\theta),$$

$$\Psi_{TE}^{int} = \frac{\sin\phi}{\omega\eta_0}\sum_n c_n^{(N)}\psi_n(k_1 r)P_n^1(\cos\theta), \tag{2.8}$$

$$\Psi_{TM}^c = \frac{\cos\phi}{\omega}\sum_n \left\{ d_n^{(M)}\psi_n(k_t(r-R_1)) + f_n^{(M)}\chi_n(k_t(r-R_1)) \right\}P_n^1(\cos\theta),$$

$$\Psi_{TE}^c = \frac{\sin\phi}{\omega\eta_0}\sum_n \left\{ d_n^{(N)}\psi_n(k_t(r-R_1)) + f_n^{(N)}\chi_n(k_t(r-R_1)) \right\}P_n^1(\cos\theta), \tag{2.9}$$

where $a_n = \frac{(-i)^{-n}(2n+1)}{n(n+1)}$, $n = 1,2,3\cdots$, $\eta_0 = \sqrt{\mu_0/\epsilon_0}$, $k_1 = \omega\sqrt{\mu_1\epsilon_1}$. $T_n^{(M)}$, $T_n^{(N)}$, $d_n^{(M)}$, $d_n^{(N)}$, $f_n^{(M)}$, and $f_n^{(N)}$ are unknown expansion coefficients, and, $\psi_n(\xi)$, $\chi_n(\xi)$ and $\zeta_n(\xi)$ represent the Riccati-Bessel functions of the first, the second, and the third kind respectively [38]. Using Eq. (2.2), the electromagnetic fields in the three regions can be expanded in terms of the corresponding scalar potentials. By applying the boundary conditions at the surface, we can get four equations at $r = R_1$ and four equations at $r = R_2$. Note that there are two equations at $r = R_1$ given by:

$$\frac{\epsilon_t}{\epsilon_1}c_n^{(N)}\psi_n(k_1 R_1) = d_n^{(N)}\psi_n(0) + f_n^{(N)}\chi_n(0) \tag{2.10}$$

$$\frac{\mu_t}{\mu_1}c_n^{(M)}\psi_n(k_1 R_1) = d_n^{(M)}\psi_n(0) + f_n^{(M)}\chi_n(0) \tag{2.11}$$

We see that $\psi_n(0) = 0$ and that $\chi_n(0)$ is an infinite term for all $n \geq 1$. Since the field in the hidden sphere should be finite, $f_n^{(N)}$ and $f_n^{(M)}$ must be kept zero. We see the field in the hidden object is decoupled with those in the other regions. From the other four equations

at the boundary of $r = R_2$, we can calculate the following coefficients:

$$T_n^{(M)} = -\frac{\psi_n'(\xi_0)\psi_n(\xi_t) - (\eta_t/\eta_0)\psi_n(\xi_0)\psi_n'(\xi_t)}{\zeta_n'(\xi_0)\psi_n(\xi_t) - (\eta_t/\eta_0)\zeta_n(\xi_0)\psi_n'(\xi_t)} \qquad (2.12)$$

$$T_n^{(N)} = -\frac{\psi_n(\xi_0)\psi_n'(\xi_t) - (\eta_t/\eta_0)\psi_n'(\xi_0)\psi_n(\xi_t)}{\zeta_n(\xi_0)\psi_n'(\xi_t) - (\eta_t/\eta_0)\zeta_n'(\xi_0)\psi_n(\xi_t)} \qquad (2.13)$$

$$d_n^{(M)} = a_n \cdot \frac{i\mu_t/\mu_0}{\zeta_n'(\xi_0)\psi_n(\xi_t) - (\eta_t/\eta_0)\zeta_n(\xi_0)\psi_n'(\xi_t)} \qquad (2.14)$$

$$d_n^{(N)} = a_n \cdot \frac{i\epsilon_t/\epsilon_0}{\zeta_n'(\xi_0)\psi_n(\xi_t) - (\eta_0/\eta_t)\zeta_n(\xi_0)\psi_n'(\xi_t)} \qquad (2.15)$$

where $\xi_0 = k_0 R_2$, $\xi_t = k_t(R_2 - R_1)$, and $\eta_t = \sqrt{\mu_t/\epsilon_t}$. If $\epsilon_t = \epsilon_0 \frac{R_2}{R_2 - R_1}$, $\mu_t = \mu_0 \frac{R_2}{R_2 - R_1}$, then $\xi_t = \xi_0$, $\eta_t = \eta_0$. Using the Wronskians for the spherical pairs of solutions, the above four equations are simplified to be:

$$T_n^{(M)} = T_n^{(N)} = 0, \quad d_n^{(M)} = \frac{\epsilon_t}{\epsilon_0} a_n, \quad d_n^{(N)} = \frac{\mu_t}{\mu_0} a_n \qquad (2.16)$$

From Eq. (2.16) we see that the scattering coefficients, $T_n^{(M)}$ and $T_n^{(N)}$, are equal to zero. Therefore, the bistatic scattering, or the radial Poynting power $< S_r > = \frac{1}{2}\Re\{\overline{E}_s \times \overline{H}_s^*\} \cdot \hat{r}$ of the scattered energy conveyed in each direction, is zero. In Chapter 3 we will see the nonzero bistatic scattering from nonideal cloaks. The exactly zero scattered field indicates the reflectionless behavior of the perfect cloak [2]. It should be mentioned that the uniqueness theorem of electromagnetic inverse problems states that zero bistatic scattering from a scatterer is impossible [39, 40] because the bistatic scattering data carry the information of the scatterer 's refractive index. However, this theorem is only applicable to isotropic scatterers while the invisibility cloaks are intrinsically anisotropic [6], so the exactly zero bistatic scattering shown here does not violate this theorem. Figure 2-2 shows the calculated electric fields and the Poynting vectors due to an E_x polarized plane wave incidence onto a cloak with $R_1 = 0.5\lambda_0$ and $R_2 = \lambda_0$ (λ_0 denotes the wavelength in free space). We see that the concealed object is completely hidden from the electromagnetic waves, corroborating the effectiveness of the cloak proposed in [2]. There is no on-axis critical ray problem [2] here since the Poynting power becomes zero as the field penetrate deep into the cloak. There is no power flowing at the inner boundary.

It is seen that the bending of power trajectories follow the prediction of ray tracing approach as shown in Ref. [2]. However, Fig. 2-2 also provides information of phase evolution inside the cloak. In general, the phase propagation direction is different from the power propagation direction due to the anisotropy of the cloak. When a wave enters into the cloak, the phase propagation slows down in the beginning when compared to its counterpart outside the cloak. In the second stage, the phase inside the cloak propagates very fast, faster than the speed of light at which the phase propagates outside the cloak. Finally, the phase inside the cloak slows down again to wait for the catching up of the phase outside the cloak. After the wave outside the cloak catches up, the waves inside and outside the cloak converge, resulting in a flat phase front as if nothing happened. It is worth mentioning that the phase velocity at the inner boundary is infinite meaning that it takes no time for the phase to cross the concealed region. This is because the concealed region is a point before the transformation and therefore the whole concealed region should share the same phase at a fixed moment. We will discuss the speed of power propagation in Chapter 3.

2.1.2 Cylindrical cloak and its surface currents

Figure 2-3 shows the configuration of the scattering from a cylindrical cloak with the inner radius R_1 and outer radius R_2 in which a time harmonic plane wave $\overline{E}_i$ is obliquely incident. Let $\overline{E}_i = (\hat{v}_i E_{vi} + \hat{h}_i E_{hi})e^{i\overline{k}\cdot\overline{r}}$, where $\overline{k} = \hat{x}k_\rho + \hat{z}k_z$, $k^2 = \omega^2\mu_0\epsilon_0$, $\hat{h}_i = \frac{\hat{z}\times\hat{k}}{|\hat{z}\times\hat{k}|}$ and $\hat{v}_i = \hat{h}_i \times \hat{k}$ [1]. Without loss of generality, we assume that the concealed region is filled with an isotropic material with permittivity ϵ_2 and permeability μ_2. The cloak layer between R_1 and R_2 is a specific anisotropic and inhomogeneous medium with permittivity tensor $\overline{\overline{\epsilon}} = \epsilon_\rho\hat{\rho}\hat{\rho}+\epsilon_\phi\hat{\phi}\hat{\phi}+\epsilon_z\hat{z}\hat{z}$ and permeability tensor $\overline{\overline{\mu}} = \mu_\rho\hat{\rho}\hat{\rho}+\mu_\phi\hat{\phi}\hat{\phi}+\mu_z\hat{z}\hat{z}$. According to Ref. [3, 6], we choose $\frac{\epsilon_\rho}{\epsilon_1} = \frac{\mu_\rho}{\mu_1} = \frac{\rho-R_1}{\rho}$, $\frac{\epsilon_\phi}{\epsilon_1} = \frac{\mu_\phi}{\mu_1} = \frac{\rho}{\rho-R_1}$, and $\frac{\epsilon_z}{\epsilon_1} = \frac{\mu_z}{\mu_1} = (\frac{R_2}{R_2-R_1})^2\frac{\rho-R_1}{\rho}$. When $\epsilon_1=\epsilon_0$ and $\mu_1=\mu_0$, the cloak corresponds to the ideal cloak.

In source free medium, the fields can be decomposed into TE^z and TM^z modes with

39
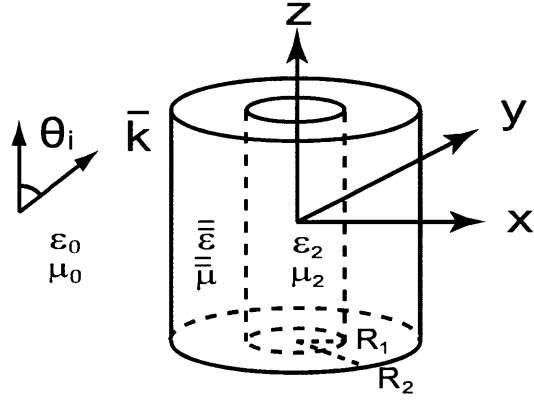
Figure 2-3: The geometry of a cylindrical cloak. The incident wave propagates in the direction of $\bar{k}$.

respect to $\hat{z}$ [41], corresponding to scalar potentials ψ_{TM}^z and ψ_{TE}^z respectively.

$$\overline{H}_{TM} = \overline{\overline{\mu}}^{-1} \cdot \nabla \times (\hat{z}\psi_{TM}^z)$$

$$\overline{E}_{TE} = -\overline{\overline{\epsilon}}^{-1} \cdot \nabla \times (\hat{z}\psi_{TE}^z)$$

$$\overline{E}_{TM} = \frac{1}{-i\omega}\overline{\overline{\epsilon}}^{-1} \cdot [\overline{\overline{\mu}}^{-1} \cdot \nabla \times (\hat{z}\psi_{TM}^z)] \tag{2.17}$$

$$\overline{H}_{TE} = \frac{1}{-i\omega}\overline{\overline{\mu}}^{-1} \cdot [\overline{\overline{\epsilon}}^{-1} \cdot \nabla \times (\hat{z}\psi_{TE}^z)]$$

Hereafter the superscript z is suppressed. After substituting Eqs. (2.17) into the Maxwell equations, we can get the wave equation for the scalar potentials as follows

$$\frac{1}{\rho - R_1}\frac{\partial}{\partial \rho}(\rho - R_1)\frac{\partial \psi}{\partial \rho} + \frac{1}{(\rho - R_1)^2}\frac{\partial^2 \psi}{\partial \phi^2}$$

$$+\frac{R_2^2}{(R_2 - R_1)^2}(\omega^2\mu_1\epsilon_1\psi + \frac{\partial^2 \psi}{\partial z^2}) = 0 \tag{2.18}$$

Using the method of separation of variables, the general expression for the two scalar potentials is obtained by

$$\psi = B_n[R_2 k_{\rho 1}\frac{(\rho - R_1)}{(R_2 - R_1)}] \cdot e^{in\phi + ik_z z} \tag{2.19}$$

where $k_{\rho 1} = \sqrt{k_1^2 - k_z^2} = \sqrt{\omega^2\epsilon_1\mu_1 - k_z^2}$, and B_n represents the solutions of Bessel equation of nth order. Similar to the spherical cloak, the scalar potentials ψ^i, ψ^s, ψ^c and ψ^{int} for

40
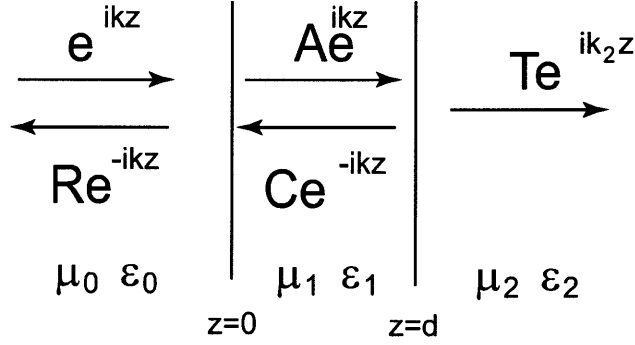
Figure 2-4: A three-layer model with a normally incident wave for demonstrating the surface currents at the inner boundary of a cylindrical cloak. The slab's permeability μ_1 goes to infinity while permittivity ϵ_1 goes to zero but their product is kept equal to $\mu_0\epsilon_0$.

the incident fields ($\rho > R_2$), the scattered fields ($\rho > R_2$), the fields inside the cloak layer ($R_1 < \rho < R_2$) and the internal fields ($\rho < R_1$) respectively for both TE and TM waves can be represented. By matching the boundary conditions, all the expanding coefficients of these scalar potentials can be deduced.

For convenience of demonstration, we consider firstly a simple TM case where a vertically polarized (E_z) plane wave is normally incident onto an ideal cylindrical cloak, i.e. $k_z = 0$ and $E_{hi} = 0$ as well as $\mu_1 = \mu_0$ and $\epsilon_1 = \epsilon_0$, which appears in Refs. [3, 6, 42]. In order to match the boundary conditions, the inner boundary of the cloak is set at $\rho = R_1 + \delta$ instead of $\rho = R_1$ and then the limit $\delta \to 0$ is taken while the parameters of the cloak are still unchanged. Consequently, four boundary equations can be listed utilizing the continuities of E_z and H_ϕ at the outer boundary (Eq.(2.20) and (2.21)) and at the inner boundary

(Eq.(2.22) and (2.23)):

$$-\frac{i^{n-1}}{\omega}E_{vi}J_n(kR_2) + a_n^{(M)}H_n(kR_2) = d_n^{(M)}J_n(kR_2) + f_n^{(M)}N_n(kR_2) \qquad (2.20)$$

$$-\frac{i^{n-1}}{\omega}E_{vi}J_n'(kR_2) + a_n^{(M)}H_n'(kR_2) = d_n^{(M)}J_n'(kR_2) + f_n^{(M)}N_n'(kR_2) \qquad (2.21)$$

$$d_n^{(M)}J_n(\frac{R_2}{R_2-R_1}k\delta) + f_n^{(M)}N_n(\frac{R_2}{R_2-R_1}k\delta) = g_n^{(M)}J_n(k_2R_1) \qquad (2.22)$$

$$\frac{R_2\delta}{(R_2-R_1)R_1}[d_n^{(M)}J_n'(\frac{R_2}{R_2-R_1}k\delta) + f_n^{(M)}N_n'(\frac{R_2}{R_2-R_1}k\delta)]$$

$$= \sqrt{\frac{\mu_0\epsilon_2}{\epsilon_0\mu_2}}g_n^{(M)}J_n'(k_2R_1) \qquad (2.23)$$

where J_n, N_n, and H_n represent the n-th order Bessel function, Neumann function, and Hankel function of the first kind, respectively; $a_n^{(M)}$, $g_n^{(M)}$, $d_n^{(M)}$, and $f_n^{(M)}$ are unknown coefficients corresponding to the scattering field, internal field and the field inside of the cloak, respectively. After solving all the equations, it is seen that $a_n^{(M)} = f_n^{(M)} = g_n^{(M)} = 0$, indicating that both the internal field and the scattering field are zero. The interesting thing is that when $n = 0$, though $f_0^{(M)} = 0$, the product $f_0^{(M)}N_0(\frac{R_2}{R_2-R_1}k\delta)$ in the limit $\delta \to 0$ is equal to $\frac{E_{vi}}{i\omega}$. Obviously, the item of this product in Eq.(2.22) is nonzero only at the inner boundary, which can be characterized as a magnetic surface current raised by the infinite μ_ϕ at the inner boundary of the cloak. Since the tangential electric field on the cloak side of the inner boundary is E_{vi}, the magnetic surface current with an amplitude E_{vi} shields the concealed object, making the field inside exactly be zero. Some study [42] mentioned the "slow convergence" of the scattering coefficients but did not realize that this is actually due to the surface current at the inner boundary.

In order to further reveal the properties of this surface current, we first consider a simplified case as shown in Fig. 2-4, where a plane wave $E_i = E_0e^{ikz}$ is normally incident onto a slab with $\epsilon_1 \to 0$ and $\mu_1 \to \infty$ but $\mu_1\epsilon_1 = \mu_0\epsilon_0$. This special material has the same property with that at the inner boundary of a cylindrical cloak, where $\epsilon_z = 0$ and $\mu_\phi = \infty$ but $\epsilon_z\mu_\phi = (\frac{R_2}{R_2-R_1})^2$. It is easy to obtain that $R = 1$ and $T = 0$ after taking the limits. The electric field at $z = 0$ is $2E_0$ while that at $z = d$ is zero. If we treat $i\omega B$ as the same role of magnetic current, we will find that the integration $\int_0^d i\omega B dz$ is exactly equal to $2E_0$. Therefore this slab acts like a perfect magnetic conductor (PMC) except that

42
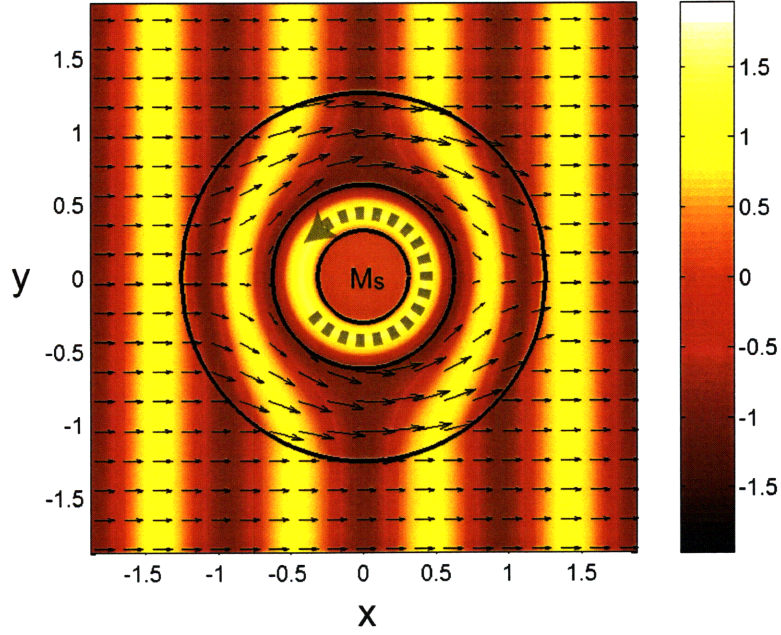
Figure 2-5: The field distribution of E_z in the xy plane due to an E_z polarized wave normally incident onto a cylindrical cloak but with the inner boundary extended inwards. The radius of the three concentric circles are $R_2 = 1.33\lambda_0$, $R_1 = \frac{1}{2}R_2$, and $R_0 = \frac{1}{4}R_2$, respectively. The arrows represent the Poynting vectors in the xy plane.

it is the volume displacement current that is distributed in the slab, not the free magnetic current on the surface of a PMC. When the thickness of the slab becomes infinitesimal, the volume displacement current becomes surface displacement current.

Similarly, we can introduce the third boundary at $\rho = R_0$ ($R_0 < R_1$) as shown in Fig. 2-5. The region between $R_0 < \rho < R_1$ is filled with the same material as the inner boundary at $\rho = R_1$, i.e. the region between $R_0 < \rho < R_1$ is homogeneous, like the slab in Fig. 2-4. The calculated electric field and the Poynting power due to an E_z polarized wave normally incident onto an ideal cylindrical cloak but with such an extended inner boundary are shown in Fig. 2-5. It is seen that there is no field in the region of $\rho < R_0$, but the E_z field in the region of $R_0 < \rho < R_1$ is nonzero. The integration $\int_{R_0}^{R_1} i\omega B_\phi d\rho$ will be the total magnetic current in this region, which has a value of E_z, equal to the surface magnetic current when $\rho = R_0$ and $\rho = R_1$ overlap as we introduced before. In other words, the

surface magnetic current M_s that was previously concentrated at the boundary of $\rho = R_1$ in the case of $R_0 = R_1$ is now distributed over the region $R_0 < \rho < R_1$. It should be noted that with the inner boundary extended (i.e. $R_0 < R_1$), B_ϕ at $\rho = R_1$ is finite, while in the case when $\rho = R_0$ and $\rho = R_1$ overlap (i.e. $R_0 = R_1$), B_ϕ at $\rho = R_1$ becomes divergent. Therefore, the fields at the inner boundary $\rho = R_1$ is dependent on the material in the region of $\rho < R_1$, which means it cannot be determined by the coordinate transformation theory [2]. In addition, although the fields can penetrate through the boundary $\rho = R_1$ in this specific case, the Poynting power along the ρ direction, P_ρ, is always zero (because H_ϕ is always zero in this region), and no power can penetrate into the concealed region. Besides, compared with the spherical cloak, we can see that the bent trajectories of power are similar in spherical and cylindrical cloaks. However, the power distribution is different. While for a spherical cloak the tangential Poynting power decreases to zero at the inner boundary, for a cylindrical cloak the tangential Poynting power P_ϕ at $\rho = R_1$ is not zero except at x axis (y=0).

For a general obliquely incident plane wave with arbitrary polarization, all the coefficients of TM and TE modes can be derived in the same way. Figure 2-6 shows the distribution of E_x component and the Poynting power in the xy and xz planes when a right-handed circularly polarized wave is incident with $\theta_i = 45°$. It is seen that perfect invisibility can still be obtained for obliquely incident waves, indicating that the cylindrical cloaking is not limited to the 2D case only [3, 6, 42]. The oblique rays traversing a cylindrical cloak have also been shown in [17] but were in the geometric limit. We can conclude that in order to completely shield a three-dimensional (3D) concealed object, the cylindrical cloak must be infinitely long. In practice, we have to rely on finite-sized cloaks. Obviously, the longer the cylinder, the better the cloaking performance. It is also worth mentioning that in the xy plane, the fields inside the cloak are no longer symmetric with respect to the x axis, while the flowing power is still distributed symmetrically. This special distribution property is unique for the obliquely incident wave having both vertical and horizontal polarizations. In xz plane, it is seen that the power direction is bent upwards and becomes more vertical, while the wave vector of the phase front is bent downwards and becomes more horizontal. Besides, the discontinuities of E_z and H_z across the inner boundary can
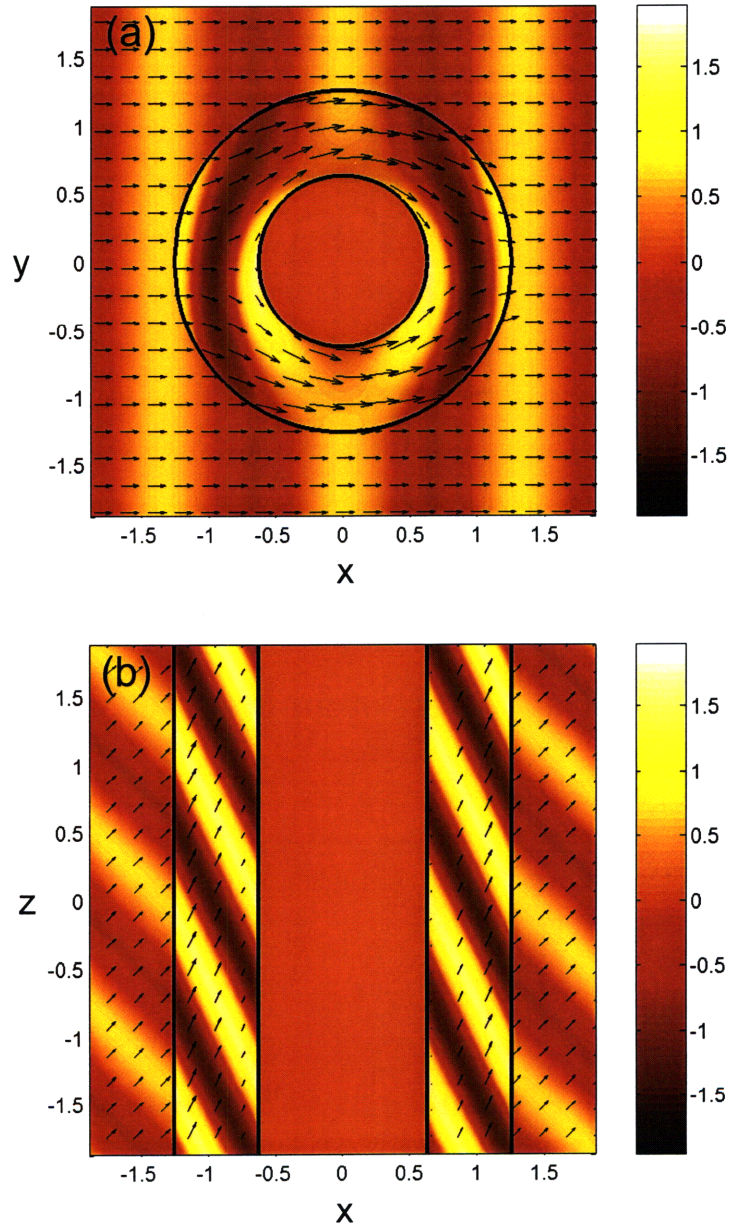
Figure 2-6: The field distribution of E_x in the (a) xy plane and (b) xz plane due to a right-handed circularly polarized incident wave with 45° incident angle. The cloak has a size of $R_2 = 1.33\lambda_0$ and $R_1 = \frac{1}{2}R_2$. The arrows represent the directions of Poynting vectors.

be similarly attributed to the electric and magnetic surface currents at the inner boundary of the cloak. For the ideal cylindrical cloak where $\mu_1 = \mu_0$ and $\epsilon_1 = \epsilon_0$, the discontinuities are $\frac{E_{hi}}{\eta_0} \sin \theta_i e^{ik_z z}$ and $E_{vi} \sin \theta_i e^{ik_z z}$, being exactly the vertical components of the incident magnetic and electrical fields respectively.

This phenomenon arises from the coordinate transformation process. In a spherical cloak, the coordinate transformation approach transforms a field vector at the origin into radial components at the inner boundary. However, this transformation in a cylindrical cloak only applies to the transverse components in the xy plane but does not do anything to the vertical component because the transform coefficient for the z component, Q_z [2, 43], is equal to one. Therefore, there must be a discontinuity across the inner boundary which induces a surface current if we assume no field exists inside the core. These surface currents do not exist before the transformation and have no counterparts in the original Cartesian coordinate system.

2.2 Surface voltage effect of an invisibility cloak with an active device inside

The mechanism of transformation-based invisibility is to create a "hole" in the transformed coordinate system and an object in the "hole" can be concealed from detection [2, 13]. From the viewpoint of transformation theory, the hole creation does not result in an electromagnetic vacuum but rather a complete separation of electromagnetic domains into a cloaked region and those outside [2, 44]. More precisely, a *true* cloak should not only cloak passive objects from incoming waves, but also cloak active devices by preventing waves from going out and being detected. The effectiveness of a transformation-based cloak design for hiding a passive object has been quantitatively analyzed in the last section. On the other hand, however, the electromagnetic wave behavior in this concealed region with an active device inside remains unknown, due to the fact that the concealed region, or the "hole", created by the transformation method does not exist before transformation and has no counterpart in the original Euclidian space. Due to the reciprocity theorem [16], the

46
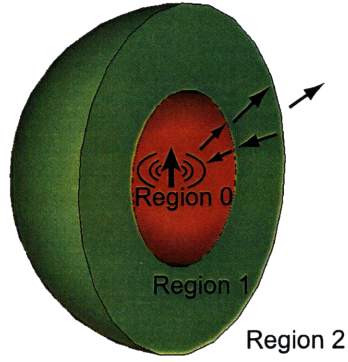
Figure 2-7: Reflection and transmission of electromagnetic waves with an electric dipole inside the concealed region of a spherical cloak. Region 0: concealed region; Region 1: cloak layer; Region 2: free space.

wave inside the concealed region is expected to be limited in this region without escaping. Here we will discuss the physical mechanism behind the reciprocity in this case.

Figure 2-7 shows the configuration of a spherical cloak with outer radius R_2 and inner radius R_1, which is the same as that in Fig. 2-1. The cloak layer within $R_1 < r < R_2$ is a specified anisotropic and inhomogeneous medium. Without loss of generality, we assume that the background material in the region $r < R_1$ has permittivity ϵ_1 and permeability μ_1. A time-harmonic electric dipole is put inside as an active device. The electromagnetic waves from the dipole as well as the response of the surrounding environment can be decomposed into TE and TM modes with respect to $\hat{r}$, corresponding to scalar potentials Ψ_{TE} and Ψ_{TM}, whose expressions in the current case have been derived in Section 2.1.1.

Since TE and TM modes in such a radially inhomogeneous medium can be shown to be decoupled [41], the derivations for these two kinds of modes are similar to each other. We start with the case that an outgoing TM wave is excited in the concealed region. This outgoing wave will induce a standing wave in region $r < R_1$, an outgoing wave and a standing wave in region $R_1 < r < R_2$, and an outgoing wave in region $r > R_2$ [41], as

47

shown in Fig. 2-7. Thus the scalar potentials in these three regions can be written as

$$\Psi_{TM}^{int} = [\zeta_n(k_1 r) + R^{TM}\psi_n(k_1 r)]P_n^m(\cos\theta)e^{im\phi} \tag{2.24}$$

$$\Psi_{TM}^{c} = [d_n^M\psi_n(k_t(r - R_1)) + f_n^M\chi_n(k_t(r - R_1))]P_n^m(\cos\theta)e^{im\phi} \tag{2.25}$$

$$\Psi_{TM}^{out} = T^{TM}\zeta_n(k_0 r)P_n^m(\cos\theta)e^{im\phi} \tag{2.26}$$

where ψ_n, χ_n, and ζ_n are Riccati-Bessel Functions of the first, the second, and the third kind respectively; R^{TM}, d_n^M, f_n^M, and T^{TM} are the unknown expansion coefficients. Especially, R^{TM} and T^{TM} are called the general reflection coefficient and general transmission coefficient, respectively [41].

For the sake of illustration, the inner boundary of the cloak is set at $r = R_1 + \delta$ instead of $r = R_1$ and then the limit $\delta \to 0$ is taken. Consequently, four boundary equations can be listed utilizing the continuities of tangential E and tangential H at the outer boundary (Eq.(2.27) and (2.28)) and at the inner boundary (Eq.(2.29) and (2.30)):

$$1/\sqrt{\mu_t \epsilon_t}[d_n^M\psi_n'(k_t(R_2 - R_1)) + f_n^M\chi_n'(k_t(R_2 - R_1))]$$
$$= 1/\sqrt{\mu_0 \epsilon_0}T^{TM}\zeta_n'(k_0 R_2) \tag{2.27}$$

$$1/\mu_t[d_n^M\psi_n(k_t(R_2 - R_1)) + f_n^M\chi_n(k_t(R_2 - R_1))]$$
$$= 1/\mu_0 T^{TM}\zeta_n(k_0 R_2) \tag{2.28}$$

$$1/\sqrt{\mu_1 \epsilon_1}[\zeta_n'(k_1(R_1 + \delta)) + R^{TM}\psi_n'(k_1(R_1 + \delta))]$$
$$= 1/\sqrt{\mu_t \epsilon_t}[d_n^M\psi_n'(k_t\delta) + f_n^M\chi_n'(k_t\delta)] \tag{2.29}$$

$$1/\mu_1[\zeta_n(k_1(R_1 + \delta)) + R^{TM}\psi_n(k_1(R_1 + \delta))]$$
$$= 1/\mu_t[d_n^M\psi_n(k_t\delta) + f_n^M\chi_n(k_t\delta)] \tag{2.30}$$

After solving all the equations, it can be obtained that $d_n^M = f_n^M = T^{TM} = 0$, indicating that no field exists in the region $r > R_1$. Meanwhile we can get that $R^{TM} = -\zeta_n(k_1 R_1)/\psi_n(k_1 R_1)$, which is important for later use. In addition, it follows that in the limit $\delta \to 0$, $f_n^M\chi_n'(k_t\delta)$ is nonzero. Obviously, the value of this product in Eq.(2.29) is nonzero only at the inner boundary, leading to the discontinuity of the tangential E field

48
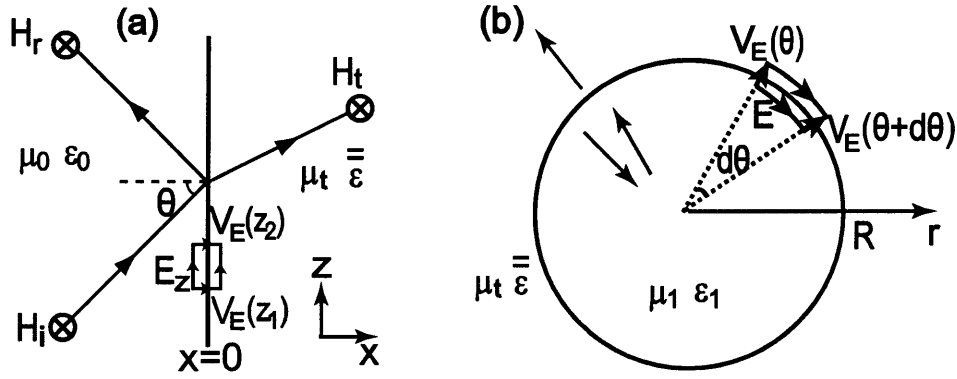
Figure 2-8: Reflection and transmission of (a) a TM wave in Cartesian coordinate system incident from free space onto an uniaxial medium whose ϵ_x goes to zero; and (b) an outgoing TM wave in spherical coordinate system from the homogeneous and isotropic hole through a homogeneous uniaxial background medium whose radial permittivity goes to zero.

across the inner boundary. This result is very interesting. Since both μ and ϵ are finite everywhere and no conductive media exist, there is no surface current to support this discontinuity, as the common boundary conditions of perfect conductor do. It should be noted that due to the same reason the displacement surface currents introduced in the cylindrical cloak [23, 45] are not applicable in the present case.

In order to understand this discontinuity, let us first consider a similar case in Cartesian coordinates as shown in Fig. 2-8(a), where a TM wave $\overline{H}_i = \hat{y}e^{ik_{ix}x+ik_z z}$ is obliquely incident ($k_z \neq 0$) from free space onto an uniaxial medium with permittivity tensor $\epsilon_x\hat{x}\hat{x} + \epsilon_t\hat{y}\hat{y} + \epsilon_t\hat{z}\hat{z}$ and permeability μ_t. The dispersion relation in this medium is $k_{tx}^2/(\omega^2\epsilon_t\mu_t) + k_z^2/(\omega^2\epsilon_x\mu_t) = 1$. Thus, when ϵ_x is very small, k_{tx} becomes imaginary and the transmitted wave becomes evanescent. In the limit $\epsilon_x \to 0$, it can be found that all fields in the region $x > 0$ vanish. More interestingly, in the limit $\epsilon_x \to 0$, the integration $\int_0^\infty E_{tx}dx$ has a finite value $-2i\eta_0 \cos\theta e^{ik_z z}/k_z$. In other words, E_{tx} is compressed on the interface like a delta function. This special finite and nonzero value can be named as an electric surface voltage V_E. The name of "voltage" is because when a free charge q moves to the interface, this voltage will push it to the other side and transfer energy qV_E to it. This voltage is not caused by conductive charges but an extreme polarization of the material on the interface, i.e. it

49
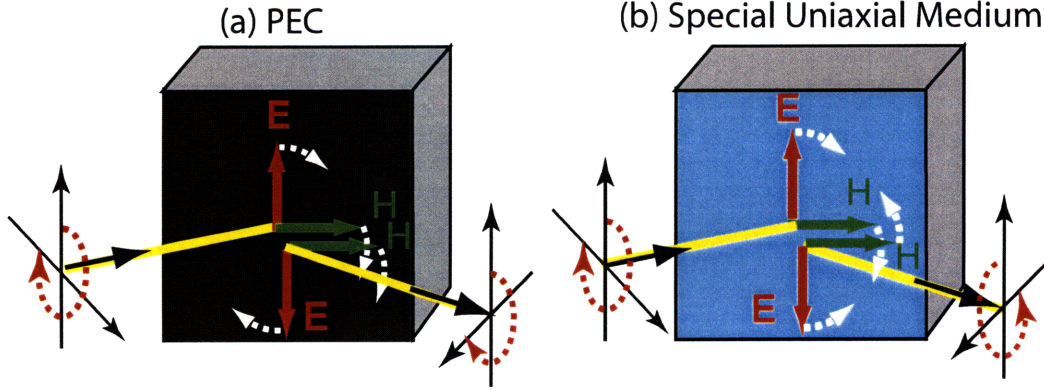
Figure 2-9: Reflection of a right-handed circularly polarized wave from (a) a PEC and (b) a medium with normal permittivity and permeability go to zero simultaneously. The dotted arrows represent the direction of rotation.

corresponds to a distribution of polarized dipole moments on the interface. In addition, the tangential electric field at the left side of the interface is $E_{iz} + E_{rz} = -2\eta_0 \cos\theta e^{ik_z z}$ while that at the right side is zero, meaning the tangential E field is discontinuous across the interface. However, since $(E_{iz} + E_{rz})\Delta z + V_E(z_2) - V_E(z_1) = 0$, as shown in Fig. 2-8(a), Faraday's law still holds on this interface. Clearly, using this uniaxial material, which is the same with the inner boundary of the cloak, E_x becomes a delta function at the boundary and forms the electric surface voltage which supports the discontinuity of the tangential E field. Meanwhile, the reflection coefficient becomes -1, meaning that this medium behaves like a PMC by means of controlling the medium's electric response. There is no physical magnetic charges flowing on the surface, but only a distribution of electric dipoles with some phase shift to match the transverse wave vector k_z.

Similarly, the reflection coefficient for a TE wave is also -1 if μ_x goes to zero. Thus, the special uniaxial medium whose ϵ_x and μ_x go to zero simultaneously behaves like a PMC for TM waves due to electric surface voltages, and a PEC for TE waves due to magnetic surface voltages. This leads to another interesting aspect of the reflection. First, in the sense that there is a complete reflection, the interface behaves like a mirror. Second, this special mirror not only keeps the polarization but also the phase information of the reflected waves. For example, for a right-handed circularly polarized wave incident onto this boundary, the reflected wave retains its handness, but for a mere PEC or PMC boundary,

the reflected wave becomes left-handed, as shown in Fig. 2-9. This property is similar to the soft and hard surface (SHS) boundary used in radar and microwave engineering [46]. But for a SHS with its conducting vector fixed, if the incident plane changes, the phase of the reflected wave also changes. However, the phase of the reflected wave in Fig. 2-9(b) is independent on the incident plane, meaning it only depends on the optical path the wave travels. So, this mirror behaves the same in any plane of incidence, and the information of a source including the polarization and phase is entirely retained in the reflected wave. From above discussion, we can see that the boundary of this special uniaxial medium is in fact a mixture of both PEC and PMC. If we treat this special uniaxial medium as a black box and only consider its boundary conditions on its surface, we can simply denote the boundary conditions as $\overline{D} \cdot \hat{n} = 0$ and $\overline{B} \cdot \hat{n} = 0$, where $\hat{n}$ is the normal direction of the surface. This set of boundary conditions are different from commonly used boundary conditions (tangential E and H being continuous) and have the physical mechanism of corresponding surface voltages.

The above discussion in Cartesian coordinate system shows that the surface voltages introduced by zero permittivity and zero permeability in the normal direction of the interface contribute to the discontinuity of the tangential electromagnetic fields across the boundary. This is also true for a spherical interface in spherical coordinate system. For example, as shown in Fig. 2-8(b), a sphere with permittivity ϵ_1 and permeability μ_1 is embedded in the homogeneous background medium with permittivity tensor $\overline{\overline{\epsilon}} = \epsilon_r \hat{r}\hat{r} + \epsilon_t \hat{\theta}\hat{\theta} + \epsilon_t \hat{\phi}\hat{\phi}$ and permeability μ_t. Similar to the case in Fig. 2-8(a), our derivation shows that for TM waves, in the limit $\epsilon_r \to 0$, no fields exist in the region $r > R_1$, but the electric surface voltage V_E is induced at the boundary. Since $E_\theta^{int} R_1 d\theta + V_E(\theta + d\theta) - V_E(\theta) = 0$, Faraday's law still holds across the boundary. The similar result can be obtained for E_ϕ component. Outgoing TE waves have similar derivation when μ_r goes to zero. Therefore the condition that the material at the inner boundary of a spherical cloak has radial permittivity and permeability of zero is sufficient for total reflection of all waves back by inducing surface voltages, no matter whether the outside medium satisfies the relation of constitutive parameters proposed in Ref. [2] or not. Mathematical treatment in time domain in Ref. [47] has also gotten the similar result on the point of complete reflection. Similar to the previous

case in Cartesian coordinate system, if we are interested only in the boundary conditions, we can denote them as $\overline{D} \cdot \hat{r} = 0$ and $\overline{B} \cdot \hat{r} = 0$ in the spherical coordinates case. This set of boundary conditions result in the reflection coefficients of both TM and TE waves to be $-\zeta_n(k_1 R_1)/\psi_n(k_1 R_1)$, as we have obtained before. We noted that there was a mathematical treatment of cloaking using the traditional boundary conditions (tangential E and H being continuous) that concluded that "finite energy solutions" to Maxwell's equations did not exist in this case [19]. Obviously, the reason is because the boundary conditions need to be modified by introducing surface voltages.

Based on the above discussion, the electric and magnetic surface voltages at the inner boundary as well as the field distribution inside the concealed region due to an electric dipole $\overline{p}$ located at an arbitrary position (r',θ',ϕ'), where $r' < R_1$, can be derived. By expanding the wave from the dipole into spherical waves, the corresponding scalar potentials Ψ^i_{TM} and Ψ^i_{TE} for the incident waves can be obtained. Since it is known that the reflection coefficient for both TE and TM waves is $-\zeta_n(k_1 R_1)/\psi_n(k_1 R_1)$, the scalar potentials of reflected waves, Ψ^r_{TE} and Ψ^r_{TM}, can be easily obtained. Consequently, the induced electric and magnetic surface voltages at the inner boundary of the spherical cloak can be calculated as follows

$$V_E = \int_{R_1^-}^{R_1^+} E_r dr = \frac{-i}{\omega\mu_1\epsilon_1}\frac{\partial}{\partial r}(\Psi^i_{TM} + \Psi^r_{TM})|_{r=R_1^-} , \qquad (2.31)$$

$$V_H = \int_{R_1^-}^{R_1^+} H_r dr = \frac{-i}{\omega\mu_1\epsilon_1}\frac{\partial}{\partial r}(\Psi^i_{TE} + \Psi^r_{TE})|_{r=R_1^-} . \qquad (2.32)$$

Figure 2-10 plots the amplitude of V_E at the inner boundary of a spherical cloak and the field H_y inside the concealed region in the xz plane, due to an electric dipole pointing in $\hat{z}$ direction and located at $(R_1/2, \pi/4, \pi)$. Firstly, it is seen that surface voltage distributions are not uniform on the surface. But for an outside observer, the dipole is invisible since no wave propagates outside. Secondly, the field inside exists in the form of standing waves. Figure 2-10(b) shows the field at the moment that the magnetic field reaches maximum. After a quarter of cycle, the magnetic field becomes zero while the electric field reaches maximum. Since E and H are always out of phase, the time-averaged Poynting power

is zero everywhere within the cloak, meaning no time-averaged power flowing inside. In other words, the energy radiated from the dipole at this moment will be returned to the dipole the next moment. Thus the total energy inside will not blow up.

It can be calculated from Eqs.(2.31) and (2.32) that, in the presence of an electric dipole inside, when ω decreases to zero, V_H becomes zero while V_E survives. Similarly, if a static magnetic dipole is inside instead of a static electric dipole, V_E vanishes while V_H survives. The cloak for the static magnetic field can be realized artificially [48]. Since there is no magnetic charge in nature, this magnetic surface voltage induced by a static magnetic dipole must exist in the form of its equivalent electric surface current. The inner boundary in Ref. [48] is made of superconductor which makes this surface current realizable.

Furthermore, the value of surface voltages can relate to another parameter directly. In derivation of the scalar potential in Ref. [22], the condition $\frac{\partial}{\partial r}\Psi_{TM} = i\omega\epsilon\mu\varphi_e$[49], where φ_e represents the auxiliary electric scalar potential, is applied. It is interesting to note that $V_E = \varphi_e|_{r=R_1^-}$. Similarly, $V_H = \varphi_m|_{r=R_1^-}$. Thus these auxiliary scalar potentials, φ_e and φ_m, which were introduced originally as mathematical tools, have direct physical counterparts at the inner boundary of the cloak, i.e. surface voltages in this case.

2.3 Mechanical responses of invisibility cloaks

When an electromagnetic wave interacts with an invisibility cloak, though the overall result is that as if no object is there, the local effect exerted by the electromagnetic waves to the cloak cannot be ignored. Electromagnetic waves propagate with power and momentum. Therefore, the cloak need to withstand some mechanical forces to guide the wave. On the other hand, according to Einstein's theory of general relativity, the gravity we commonly see is due to the bending of time-space, or, the bending of time-space and the gravity are just two aspects of the same thing. Applying the similar principle to a cloak created by squeezing the electromagnetic space, we might be able to make an analogy of the gravity and conjecture that a "force field" must exist in the cloak. The electromagnetic waves propagate along the curved trajectories because of this force field. In this section we study the mechanical interactions between the cloak and the electromagnetic wave. We take the
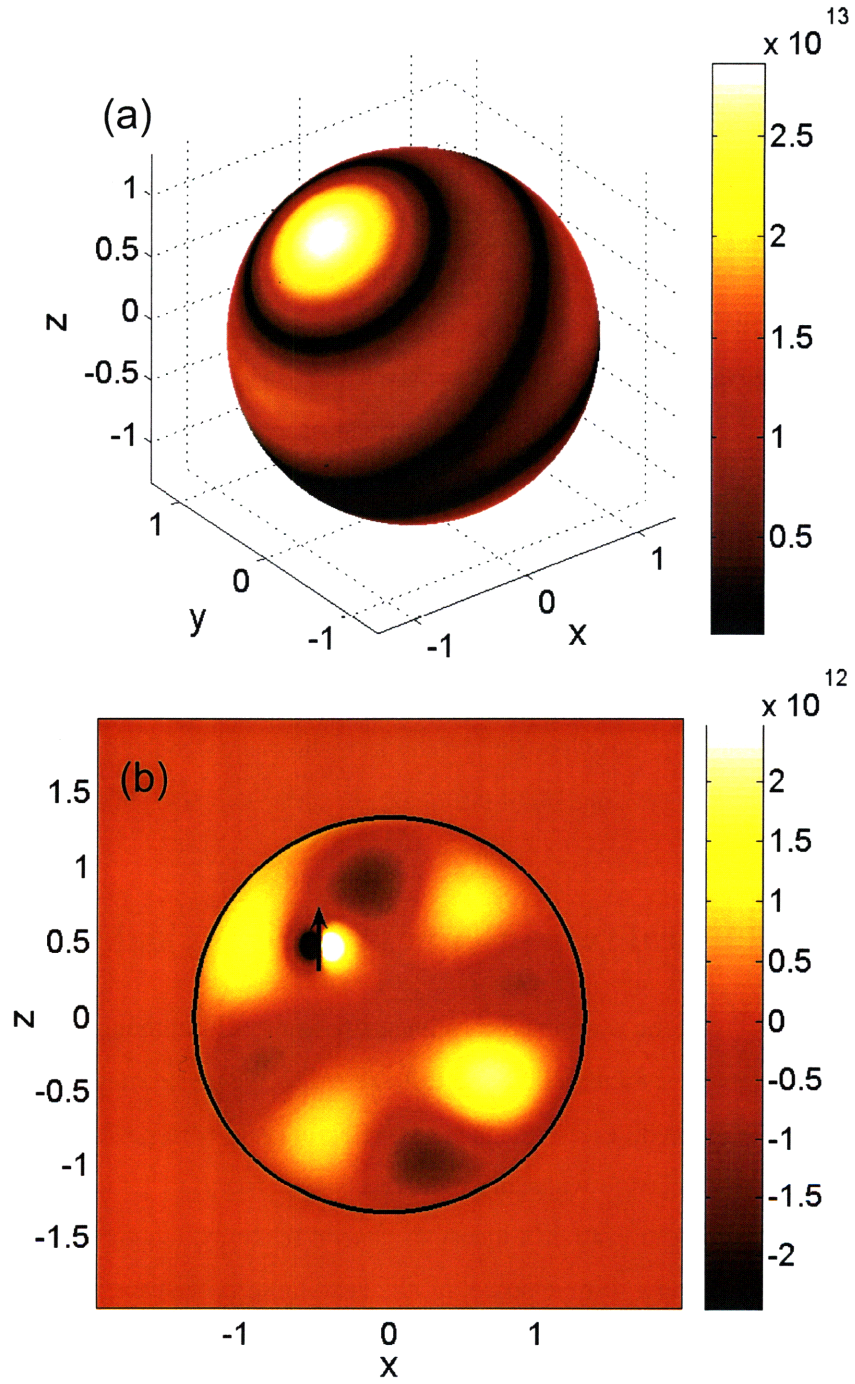
Figure 2-10: Distributions of (a) the amplitude of V_E at the inner boundary and (b) H_y in the concealed region $r < R_1$ due to an unit electric dipole oriented in z direction and located at $(R_1/2, \pi/4, \pi)$ indicated by a small arrow in (b). $R_1 = 1.33\lambda_1$.

54

position that when the electromagnetic waves exert some local forces to the cloak, at the same time the cloak in turn exerts the corresponding recoil forces to the electromagnetic waves.

2.3.1 Electromagnetic forces on a spherical cloak

We first take the spherical cloak as an example and study the mechanical effects of electromagnetic wave on the spherical cloak by directly calculating the Lorentz force inside of the cloak. The bulk bound charge density and surface bound charge density are calculated, and therefore the forces of the wave imposed on these charges can be derived.

We start with a three dimensional spherical cloak with the inner radius R_1 and the outer radius R_2. The cloak shell within $R_1 < r < R_2$ is a radially uniaxial and inhomogeneous medium with permittivity tensor $\bar{\bar{\epsilon}} = \epsilon_r \hat{r}\hat{r} + \epsilon_t \hat{\theta}\hat{\theta} + \epsilon_t \hat{\phi}\hat{\phi}$ and permeability tensor $\bar{\bar{\mu}} = \mu_r \hat{r}\hat{r} + \mu_t \hat{\theta}\hat{\theta} + \mu_t \hat{\phi}\hat{\phi}$. Here we consider an arbitrary radial compression function $f(r)$ as the transformation mapping from the the physical spherical coordinate system (r, θ, ϕ) to the original spherical coordinate system (r', θ', ϕ'), where $r' = f(r)$, $\theta' = \theta$ and $\phi' = \phi$. The constitutive parameters ϵ_t, ϵ_r, μ_t, and μ_r can be derived based on the transformation method:

$$
\begin{aligned}
\epsilon_t &= \epsilon_0 f'(r), \quad \epsilon_r = \epsilon_0 \frac{f^2(r)}{r^2 f'(r)} \\
\mu_t &= \mu_0 f'(r), \quad \mu_r = \mu_0 \frac{f^2(r)}{r^2 f'(r)}
\end{aligned}
\tag{2.33}
$$

where ϵ_0 and μ_0 are the permittivity and permeability of free space. An E_x polarized plane wave with unit amplitude, $E_i = \hat{x} e^{ik_0 z}$, is incident upon the spherical cloak, where $k_0 = \omega \sqrt{\mu_0 \epsilon_0}$ is the wave number in air. The electromagnetic field inside the cloak layer can be calculated as follows:

$$
\begin{aligned}
E_r^c &= f'(r) \sin \theta \cos \phi \, e^{ik_0 f(r) \cos \theta} \\
E_\theta^c &= \frac{f(r)}{r} \cos \theta \cos \phi \, e^{ik_0 f(r) \cos \theta} \\
E_\phi^c &= -\frac{f(r)}{r} \sin \phi \, e^{ik_0 f(r) \cos \theta}
\end{aligned}
\tag{2.34}
$$

$$H_r^c = \frac{1}{\eta_0} f'(r) \sin\theta \sin\phi \; e^{ik_0 f(r)\cos\theta}$$

$$H_\theta^c = \frac{1}{\eta_0} \frac{f(r)}{r} \cos\theta \sin\phi \; e^{ik_0 f(r)\cos\theta} \qquad (2.35)$$

$$H_\phi^c = \frac{1}{\eta_0} \frac{f(r)}{r} \cos\phi \; e^{ik_0 f(r)\cos\theta}$$

Note that the field in the core is zero while the field outside of the cloak (free space region) can be expressed using Eqs. (2.34) and (2.35) except that the transformation function in the free space region is determined by $f^{air}(r) = r$. Once the field inside of the spherical cloak is obtained, the force inside of the medium can be calculated directly using the Lorentz force formula. The time-averaged Lorentz force density due to time-harmonic excitation wave is [50]

$$< \overline{f} >= \frac{1}{2} \Re\{ (-\nabla \cdot \overline{P})\overline{E}^* + (-\nabla \cdot \mu_0 \overline{M})\overline{H}^*$$

$$-i\omega\overline{P} \times \overline{B}^* + i\omega\mu_0 \overline{M} \times \overline{D}^* \} \qquad (2.36)$$

where $\Re$ means taking the real part of a complex quantity and * denotes the complex conjugate. The polarization and magnetization are defined as $\overline{P} = \overline{D} - \epsilon_0 \overline{E}$ and $\mu_0 \overline{M} = \overline{B} - \mu_0 \overline{H}$, respectively. The first two terms in Eq. (2.36) contribute via a force density on bound electric and magnetic charges, while the final two terms represent the force density on both bound and free electric and magnetic currents. In a source free region, $\nabla \cdot \overline{D} = 0$, $\nabla \cdot \overline{B} = 0$, we can get $-\nabla \cdot \overline{P} = \epsilon_0 \nabla \cdot \overline{E}$ and $-\nabla \cdot \mu_0 \overline{M} = \mu_0 \nabla \cdot \overline{H}$. It should be noted that in a homogenous material, both $\nabla \cdot \overline{E}$ and $\nabla \cdot \overline{H}$ are zero everywhere, therefore the force density on the bound electric and magnetic charges exist only at the boundary of two homogenous materials. However, in the spherical cloak case, the materials are both anisotropic and inhomogeneous, the force density on bound electric and magnetic charges may exist in the whole region of the cloak. Substitution of Eqs. (2.34) and (2.35) into Eq. (2.36) yields the bulk force density in the region of $R_1 < r < R_2$:

$$< \overline{f}_{bulk} >= \frac{1}{2} \epsilon_0 \sin\theta \left[f''(r) + \frac{2f'(r)}{r} - \frac{2f(r)}{r^2} \right]$$

$$\cdot \left[\hat{r} f'(r) \sin\theta + \hat{\theta} \frac{f(r)}{r} \cos\theta \right] \qquad (2.37)$$

56

On the outer surface of the cloak, Eq. (2.36) is simplied to be

$$< \overline{f}_{surf} >= \frac{1}{2} \Re\{\rho_e \overline{E}_{avg}^* + \rho_h \overline{H}_{avg}^*\} \tag{2.38}$$

where $\rho_e = \hat{r} \cdot \epsilon_0(\overline{E}^{air} - \overline{E}^c)$, $\rho_h = \hat{r} \cdot \mu_0(\overline{H}^{air} - \overline{H}^c)$ are the bound electric and magnetic surface charge density respectively, and $\overline{E}_{avg} = (\overline{E}^{air} + \overline{E}^c)/2$, $\overline{H}_{avg} = (\overline{H}^{air} + \overline{H}^c)/2$ are the average electric and magnetic field at the surface. It is worth mentioning that the use of the average is not just a matter of choice. From the physical point of view, the charges at the boundary produce a local field in normal direction that has the same magnitude but opposite directions on the two sides of the interface. Therefore it is this locally generated field that is responsible for the field's discontinuity. Averaging the field across the interface eliminates the local field, since the charge cannot exert a force on itself.

Substitution of Eqs. (2.34), (2.35) and the field equation in the free space into Eq. (2.38) yields the surface force density at $r = R_2$:

$$< \overline{f}_{r=R_2} >= \frac{1}{2} \epsilon_0 \sin \theta \left\{ \hat{r} \frac{1}{2}[1 - f'^2(R_2)] \sin \theta + \hat{\theta}[1 - f'(R_2)] \cos \theta \right\} \tag{2.39}$$

Similarly, the surface force density at the inner surface of the cloak ($r = R_1$) can be derived by assuming the field inside the inner core is zero:

$$< \overline{f}_{r=R_1} >= \hat{r} \frac{1}{4} \epsilon_0 f'^2(R_1) \sin^2 \theta \tag{2.40}$$

It can be seen that neither the bulk force density nor the surface force density have ϕ component, which means there is no angular momentum transfer with respect to the z axis due to the rotational symmetry of the spherical cloak. In addition, the surface force at the inner boundary has only r component, because there are no tangential field components at the inner surface. However, the surface force at the outer boundary has both r and θ components.

For a linearly transformed spherical cloak where $f(r) = \frac{R_2}{R_2-R_1}(r-R_1)$, the constitutive parameters of the spherical cloak are $\epsilon_t = \epsilon_0 \frac{R_2}{R_2-R_1}$, $\epsilon_r = \epsilon_0 \frac{R_2}{R_2-R_1}(\frac{r-R_1}{r})^2$, $\mu_t = \mu_0 \frac{R_2}{R_2-R_1}$, $\mu_r = \mu_0 \frac{R_2}{R_2-R_1}(\frac{r-R_1}{r})^2$. Substituting the linear transformation function into Eqs. (2.41,

2.52, 2.53), we can get the force distribution inside the linearly transformed cloak:

$$< \overline{f}_{bulk} >= \epsilon_0 \sin\theta \frac{R_1 R_2^2}{(R_2 - R_1)^2} \frac{1}{r^2} \cdot \left[\hat{r} \sin\theta + \hat{\theta}\left(1 - \frac{R_1}{r}\right)\cos\theta \right] \qquad (2.41)$$

$$< \overline{f}_{r=R_2} >= \frac{1}{2}\epsilon_0 \sin\theta \frac{-R_1}{R_2 - R_1} \cdot \left[\hat{r} \frac{2R_2 - R_1}{2(R_2 - R_1)} \sin\theta + \hat{\theta}\cos\theta \right] \qquad (2.42)$$

$$< \overline{f}_{r=R_1} >= \hat{r}\frac{1}{4}\epsilon_0 \left(\frac{R_2}{R_2 - R_1} \right)^2 \sin^2\theta \qquad (2.43)$$

Assuming the incident wave has a wavelength of $\lambda_0 = 0.1$ m, we can calculate the total electric field intensity in the xz plane and the bulk force density inside of the cloak as well as the surface force density on the inner and outer boundaries as shown in Fig. 2-11. If we define the polar axis to be along the wave propagation direction (z direction), we can see that the force at the polar regions which corresponds to $\theta = 0$ and $\theta = \pi$ is exactly zero. This means that the polar region (at $\theta = 0$ and $\theta = \pi$) which is directly impinged upon by the electromagnetic waves withstands no electromagnetic force while the equatorial region (at $\theta = \pi/2$) withstands finite optical forces. The maximum bulk force density is $3.53 \times 10^{-10} \text{N/m}^3$. The maximum value of the surface force density on the outer surface is $6.63 \times 10^{-12} \text{N/m}^2$ located at $(r, \theta) = (R_2, \pi/2)$. The maximum value of the surface force density on the inner surface is $8.84 \times 10^{-12} \text{N/m}^2$ located at $(r, \theta) = (R_1, \pi/2)$.

In order to view the bulk force clearly, we plot each component of the bulk force in Fig. 2-12, where Fig. 2-12(a) shows the r component of the force while Fig. 2-12(b) shows the θ component of the force in the xz plane. The r component of the force is dominant and is always pointing outward, tending to expand the cloak medium. The force is much bigger at the equatorial region of the cloak corresponding to $\theta = \pi/2$ than that at the polar regions corresponding to $\theta = 0$ and $\theta = \pi$. The θ component of the force shown in Fig. 2-12(b) is smaller by an order of magnitude when compared to the r component. The θ component shows a symmetric pattern in the xz plane, and the force in the region of $\theta > 0$ is positive while in the region of $\theta < 0$ is negative.

Figure 2-11: E_x field distribution and Lorentz force density distribution in the xz plane due to an E_x polarized plane wave incident onto an ideal spherical cloak with $R_1 = \lambda_0$ and $R_2 = 2\lambda_0$.
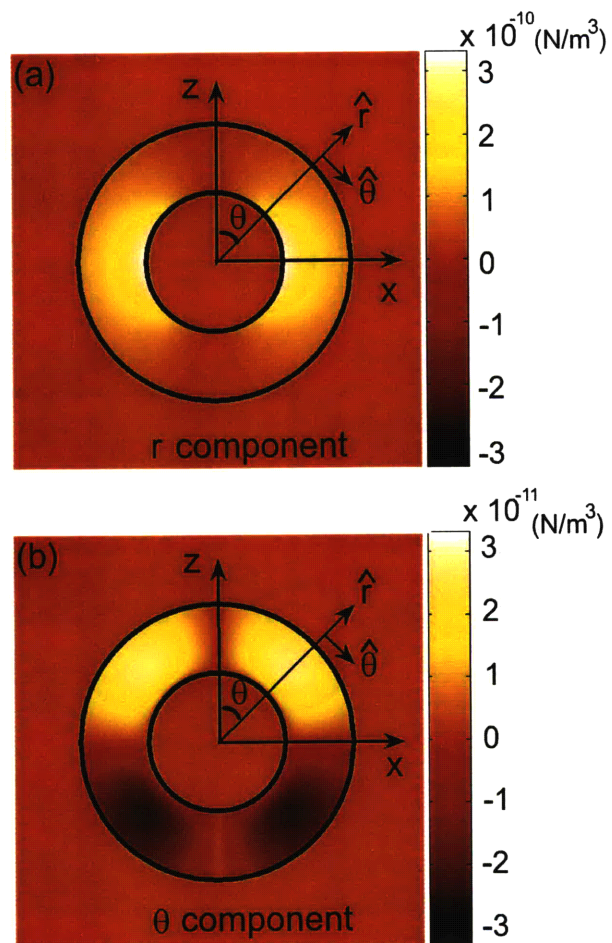
Figure 2-12: (a) The r component and (b) θ component of the bulk Lorentz force density in the xz plane inside the spherical cloak with $R_1 = 1\lambda_0$ and $R_2 = 2\lambda_0$ due to an E_x polarized plane wave passing through. $\lambda_0 = 0.1$ m.
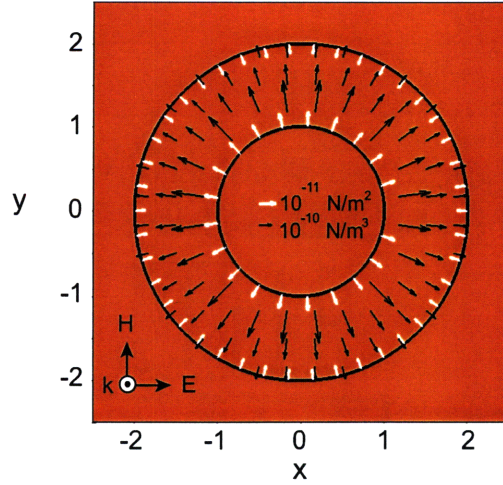
Figure 2-13: Bulk and surface Lorentz force density distributions in the xy plane within an ideal spherical cloak with $R_1 = 1\lambda_0$ and $R_2 = 2\lambda_0$ due to an E_x polarized plane wave passing through. λ_0=0.1 m.

It should be noted that all the bulk force and the surface force are rotationally symmetric with respect to the z axis, as shown in Fig. 2-13, where we plot both the bulk force density (marked in black) and the surface force density (marked in white) in the xy plane. The surface force density has a unit of N/m^2 and the bulk force density has a unit of N/m^3. Since the force distribution are symmetric with respect to the z axis, the total Lorentz force for an ideal cloak is exactly zero, which means there is no momentum transfer from the electromagnetic waves to the cloak. However, the expanding force along the $\hat{r}$ direction and the shrinking force along the $-\hat{r}$ direction are not in balance. The total force on the half cloak located at $x > 0$ is $\hat{x}1.82 \times 10^{-13}$N while the total force on the other half cloak located at $x < 0$ is $-\hat{x}1.82 \times 10^{-13}$N. These two forces of the same amplitude pull the two halves of the cloak in an opposite direction. Therefore, the effect is to expand the cloak but the total radiation force on the whole cloak is zero.

The Lorentz force density on the spherical cloak can also be calculated by using the Maxwell stress tensor [16, 51]:

$$<\overline{f}> = -\frac{1}{2}\Re\{\nabla \cdot \overline{\overline{T}}\} \tag{2.44}$$

61

where

$$< \overline{\overline{T}} > = \frac{1}{2}(\epsilon_0|\overline{E}|^2 + \mu_0|\overline{H}|^2)\overline{\overline{I}} - \epsilon_0\overline{E}\,\overline{E}^* - \mu_0\overline{H}\,\overline{H}^* \qquad (2.45)$$

takes the Chu's formulation of the Maxwell stress tensor [52]. The total force $\overline{F}$ on the cloak is found by integrating a surface that just encloses the entire cloak so that $\overline{\overline{T}}$ is evaluated at $r = R_2^+$,

$$\overline{F} = -\frac{1}{2}\Re\left\{\oint_A dA[\hat{r} \cdot \overline{\overline{T}}(\overline{r})]\right\} \qquad (2.46)$$

The calculated total force using tensor form is also shown to be zero because the scattering field is zero. Therefore, the Maxwell stress tensor and the distributed Lorentz force are in agreement when applied to calculating the force.

After calculating the Lorentz force distribution, we can discuss the effects exerted by the cloak to the electromagnetic waves. From Fig. 2-11 we can see that most of the forces are pointing outwards except those on the outer boundary which are pointing inwards. While Lorentz forces are exerted to the cloak by electromagnetic waves or photons, we can also consider that the electromagnetic waves or photons are subject to the recoil forces since the force action is mutual. Now we discuss the reason why directions of forces on the outer boundary and inside the cloak layer are quite different. By tracing the trajectory of a ray (or photons) through the cloak, we can see that it is bent three times. The first occurs on the outer boundary when the photons start entering into the cloak. We can see an abrupt direction change of the ray at this incident point on the outer boundary, meaning the photons at this point are pulled abruptly. The second is the turning around of the ray inside the cloak layer, as if the photons are doing circular motion. The third occurs at the outer boundary when the ray goes out. This emitting point, symmetric with the incident point, is the place where the photons are pulled back to their original trajectory. The bending at the incident point at the outer boundary is due to the surface bound charges. Since these bound charges are concentrated on the boundary, they are able to change the direction of rays abruptly. We can see that by bending the ray or photons at the outer boundary, the recoil force must point outwards, meaning the Lorentz force on the outer boundary need

62

to point inwards. Within the cloak layer, photons are moving along curvatures, requiring a centripetal force. The centripetal force is the recoil force of the Lorentz force exerted to the cloak layer. Therefore we can see that the dominant r component of the Lorentz force is always positive because the force needs to drag the photons to turn around the center. However, this turning around is not strictly centered at the origin, but has a slight deviation. Therefore, the θ component of the bulk force is important to tune the center of the circulating motion slightly, though its value is relatively small.

2.3.2 Electromagnetic forces on a cylindrical cloak

In the above section we discussed the Lorentz force distribution inside a spherical cloak. The same procedure can also be applied to a cylindrical cloak.

Take a cylindrical cloak with inner radius R_1 and outer radius R_2 for instance. The cloak shell within $R_1 < \rho < R_2$ is an anisotropic and inhomogeneous medium with permittivity tensor $\bar{\bar{\epsilon}} = \epsilon_\rho \hat{\rho}\hat{\rho} + \epsilon_\phi \hat{\phi}\hat{\phi} + \epsilon_z \hat{z}\hat{z}$ and permeability tensor $\bar{\bar{\mu}} = \mu_\rho \hat{\rho}\hat{\rho} + \mu_\phi \hat{\phi}\hat{\phi} + \mu_z \hat{z}\hat{z}$. Here we consider an arbitrary radial compression function $f(\rho)$ as the transformation mapping from the the physical cylindrical coordinate system (ρ, ϕ, z) to the original cylindrical coordinate system (ρ', ϕ', z'). The constitutive parameters ϵ_ρ, ϵ_ϕ, ϵ_z, μ_ρ, μ_ϕ and μ_z can be derived based on the transformation:

$$
\begin{aligned}
\epsilon_\rho &= \epsilon_0 \frac{f(\rho)}{\rho f'(\rho)}, \quad \epsilon_\phi = \epsilon_0 \frac{\rho f'(\rho)}{f(\rho)}, \quad \epsilon_z = \epsilon_0 \frac{f(\rho)f'(\rho)}{\rho} \\
\mu_\rho &= \mu_0 \frac{f(\rho)}{\rho f'(\rho)}, \quad \mu_\phi = \mu_0 \frac{\rho f'(\rho)}{f(\rho)}, \quad \mu_z = \mu_0 \frac{f(\rho)f'(\rho)}{\rho}
\end{aligned}
\tag{2.47}
$$

where ϵ_0 and μ_0 are the permittivity and permeability of free space. The time-harmonic incident wave is $\bar{E}_i = (\hat{v}_i E_{vi} + \hat{h}_i E_{hi})e^{i\bar{k}\cdot\bar{r}}$, where $\bar{k} = \hat{x}k_\rho + \hat{z}k_z$, $k^2 = \omega^2\mu_0\epsilon_0$, $\hat{h}_i = \frac{\hat{z}\times\hat{k}}{|\hat{z}\times\hat{k}|}$ and $\hat{v}_i = \hat{h}_i \times \hat{k}$ [1]. Here we only consider the case of vertical polarization, i.e. $E_{hi} = 0$. The horizontal polarization, i.e. $E_{vi} = 0$, can be considered as the dual case. The incident angle α can be defined as $\alpha = \tan^{-1}\frac{k_z}{k_\rho}$. The electromagnetic field inside the cloak layer

can be calculated as follows:

$$E_\rho^c = -f'(\rho) \sin \alpha \cos \phi \, e^{ik_\rho f(\rho) \cos \phi + ik_z z}$$

$$E_\phi^c = \frac{f(\rho)}{\rho} \sin \alpha \sin \phi \, e^{ik_\rho f(\rho) \cos \phi + ik_z z} \tag{2.48}$$

$$E_z^c = \cos \alpha \, e^{ik_\rho f(\rho) \cos \phi + ik_z z}$$

$$H_\rho^c = -\sqrt{\frac{\epsilon_0}{\mu_0}} f'(\rho) \sin \phi \, e^{ik_\rho f(\rho) \cos \phi + ik_z z}$$

$$H_\phi^c = -\sqrt{\frac{\epsilon_0}{\mu_0}} \frac{f(\rho)}{\rho} \cos \phi \, e^{ik_\rho f(\rho) \cos \phi + ik_z z} \tag{2.49}$$

$$H_z^c = 0$$

Applying the Lorentz force formula Eq. (2.36), we can get the force densities exerted to the bound charges within the cloak and on the boundaries.

$$< \overline{f}_{bulk} > = \epsilon_0 \left[\frac{f'(\rho)}{\rho} + f''(\rho) + \frac{f(\rho)}{\rho^2} \right] \left\{ \hat{\rho}(\sin^2 \alpha \cos^2 \phi + \sin^2 \phi) f'(\rho) \right.$$

$$\left. + \hat{\phi} \sin \phi \cos \phi \cos^2 \alpha \frac{f(\rho)}{\rho} - \hat{z} \sin \alpha \cos \alpha \cos \phi \right\} \tag{2.50}$$

$$< \overline{f}_{\rho=R_2} > = \frac{1}{2} \epsilon_0 (1 - f'(R_2)) \left\{ \hat{\rho} \frac{1 + f'(R_2)}{2} (\sin^2 \alpha \cos^2 \phi + \sin^2 \phi) \right. \tag{2.51}$$

$$\left. + \hat{\phi} \sin \phi \cos \phi \cos^2 \alpha - \hat{z} \sin \alpha \cos \alpha \cos \phi \right\} \tag{2.52}$$

$$< \overline{f}_{\rho=R_1} > = \frac{1}{4} \epsilon_0 f'(R_1) \left\{ \hat{\rho} f'(R_1)(\sin^2 \alpha \cos^2 \phi + \sin^2 \phi) \right.$$

$$\left. - \hat{z} \sin \alpha \cos \alpha \cos \phi \right\} \tag{2.53}$$

It is easily seen that for the ρ and ϕ components, due to the symmetry, the total integration of these components must be zero. For the z component, its integration over ϕ from 0 to 2π will automatically give the result of zero. Therefore the total force exerted to the cylindrical cloak must be zero.

For simplicity of demonstration we consider normal incidence. By setting $R_2 = 2R_1 =$
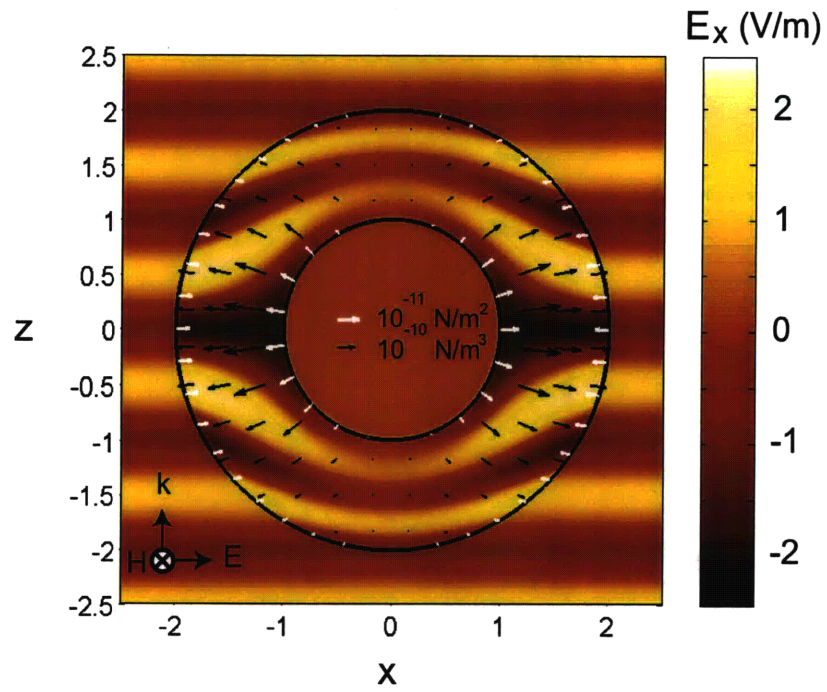
64
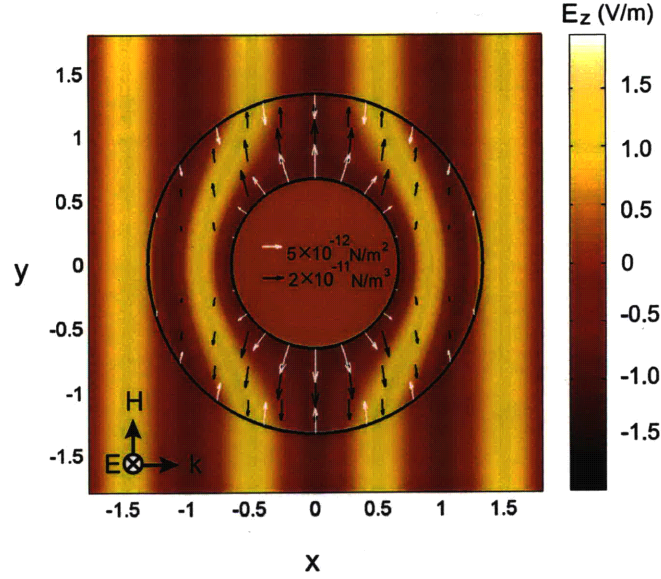
Figure 2-14: E_z field distribution and Lorentz force density distribution in the xy plane due to a vertically polarized plane wave incident onto an ideal cylindrical cloak with $R_2 = 1.33\lambda_0$ and $R_1 = \frac{1}{2}R_2$ at normal incidence. $\lambda_0 = 0.94$ m.

$1.33\lambda_0$ ($\lambda_0 = 0.94$ m) and the incident angle $\alpha = 0$, we can plot the force distribution inside the cylindrical cloak when a vertically polarized wave is normally incident with E filed of unit amplitude, as shown in Fig. 2-14. It is seen that the force distribution is similar to the case of a spherical cloak. The forces at the outer surface of the cloak point inward while the forces in the other regions point outward. There are slight differences between the forces within the cylindrical cloak and the forces within the spherical cloak due to the geometrical difference.

When the incident angle is tilted and set to be $\alpha = \pi/4$, the force distribution is quite different, as shown in Fig. 2-15. It is seen from Fig. 2-15(a) that in the xy plane, the force along the y axis ($\phi = 0$ and $\phi = \pi$) is not zero. From Fig. 2-15(b), we can see that all the bulk forces and surface forces have z components. It is interesting to note that within the cloak, the bulk forces are perpendicular to the direction of Poynting powers in the xz plane while the power's direction still remains a straight line. This phenomenon is different from conventional cases in a common material and may need more studies.

65
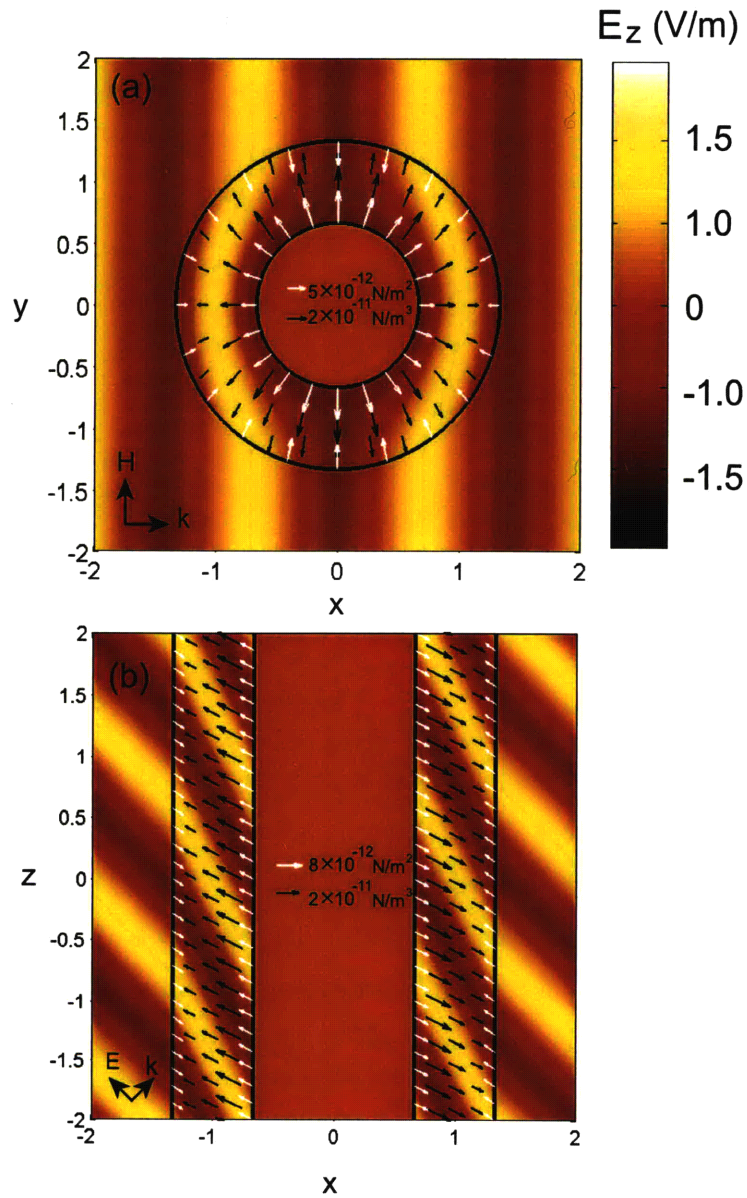
Figure 2-15: E_z field distribution and Lorentz force density distribution in (a) the xy plane and (b) the xz plane due to a vertically polarized plane wave incident onto an ideal cylindrical cloak with $R_2 = 1.33\lambda_0$ and $R_1 = \frac{1}{2}R_2$ with incident angle of $45°$. $\lambda_0 = 0.94$ m.

2.4 Summary

In this chapter, the physics behind perfect invisibility cloaks is explored by analytically calculating the spatial distribution of electromagnetic fields. The scattering models of the spherical cloak and the cylindrical cloak are firstly established and wave functions inside the cloak are derived. Main conclusions are as follows.

- Perfect invisibility can be characterized as exactly zero bistatic scattering.

- An external electromagnetic wave illuminating a cylindrical cloak will induce electric and magnetic surface currents at the inner boundary of this cloak. These surface currents do not exist in the original electromagnetic space and have no counterparts in the transformation.

- A spherical cloak is able to cloak perfectly an active device that radiates from the concealed region. The mechanism is that the outgoing radiation will induce surface voltages at the inner boundary of the cloak that reflect all waves back. These surface voltages lead to a new set of boundary conditions.

- The mechanical response of the cloak to external electromagnetic waves is analyzed by calculating the Lorentz force distribution. It is shown that an incoming plane wave tends to expand the bulk of a cloak while squeezing the outer boundary of the cloak at the same time. The recoil forces can be treated as the reason of bending of ray trajectories.

.

Chapter 3

Effects of Imperfections on Invisibility Cloaks

The requirement for perfect invisibility is quite stringent. The constitutive parameters must satisfy the specific conditions which contain continuously varying anisotropy and inhomogeneity. Especially, the constitutive parameters possess extreme values, either zero or infinity. All of these factors imply that it is quite difficult to implement the required constitutive parameters in practice and thus it is necessary to study imperfect cases. This chapter is concerned with imperfections caused by mismatches and frequency dispersions.

3.1 Scattering from mismatched cloaks

3.1.1 Spherical cloak with perturbed constitutive parameters

In last chapter we derived the wave equations and showed the exactly zero scattering from a perfect spherical cloak from Eqs. (2.12–2.15). In fact, Eqs. (2.12–2.15) are able to provide further information. For example, it is known that loss is often an important issue. When the electric and magnetic loss tangents are introduced, the scattering coefficients $T_n^{(M)}$ and $T_n^{(N)}$ become nonzero. In Fig. 3-1, we plot the bistatic scattering as a function of the scattering angle θ for the loss tangent of 0.01, 0.1, and 1, respectively. The vertical axis represents the normalized differential scattering cross sections, $\frac{|S_1(\theta)|^2}{k_0^2 \pi R_2^2}$, $\frac{|S_2(\theta)|^2}{k_0^2 \pi R_2^2}$, where
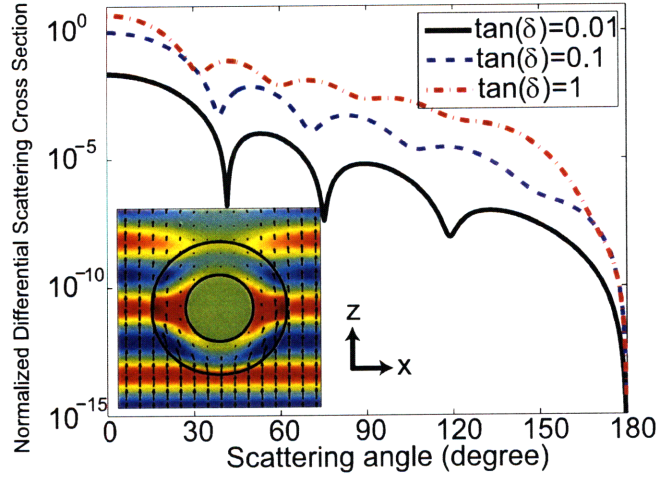
Figure 3-1: Normalized differential scattering cross sections $|S_1(\theta)|^2/(k_0^2 \pi R_2^2)$ and $|S_2(\theta)|^2 /(k_0^2 \pi R_2^2)$ [1] for a cloak ($R_1 = 0.5\lambda_0$, $R_2 = \lambda_0$) with a specified loss tangent introduced in each component of the permittivity and permeability. The inset shows the E_x field for the case of $\tan \delta = 0.1$.

$S_1(\theta)$ and $S_2(\theta)$ are defined by [1]:

$$S_1(\theta) = -\sum_n \frac{(2n+1)}{n(n+1)}[T_n^{(M)}\pi_n(\theta) + T_n^{(N)}\tau_n(\theta)]$$

$$S_2(\theta) = -\sum_n \frac{(2n+1)}{n(n+1)}[T_n^{(M)}\tau_n(\theta) + T_n^{(N)}\pi_n(\theta)]$$

(3.1)

In the above two equations $\pi_n(\theta)$ and $\tau_n(\theta)$ are related to the associated Legendre functions by $\pi_n(\theta) = -\frac{P_n^1(\cos\theta)}{\sin\theta}$ and $\tau_n(\theta) = -\frac{dP_n^1(\cos\theta)}{d\theta}$, respectively [38]. For the configuration shown in Fig. 2-1, $S_1(\theta)$ and $S_2(\theta)$ represent the scattering patterns in the yz and xz planes respectively. The two curves of $S_1(\theta)$ and $S_2(\theta)$ overlap because $T_n^{(M)} = T_n^{(N)}$. From Fig. 3-1 we see that the scattered power increases as the loss increases. A more interesting phenomenon is that the backscattering magnitude is always zero (because $T_n^{(M)} = T_n^{(N)}$, and $\pi_n(\theta) = -\tau_n(\theta)|_{\theta=180°}$), which is very different from conventional scattering from regular particles [1]. The calculated field distribution in the xz plane for the spherical cloak with $\tan \delta = 0.1$ (Fig. 3-1, inset) is similar to the simulation results of a cylindrical cloak with the same type of loss [3]. However, our analytical calculation shows that only

70

the spherical cloak in this particular lossy case exhibits exactly zero backscattering. This unique property of the spherical cloak indicates that the cloaked object can still completely hide from a monostatic radar detection.

Since the constitutive parameters for a perfect cloak are very difficult to realize, non-ideal material parameters are more often used in the measurements [3, 6]. Hence, it is worth studying how the mismatched material parameters quantitatively affect the performance of the cloak. We calculate the normalized scattering cross section $Q_{scat} = \frac{2}{(k_0 a)^2} \sum_n (2n + 1)(|T_n^{(M)}|^2 + |T_n^{(N)}|^2)$ [1] as ϵ_t changes under three cases: (Case I) keep $\mu_t = \mu_0 \frac{R_2}{R_2 - R_1}$ constant; (Case II) keep the impedance $\eta_t = \sqrt{\mu_t/\epsilon_t} = \eta_0$ constant; and (Case III) keep the refractive index $n_t = \sqrt{\frac{\mu_t \epsilon_t}{\mu_0 \epsilon_0}} = \frac{R_2}{R_2 - R_1}$ constant. The results are shown in Fig. 3-2(a), where the horizontal axis ϵ_t is normalized by the ideal parameter $\epsilon_0 \frac{R_2}{R_2 - R_1}$. We see that when ϵ_t is equal to the ideal parameter, the corresponding μ_t in the three cases are all equal to $\mu_0 \frac{R_2}{R_2 - R_1}$, and Q_{scat} is equal to 0, meaning the cloak is perfect. When ϵ_t is slightly changed from the ideal parameter, Q_{scat} in Case I and Case II increase from zero more rapidly than that in Case III. This is because in Case III, the refractive index is kept constant, and the direction of Poynting vector inside the cloak is mostly close to the ideal case, as shown in Fig. 3-2(b). Therefore, we can conclude that the bistatic scattering performance of the cloak is more sensitive to $\eta_t = \sqrt{\mu_t/\epsilon_t}$ than $n_t = \sqrt{\mu_t \epsilon_t}$. However, it should be noted that from Eqs. (2.12, 2.13, 3.1) the cloak in case II is still invisible with monostatic detection since the matched impedance results in a zero backscattering.

It is important to note that all the above analysis are valid independent of the material parameters of the hidden object. Even when the material parameters of the cloak are imperfect, the incident fields still cannot penetrate into the hidden object, and the scattered power is totally introduced by the cloak itself. This unusual phenomenon is based on the assumption that the material parameters of the cloak in the radial and transverse axis always have the same form of $\kappa_r = \kappa_t \frac{(r - R_1)^2}{r^2}$, where κ represents μ or ϵ. Hence, Eqs. (2.5, 2.10, 2.11) always hold, leading to $f_n^{(N)} = 0$ and $f_n^{(M)} = 0$, and the material parameters in the hidden object give no contribution to the outside field. If some perturbations are introduced in the relationship of the radial and transverse material parameters, the solution of Eqs. (2.4) should be revisited, and the interaction of the outside field with the hidden object cannot be

71
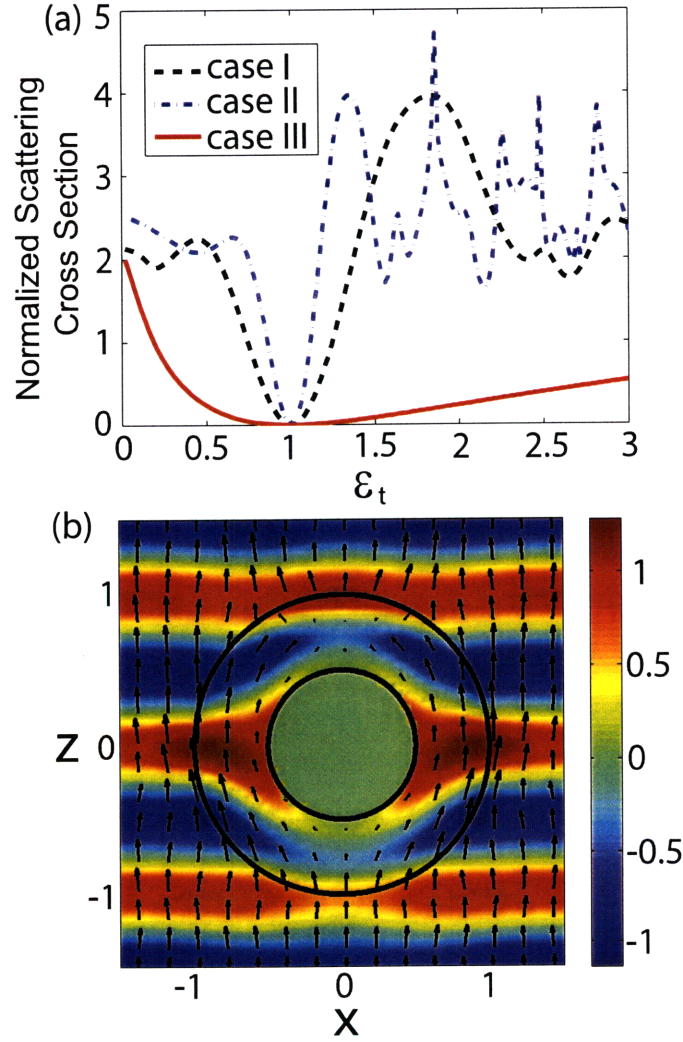
Figure 3-2: (a) Normalized scattering cross section Q_{scat} [1] of a cloak as functions of ϵ_t for three different cases: (Case I) keep $\mu_t = \mu_0 \frac{R_2}{R_2-R_1}$ constant; (Case II) keep $\eta_t = \eta_0$ constant; and (Case III) keep $n_t = \frac{R_2}{R_2-R_1}$ constant. (b) E_x field distribution and Poynting vectors for Case III with $\epsilon_t = 2\epsilon_0 \frac{R_2}{R_2-R_1}$ and $\mu_t = \frac{1}{2}\mu_0 \frac{R_2}{R_2-R_1}$.

omitted.

3.1.2 Cylindrical cloak with perturbed constitutive parameters

For a cylindrical cloak, though the geometry is relatively simpler, the condition for perfect invisibility is still difficult to be realized. Here we apply the same procedure as that in last section to a cylindrical cloak.

By taking the far-field approximation, we can get the far-field scattering information from a cylindrical cloak with some loss or mismatch. The scattering cross section (normalized by the geometrical cross section $2R_2$) Q_{scat} can be derived correspondingly as follows,

$$
Q_{scat} = \frac{2\omega\eta_o \sin\theta_i}{(E_{vi}^2 + E_{hi}^2)R_2}
$$
$$
\cdot \left\{ \frac{1}{\epsilon_0} \sum_{n=-\infty}^{\infty} |a_n^{(N)}|^2 + \frac{1}{\mu_0} \sum_{n=-\infty}^{\infty} |a_n^{(M)}|^2 \right\} \tag{3.2}
$$

Where $a_n^{(M)}$ and $a_n^{(N)}$ are the scattering coefficients for TM and TE waves respectively. The differential scattering efficiency in each unit radian angle can also be derived as follows,

$$
Q_{scat}/\text{angle} = \frac{\omega\eta_0 \sin\theta_i}{(E_{vi}^2 + E_{hi}^2)R_2\pi}
$$
$$
\cdot \left\{ \frac{1}{\epsilon_0} | \sum_{n=-\infty}^{\infty} a_n^{(N)} e^{in\phi}(-i)^n|^2 + \frac{1}{\mu_0} | \sum_{n=-\infty}^{\infty} a_n^{(M)} e^{in\phi}(-i)^n|^2 \right\} \tag{3.3}
$$

We introduce a loss tangent for each component of the constitutive parameters of an ideal cylindrical cloak, similar to the case we studied in last section. Figure 3-3 plots the differential normalized scattering cross sections as a function of the scattering angle in the xy plane for loss tangents of $0.001, 0.01, 0.1$ and 1 respectively, due to a 2 GHz vertically polarized and normally incident wave. The size of the cloak is the same as that in Sec. 2.1.2. Generally, with the increase of loss, the scattering increases. However, the backward scattering is no longer zero, which is different with the spherical cloak with the same losses. It is worth noting that the scattering angle at which the minimum scattering occurs is 180°,

73
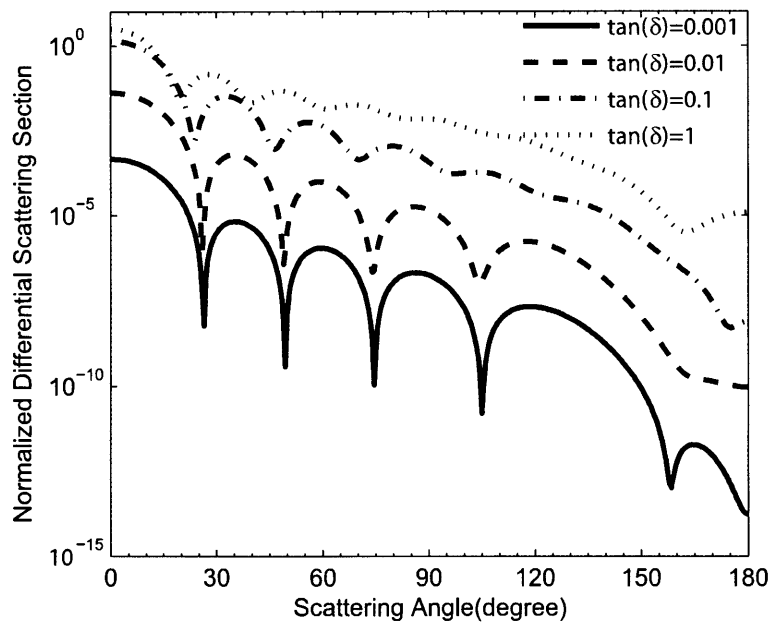
Figure 3-3: The scattering pattern in the xy plane due to a vertically polarized and normally incident wave with different loss tangents for each component of the constitutive parameters. The size of the cloak is the same as that in Fig. 2-5 and Fig. 2-6.

i.e. the backward direction, only when the loss tangent is small. With the increase of the loss tangent, this angle decreases, meaning the backward direction is no longer where the minimum scattering occurs.

Another issue is how the mismatches of the constitutive parameters affect the cloak performance. We find that a slight mismatch of constitutive parameters while keeping the refractive index constant can still provide a good performance of a cylindrical cloak. This property is very similar with the spherical cloak as shown in last section.

3.2 Dispersion effect on invisibility cloaks

All materials in nature are intrinsically dispersive, i.e. the constitutive parameters are functions of frequency. For metamaterials, which are the building blocks for invisibility cloaks, the dispersion is even more significant since a typical metamaterial works by constructing a local resonance to tune its electric and magnetic responses [53, 54]. Here we use a spherical cloak as an example and focus on the effect of dispersion.

In an ideal spherical cloak, the radial constitutive parameters ϵ_r and μ_r are required to vanish at the inner boundary [2] at the single frequency which can be named as the "cloaking frequency". Since any physical wave has nonzero bandwidth, the transition of ϵ_r and μ_r from positive to negative will be formed within the cloak at frequencies entirely below or above the cloaking frequency because of dispersions which usually possess the forms of Drude and Lorentz types for most metamaterials. Similar positive-to-negative transition of constitutive parameters has been shown to cause some peculiar phenomena such as negative refraction [54] and superlens [55]. Resonances caused by surface polaritons between positive and negative index media has also been shown to produce strong anomalous scattering [56]. Therefore, it is necessary to analyze the influence of this transition of constitutive parameters on the performance of the cloak.

3.2.1 Multi-layer algorithm applicable to a dispersive cloak

The configuration of a 3D spherical cloak with inner radius R_1 and outer radius R_2 follows that in Fig. 2-1. The cloak shell within $R_1 < r < R_2$ is a radially uniaxial and inhomoge-

neous medium with permittivity tensor $\bar{\bar{\epsilon}} = \epsilon_r(r)\hat{r}\hat{r} + \epsilon_t\hat{\theta}\hat{\theta} + \epsilon_t\hat{\phi}\hat{\phi}$ and permeability tensor $\bar{\bar{\mu}} = \mu_r(r)\hat{r}\hat{r} + \mu_t\hat{\theta}\hat{\theta} + \mu_t\hat{\phi}\hat{\phi}$. An E_x polarized plane wave, $\overline{E}_\imath = \hat{x}e^{ik_0 z}$, is incident upon the cloak. The electromagnetic wave in the cloak shell can be decomposed into TM and TE modes with respect to $\hat{r}$ [41], corresponding to scalar potentials Ψ_{TM} and Ψ_{TE}. Since TM and TE modes have similar derivations, we focus on the former. The r dependent function $f(r)$ of Ψ_{TM} satisfies Eq. (3.4) (i.e. Eq. (2.4) in Section 2.1.1), where $k_t^2 = \omega^2 \epsilon_t \mu_t$.

$$\left\{ \frac{\partial^2}{\partial r^2} + \left[k_t^2 - (\epsilon_t/\epsilon_r)\frac{n(n+1)}{r^2} \right] \right\} f(r) = 0. \tag{3.4}$$

By utilizing the relation between constitutive parameters specified in [2] at the cloaking frequency, i.e. $\epsilon_r = \epsilon_t \frac{(r-R_1)^2}{r^2}$, $f(r)$ can be converted to the Riccati-Bessel function [22]. However, ϵ_t/ϵ_r is a function of frequency and position, which makes this specified relation no longer hold at a deviated frequency.

In order to solve this difficulty, we shall revisit Eq. (3.4). Since ϵ_r does not vary much with variation of r, we can divide the cloak shell in $R_1 < r < R_2$ into a lot of thin layers, which is similar to the recipe applied in practice [6]. Then both ϵ_r and ϵ_t in each layer of $R^{(j)} < r < R^{(j+1)}$ can be treated as constants, such that Eq. (3.4) has solutions

$$f(r) = a_{jn}\psi_\nu(k_t r) + a_{jn}\tilde{R}_{jn}^{TM}\zeta_\nu(k_t r), \quad j = 1, 2, \cdots N \tag{3.5}$$

where ψ_ν and ζ_ν are Riccati-Bessel functions of the first and the third kind, respectively, with a complex order $\nu = \sqrt{\frac{\epsilon_t}{\epsilon_r}n(n+1) + \frac{1}{4}} - \frac{1}{2}$, and $\tilde{R}_{jn}^{TM}$ is defined as the general reflection coefficient of nth order in the jth layer. The field solution in each layer can then be expressed with different coefficients a_{jn} and $\tilde{R}_{jn}^{TM}$ as unknowns. By matching the boundary conditions between adjacent layers, we first calculate the reflection and transmission coefficients due to a single reflection and transmission across the interface between adjacent

76

layers numbered j and $j-1$ as follows,

$$R_{j,j-1}^{TM} = \frac{\begin{aligned}&\frac{\mu_{t,j-1}}{\mu_{t,j}}\psi_{\nu,j}(k_{t,j}R^{(j-1)})\psi_{\nu,j-1}{}'(k_{t,j-1}R^{(j-1)})\\&-\sqrt{\frac{\mu_{t,j-1}\epsilon_{t,j-1}}{\mu_{t,j}\epsilon_{t,j}}}\psi_{\nu,j-1}(k_{t,j-1}R^{(j-1)})\psi_{\nu,j}{}'(k_{t,j}R^{(j-1)})\end{aligned}}{\begin{aligned}&\sqrt{\frac{\mu_{t,j-1}\epsilon_{t,j-1}}{\mu_{t,j}\epsilon_{t,j}}}\psi_{\nu,j-1}(k_{t,j-1}R^{(j-1)})\zeta_{\nu,j}{}'(k_{t,j}R^{(j-1)})\\&-\frac{\mu_{t,j-1}}{\mu_{t,j}}\zeta_{\nu,j}(k_{t,j}R^{(j-1)})\psi_{\nu,j-1}{}'(k_{t,j-1}R^{(j-1)})\end{aligned}} \tag{3.6}$$

$$R_{j-1,j}^{TM} = \frac{\begin{aligned}&\sqrt{\frac{\mu_{t,j}\epsilon_{t,j}}{\mu_{t,j-1}\epsilon_{t,j-1}}}\zeta_{\nu,j}(k_{t,j}R^{(j-1)})\zeta_{\nu,j-1}{}'(k_{t,j-1}R^{(j-1)})\\&-\frac{\mu_{t,j}}{\mu_{t,j-1}}\zeta_{\nu,j-1}(k_{t,j-1}R^{(j-1)})\zeta_{\nu,j}{}'(k_{t,j}R^{(j-1)})\end{aligned}}{\begin{aligned}&\frac{\mu_{t,j}}{\mu_{t,j-1}}\psi_{\nu,j-1}(k_{t,j-1}R^{(j-1)})\zeta_{\nu,j}{}'(k_{t,j}R^{(j-1)})\\&-\sqrt{\frac{\mu_{t,j}\epsilon_{t,j}}{\mu_{t,j-1}\epsilon_{t,j-1}}}\zeta_{\nu,j}(k_{t,j}R^{(j-1)})\psi_{\nu,j-1}{}'(k_{t,j-1}R^{(j-1)})\end{aligned}} \tag{3.7}$$

$$T_{j,j-1}^{TM} = \frac{i}{\begin{aligned}&\frac{\mu_{t,j}}{\mu_{t,j-1}}\psi_{\nu,j-1}(k_{t,j-1}R^{(j-1)})\zeta_{\nu,j}{}'(k_{t,j}R^{(j-1)})\\&-\sqrt{\frac{\mu_{t,j}\epsilon_{t,j}}{\mu_{t,j-1}\epsilon_{t,j-1}}}\zeta_{\nu,j}(k_{t,j}R^{(j-1)})\psi_{\nu,j-1}{}'(k_{t,j-1}R^{(j-1)})\end{aligned}} \tag{3.8}$$

$$T_{j-1,j}^{TM} = \frac{i}{\begin{aligned}&\sqrt{\frac{\mu_{t,j-1}\epsilon_{t,j-1}}{\mu_{t,j}\epsilon_{t,j}}}\psi_{\nu,j-1}(k_{t,j-1}R^{(j-1)})\zeta_{\nu,j}{}'(k_{t,j}R^{(j-1)})\\&-\frac{\mu_{t,j-1}}{\mu_{t,j}}\zeta_{\nu,j}(k_{t,j}R^{(j-1)})\psi_{\nu,j-1}{}'(k_{t,j-1}R^{(j-1)})\end{aligned}} \tag{3.9}$$

After obtaining these single reflection and transmission coefficients, we can easily get the general reflection coefficients by

$$\tilde{R}_{jn}^{TM} = R_{j,j-1}^{TM} + \frac{T_{j-1,j}^{TM}\tilde{R}_{j-1,j-2}^{TM}T_{j,j-1}^{TM}}{1 - R_{j-1,j}^{TM}\tilde{R}_{j-1,j-2}^{TM}} \tag{3.10}$$

Moreover,

$$a_{jn} = \frac{T_{j+1,j}}{1 - R_{j,j+1}\tilde{R}_{j,j-1}}a_{j+1,n} \tag{3.11}$$

The coefficients for TE waves can be treated as a dual case and obtained similarly. There-

77

fore, all the fields over the whole space can be determined in a straightforward manner.

To validate this algorithm, we study the dependence of normalized scattering cross section (normalized to πR_2^2) on the number of layers. The parameters at each layer's center are set to match those proposed in Ref. [2] and $R_2 = 2R_1 = 1.5\lambda_0$ at the cloaking frequency of 10 GHz, where $\lambda_0 = 3$cm. The concealed region $r < R_1$ is specified to be a PEC. It can be found that as the number of layers increases, the scattering cross section drops rapidly. When the number of layers reaches 100, the normalized scattering cross section reaches 10^{-7}, which is close to "perfect invisibility".

3.2.2 Distributed penetration depth and blue-shift effect

Since each layer's parameters can be specified arbitrarily, we are able to deal with more complicated situations including cases with anisotropic loss and dispersion. Since ϵ_t and μ_t are larger than 1 and do not vary within the whole cloak shell, they can be treated as constants over the frequency band of interest. The radial constitutive parameters ϵ_r and μ_r can be thought of as being achieved by embedding radially uniaxial metamaterials in a background with ϵ_t and μ_t. Subsequently, Drude model [57] and Lorentz model [58] are applied to ϵ_r and μ_r, respectively, as follows:

$$\epsilon_r = \epsilon_t\left(1 - \frac{f_p^2}{f(f + i\gamma_1)}\right) \tag{3.12}$$

$$\mu_r = \mu_t\left(1 - \frac{F}{1 + i\gamma_2/f - f_0^2/f^2}\right) \tag{3.13}$$

For simplicity, we set $\gamma_1 = \gamma_2 = \gamma$ and $F = 0.78$. Forcing the real parts of parameters at the center of each layer to match the relation proposed in Ref. [2] at the cloaking frequency, the corresponding f_p and f_0 for each layer can be calculated as well as subsequent ϵ_r and μ_r at other frequencies.

Now we first consider the case where $\gamma \neq 0$. Then ϵ_r in Eq. (3.4) is always nonzero. Figure 3-4 shows the normalized scattering cross section spectrum of a dispersive cloak with different losses where the number of layers is set as $N = 100$. By decreasing γ, the curve of normalized scattering cross section is convergent. It can be seen that though
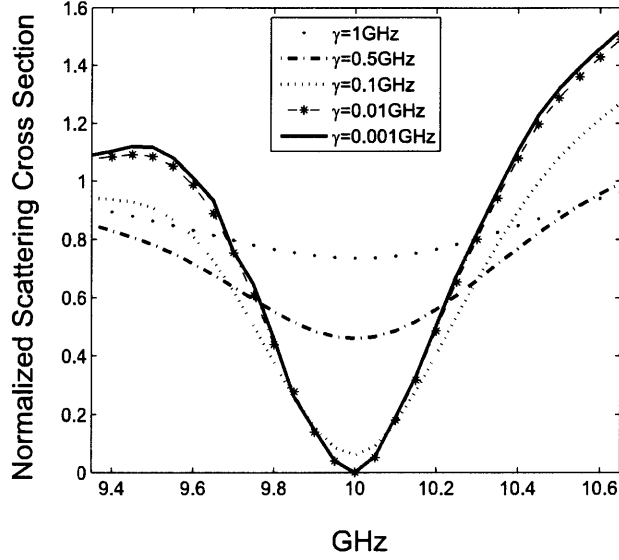
Figure 3-4: Dependence of scattering cross section (normalized to πR_2^2) on different frequencies and losses. $R_2 = 2R_1 = 1.5\lambda_0$. $\lambda_0 = 3$cm. In the concealed region $r < R_1$ is PEC.

invisibility is sensitive to frequency deviation, extremely low normalized scattering cross section can still be obtained within a small finite bandwidth around the cloaking frequency. This result excludes the possibility of some kind of large anomalous scattering [56] in the vicinity of the cloaking frequency. Moreover, the working bandwidth of the cloak depends on the sensitivity of the detector outside. For example, if we set 0.04 as the upper limit of the undetectable normalized scattering cross section, then the working bandwidth of the cloak is about 100 MHz around the cloaking frequency of 10 GHz. An arbitrary nonzero scattering cross section limit can always be satisfied by narrowing the bandwidth.

Next we consider the other case where $\gamma = 0$. What is different in this case is that, if the frequency is below the cloaking frequency, then the normal dispersion requires that ϵ_r (or μ_r if TE waves are considered) close to the inner boundary be negative and Eq. (3.4) has a singularity at the position where ϵ_r is zero. This singularity will form an impenetrable wall for TM waves as we will demonstrate in the following. Similarly, another singularity caused by μ_r of zero value will form a wall for TE waves. Figure 3-5(a) shows the distribution of E_x in xz plane when a E_x polarized incident plane wave ($\overline{E_i} = \hat{x}e^{ik_1z}$) is passing

79

through the cloak along z direction. For the sake of illustration, we choose the frequency deviation to be -532 MHz and $\gamma = 0.0001\text{GHz}$. Since most contribution of E_x field in xz plane except near the z axis comes from TM waves, it can be seen that the TM field is expelled by a very thin "wall" within the shell which little TM field can penetrate. The position of this "wall" coincides with the position where ϵ_r is zero. In yz plane which is not shown in this letter, we can see a similar "wall" for H_y field except with a different location because μ_r has different dispersion and thus different location of zero value. The influence of loss on the field distribution is shown in Fig. 3-5(b) where the amplitude of E_x field along the direction $(\theta = 2\pi/3, \phi = 0)$ where TM field is dominant is plotted. It can be seen that with decreasing γ, the field outside of the "wall" $(r > R_w^{TM})$ is almost unchanged and the field inside of the "wall" $(r < R_w^{TM})$ is decreasing fast while the "wall" at $r = R_w^{TM}$ becomes thinner and sharper. Further decreasing of γ requires increasing the number of layers N which is not shown in Fig. 3-5. In the limit of $\gamma \to 0$, the field at $r = R_w^{TM}$ (or $r = R_w^{TE}$ for TE waves) will diverge and all TM fields will be blocked for $r > R_w^{TM}$ while for TE fields, for $r > R_w^{TE}$. Similar "wall" effects have been found to prevent waves excited by an active device inside the concealed region from going out at the cloaking frequency, as we have seen in Section 2.2. But here this effect is induced by the incoming wave directly when the frequency is deviated from the cloaking frequency. A more rigorous argument can be made as follows. Following the derivation in Section 2.2, suppose a layer within the cloak shell has ϵ_r and thickness d, then it can be found that in the limit of $\epsilon_r \to 0$, the TM field inside this layer as well as all the space it encloses decreases to zero while the TM field on the surface of the layer diverges, no matter how small d is. Since this "wall" for TM waves requires the tangential H field to vanish, it can be treated as a PMC wall. Similarly, another wall expelling TE waves is a PEC wall.

This peculiar "wall" effect will form a rainbow-like field distribution inside the cloak since different frequency components penetrate into different depths from $r = R_2$ to $r = R_1$, as shown in Fig. 3-6 where six frequencies are considered. Such a frequency selection challenges a basic concept in optics, group velocity. The group velocity at the inner boundary of the cloak has been calculated from the point of view of geometrical optics to study causality of the cloak [20, 21]. However, what really happens at the inner
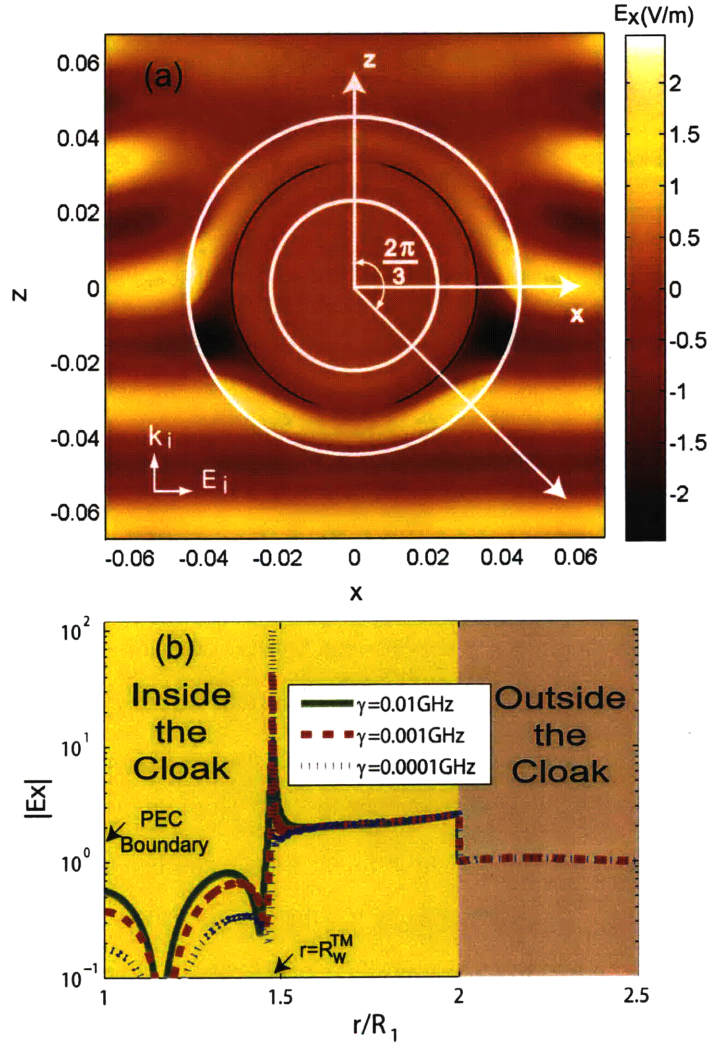
Figure 3-5: Field distribution of (a) E_x in xz plane and (b) $|E_x|$ along the direction ($\theta = 2\pi/3, \phi = 0$) when a x-polarized incident plane wave with frequency 9.468 GHz is passing through the cloak along z direction. The size of the cloak is the same as Fig. 3-4. The number of layers N=300.
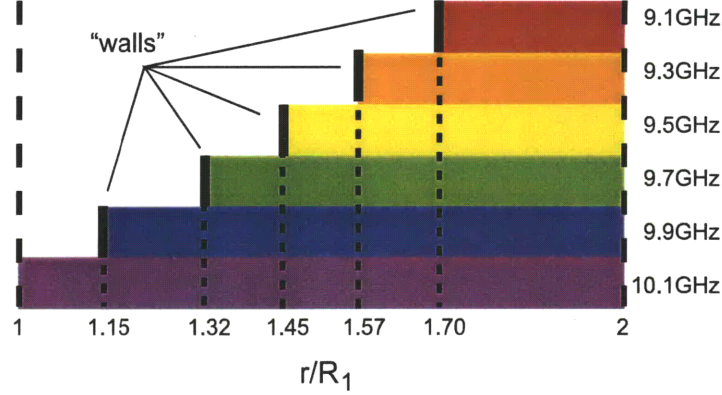
Figure 3-6: Fields of different frequencies have different depths of penetration within the cloak. Here only TM fields are considered. All other parameters follow Fig. 3-5.

boundary should be based on the field solution directly. As we all know, the group velocity at the cloaking frequency of f_c represents the speed of the envelop formed by two close frequency components $f_c - \delta f$ and $f_c + \delta f$. For the wave with frequency $f_c + \delta f$, it is able to reach the inner boundary $r = R_1$. But for the wave with frequency $f_c - \delta f$, as we have shown, will be stopped somewhere in-between by the PMC and PEC walls and thus never reach the inner boundary $r = R_1$. Therefore the group velocity at $r = R_1$ is meaningful only for the frequencies above the cloaking frequency, i.e. $f > f_c$. As a result, the group velocity at $r = R_1$ at the cloaking frequency loses its physical meaning.

The different responses of cloak to different frequencies can lead to another interesting phenomenon. At the cloaking frequency f_c, the strictly monochromatic wave will pass through the cloak without any distortion [2, 17, 22]. So an observer looking at an object emitting or reflecting this monochromatic wave behind the cloak will see exactly the same object as if there is no block in front of it. But is this true for a more physical quasi-monochromatic wave possessing a narrow band? For the wave with frequency slightly deviated above at $f_c + \delta f$, the most part of the cloak shell does not change much except the part close to the inner boundary $r = R_1$. Thus only a narrow spectrum of wave can reach the PEC core within $r < R_1$. From the view of the observer outside, the scattering looks as if it is from a very small PEC particle, i.e. Rayleigh scattering occurs in this case [20]. For a very small PEC particle with $kR \ll 1$, the first order scattering coefficients

82
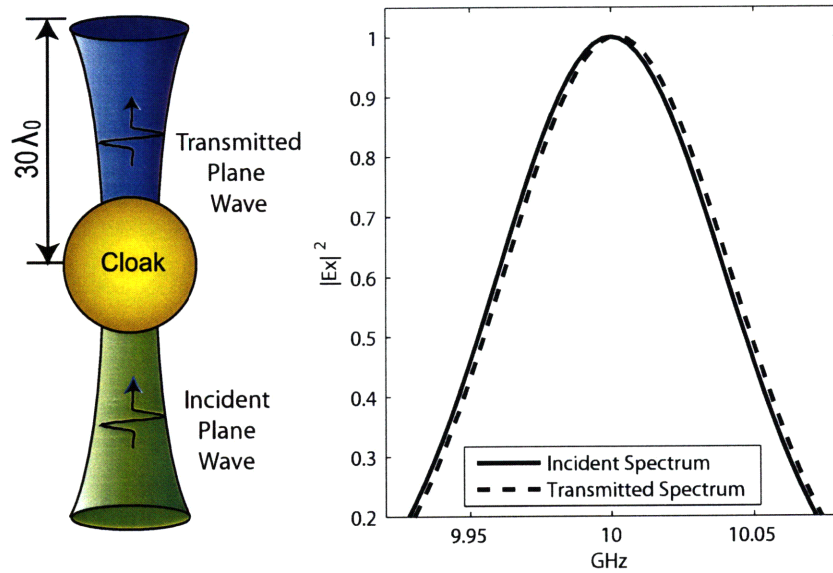
Figure 3-7: The frequency center of a quasi-monochromatic incident plane wave is blue-shifted in the forward direction after passing through the cloak. The dimension of the cloak follows Fig. 3-4. The transmitted wave is measured at the location $30\lambda_0$ apart from the cloak.

R_{01}^{TM} and R_{01}^{TE} becomes dominant [16], where $R_{01}^{TM} = -\psi'(kR)/\zeta'(kR) \approx 2i/3(kR)^3$ and $R_{01}^{TE} = -\psi(kR)/\zeta(kR) \approx -i/3(kR)^3$. The phase of scattering wave in the forward direction ($\theta = 0$) depends on the phase of $-i\sum(R_{0n}^{TM} + R_{0n}^{TE})$ [1] which in this case is $-i(R_{01}^{TM} + R_{01}^{TE}) \approx +1/3(kR)^3$. The positive sign indicates that the forward scattering field will constructively interfere with the original incident field. Thus the wave after passing the cloak will be reinforced. But for the incident wave with frequency slightly deviated below at $f_c - \delta f$, the observer outside will regard the scattering of TM waves as if it is from a PMC particle and the scattering of TE waves as if it is from a PEC particle because of the PMC and PEC walls close to the inner boundary. Thus in this case $R_{01}^{TM} = R_{01}^{TE} = -\psi(kR)/\zeta(kR) \approx -i/3(kR)^3$, which gives $-i(R_{01}^{TM} + R_{01}^{TE})$, a negative value. Thus the field after the wave passes the cloak will be decreased. After noting these differences, we can study the behavior of this quasi-monochromatic wave passing through the cloak. Since the frequency components $f > f_c$ are reinforced while the other frequency components $f < f_c$ are weakened, the frequency center of this incident wave will be blue-shifted after passing the cloak in the forward direction, i.e., shifted toward a higher frequency. Thus the observer looking at the object emitting or reflecting this quasi-monochromatic wave behind the cloak will see a blue-shifted wave. Figure 3-7 plots this shift effect for a quasi-monochromatic incident plane wave with Gaussian distribution in frequency spectrum with mean of 10 GHz and variation of 50^2 MHz^2. The transmitted wave is measured at the location $30\lambda_0$ apart from the cloak. It should be noted that this blue-shift is caused by the shift of frequency center of the narrow band wave, which does not mean any change of frequency itself. Furthermore, this blue-shift effect does not depend on the size of the cloak, but the normal dispersions of radial constitutive parameters. For anomalous dispersions which rarely occur, a red-shift effect will arise.

3.2.3   Signal transport and time-delay

How a light signal propagates through a physical dispersive invisibility cloak is one of the fundamental problems in studying transformation-based invisibility cloaking. Here, we present a full-wave method on the transmission of a Gaussian pulse through a spherical

invisibility cloak with causal dispersions. This study helps to provide a complete picture of energy propagation through an invisibility cloak.

To study the light signal propagation through a physical dispersive cloak, we consider several key quantities: group velocity, energy transport velocity, time-delay, and distortion of energy distribution. Previous single frequency analyses [2, 3, 6, 13, 17, 22, 23, 27, 42, 59, 60] did not provide results of the group velocity and the energy transport velocity. Some studied the group velocity and the energy transport velocity inside a cloak from the view of ray theory [20, 21]. Ray theory gives good demonstrations for a dispersionless case, because it can show the paths of rays inside the cloak. However, when it is applied to a dispersive cloak, the analysis in Ref. [20] raised the issue that such a cloak may violate causality, since the group velocity at the inner boundary diverges. In addition, Ref. [21] stated that a ray would take nearly infinite time to reach from one side of the cloak to another side if it points at the origin of the cloak, since the energy transport velocity approaches zero at the inner boundary. Furthermore, the ray theory approach applied in previous studies did not address the issues of scattering and distortion of energy distribution during the process of energy transport. Time-domain simulation [61] does produce some useful results, but is not able to provide as much insight into the physics to answer these questions as an analytical approach does. These problems must be carefully examined before we get a clear picture of energy propagation through a dispersive invisibility cloak.

We study these problems by using a real signal (a Gaussian pulse) together with full-wave analysis. The instantaneous field and Poynting vector at each point in space and time can be calculated, from which we show that inside the cloak, the local group velocity and the energy transport velocity may no longer be clearly defined due to the serious local distortion of the signal. However, if the bandwidth is sufficiently narrow, we can still define the time-delay of the signal on a target plane behind the cloak, and examine the spatial distortion of the transmitted pulse/energy.

Figure 3-8 shows an isolated signal carried with carrier-frequency f_0 (with period T_0 and wavelength λ_0) and characterized by a Gaussian envelope $C(t) = e^{-t^2/2\sigma^2}$. Thus the complete signal of this Gaussian pulse sent at the input plane at $z = -d_1$ is $\overline{E}(t, -d_1) = \hat{x}C(t)\cos(2\pi f_0 t)$. This $\hat{x}$-polarized Gaussian pulse is incident along $\hat{z}$ direction onto a
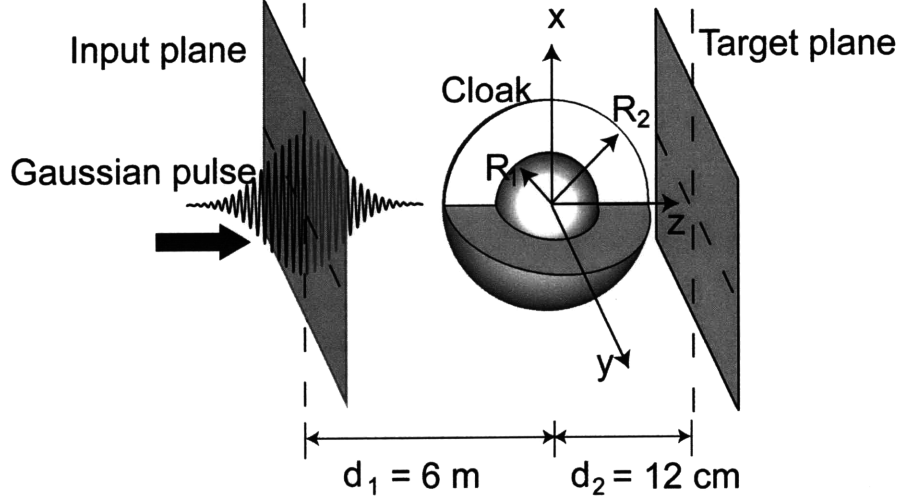
Figure 3-8: Propagation of an isolated narrow-band Gaussian pulse through a frequency-dispersive spherical invisibility cloak with a target plane set up at $z = 12$ cm. The pulse peak is at $z = -6$ m when $t = 0$. $R_2 = 2R_1 = 9$ cm.

dispersive spherical cloak that is designed to conceal arbitrary objects perfectly only at the carrier-frequency f_0 [2]. The cloak layer within $R_1 < r < R_2$ is an anisotropic and inhomogeneous medium with permittivity tensor $\bar{\bar{\epsilon}} = \epsilon_r \hat{r}\hat{r} + \epsilon_t \hat{\theta}\hat{\theta} + \epsilon_t \hat{\phi}\hat{\phi}$ and permeability tensor $\bar{\bar{\mu}} = \mu_r \hat{r}\hat{r} + \mu_t \hat{\theta}\hat{\theta} + \mu_t \hat{\phi}\hat{\phi}$. It is chosen such that at f_0, $\epsilon_t/\epsilon_0 = \mu_t/\mu_0 = R_2/(R_2 - R_1)$ and $\epsilon_r/\epsilon_t = \mu_r/\mu_t = (r - R_1)^2/r^2$ [2]. We adopt the same dispersion types as in Section 3.2.2, i.e.

$$\epsilon_r = \epsilon_t(1 - \frac{f_p^2}{f(f + i\gamma_1)}) \tag{3.14}$$

$$\mu_r = \mu_t(1 - \frac{F}{1 + i\gamma_2/f - f_0^2/f^2}) \tag{3.15}$$

where ϵ_t and μ_t are assumed to be constants over the frequency range of interest, f_p and f_0 are parameters for Drude model and Lorentz model respectively, $F = 0.78$, and γ_1 and γ_2 are set to be zero. The background is free space. We set a target plane at $z = d_2$. The signal propagation through each point in this target plane is monitored.

86

The original Gaussian pulse can be expressed by a Fourier integral as follows

$$\overline{E}_{inc}(\overline{r}, t) = \hat{x}\Re \left\{ \int_0^\infty E_{inc}(\omega)e^{ik(z+d_1)-i\omega t} d\omega \right\} \tag{3.16}$$

where $\Re$ means taking the real part, $E_{inc}(\omega)$ is the Fourier transform of $E(t, -d_1)$ and $k = \omega\sqrt{\mu_0\epsilon_0}$. To facilitate calculation, we truncate the original signal from $-T$ to T and let it be periodic with a period of $2T$. A very large period of $2T$ will not affect our treatment of a single Gaussian pulse significantly. The Fourier integral can then be written as a Fourier series

$$\overline{E}_{inc}(\overline{r}, t) = \hat{x}\Re \left\{ \sum_{n=0}^\infty E_n e^{ink_0(z+d_1)-in\omega_0 t} \right\} \tag{3.17}$$

where E_n is the coefficient of the nth order item, $\omega_0 = \pi/T$ and $k_0 = \omega_0\sqrt{\mu_0\epsilon_0}$. Due to the narrow band property of the original signal, we can discard the items in the Fourier series except those from $n = N_1$ to $n = N_2$ with frequencies close to f_0. Thus the total electrical field in presence of the dispersive spherical cloak can be expressed as

$$\overline{E}(\overline{r}, t) = \Re \left\{ \sum_{n=N_1}^{N_2} \left[\hat{x}E_n e^{ink_0(z+d_1)} + \overline{E}_{scat}(\overline{r}) \right] e^{-in\omega_0 t} \right\} \tag{3.18}$$

where $\overline{E}_{scat}$ is the scattering field for nth order item with frequency $n\omega_0$, which can be solved by using a multi-layer algorithm as we have shown in Section 3.2.2. After obtaining $\overline{E}(\overline{r}, t)$ in time-domain, we are able to predict the signal or the energy propagation.

As a concrete example, an input Gaussian pulse is modulated at $f_0 = 10\,\text{GHz}$ with $\sigma = 20T_0 = 2\,\text{ns}$. We truncate this signal from $-20\,\text{ns}$ to $= 20\,\text{ns}$ ($T = 20\,\text{ns}$). Then the frequency spectrum is discretized by the sampling gap $\delta f = 25\,\text{MHz}$. We choose the time-harmonic plane wave items covering the range from $10\,\text{GHz} - 375\,\text{MHz}$ to $10\,\text{GHz} + 375\,\text{MHz}$. In other words, we reconstruct the original Gaussian pulse by using 31 time-harmonic plane waves with different frequencies. Amplitude of each plane wave can be determined with straightforward calculation. The outer radius of the spherical cloak R_2 is 9 cm ($3\lambda_0$) and the inner radius R_1 is 4.5 cm ($1.5\lambda_0$). Region $r < R_1$ is PEC. In the multi-layer algorithm, the number of layers N is set to be 200. We set $d_1 = 200\lambda_0 = 6\,\text{m}$
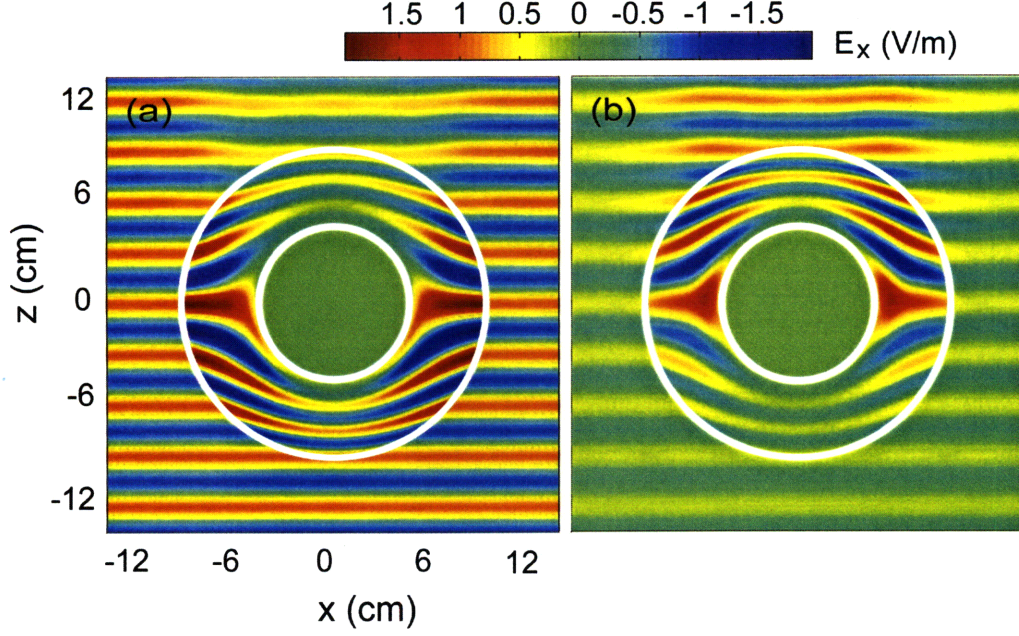
Figure 3-9: E_x field distribution when the Gaussian pulse is passing through the dispersive spherical cloak at (a) $t = 20\,\text{ns}$ and (b) $t = 23\,\text{ns}$.

and $d_2 = 4\lambda_0 = 12\,\text{cm}$.

To be consistent with Ref. [62] about the definition of the arrival moment as *the exact moment when the main part of the signal arrives*, we first calculate the instantaneous Poynting power transferred through the target plane as

$$S_z(t,x,y,d_2) = \overline{E}(t,x,y,d_2) \times \overline{H}(t,x,y,d_2) \cdot \hat{z} \qquad (3.19)$$

where (x,y,d_2) is a point in the target plane. Then the total accumulated energy that would transport through a given point in the target plane can be calculated as $W = \int_{4T_0}^{4T_0+2T} S_z dt$. In our numerical integration, the integration step length is set as $\delta t = T_0/20 = 0.005\,\text{ns}$. Based on that, we can pick the exact moment when half of the total accumulated energy has been transferred as the arrival moment t_a of the signal reaching the target plane. Time-delay of the signal is defined as $t_a - t_{inc}$, where t_{inc} is the arrival moment of the incident signal in absence of the cloak and the PEC core.

Now let us discuss the results. Figure 3-9(a) and (b) show the E_x field distribution at the

88

moments of $t = 20\,\mathrm{ns}$ and $t = 23\,\mathrm{ns}$, respectively. At $t = 20\,\mathrm{ns}$, the peak of the incident Gaussian pulse is passing the center of the cloak. It is seen that the energy, or the wave envelope, is slowed down inside the cloak. When the pulse is passing by, some energy is stored inside the cloak. After the pulse leaves, the energy is released. It is worth mentioning that during the whole process, the *phase* of the signal exhibits minimal disturbance. The reason is that, although the cloak is created from the coordinate transformation theory, the theory itself does not provide any direct information about the energy propagation but only shows the perfect transmission of the wave's phase through an invisibility cloak. Therefore, the causality of the cloak cannot be judged by analyzing the behavior of an infinitely long sine wave at a single frequency but should be based on tracing the motion of the wave envelope which represents the energy's location. We can see from Fig. 3-9(b) that the transmission of the pulse through the cloak is delayed due to a longer physical distance when compared to a free space case. Vividly, the ray's true path in physical space has been elongated as shown in Refs. [2, 13]. However, is it true that a longer ray path must lead to a larger delay of the wave signal and energy propagation?

Figure 3-10 shows the instantaneous Poynting power S_z at the points (4.5, 0, 12), (2.25, 0, 12) and (0, 0, 12) cm in the target plane compared to the incident signal's instantaneous Poynting power in absence of the cloak and the PEC core. It should be pointed out that the instantaneous Poynting power has fast oscillations inside the modulation envelope. We can see that the signals transported through the cloak have well-defined arrival moments and are indeed delayed when compared to the incident signal. However, it is very interesting to note that the signal coming along the center of the cloak, i.e. passing through $(0, 0, 12)$ cm in the target plane, is faster than signals at some other points. In Fig. 3-11, we plot the time-delay distribution using the previously defined arrival moment in the target plane, and it exhibits a volcano-like shape with a pit at the center. This result is quite counterintuitive, since according to the geometrical description, the rays traveling closest to the z axis should have the longest distance to go. In fact, calculation based on geometric optics shows that the ray pointing at the center of the cloak would take nearly infinite time to reach from one side to the other of the cloak [21]. However, the energy propagation is governed by Maxwell's equations and it may not satisfy the ray approximation. Historically, it has been shown
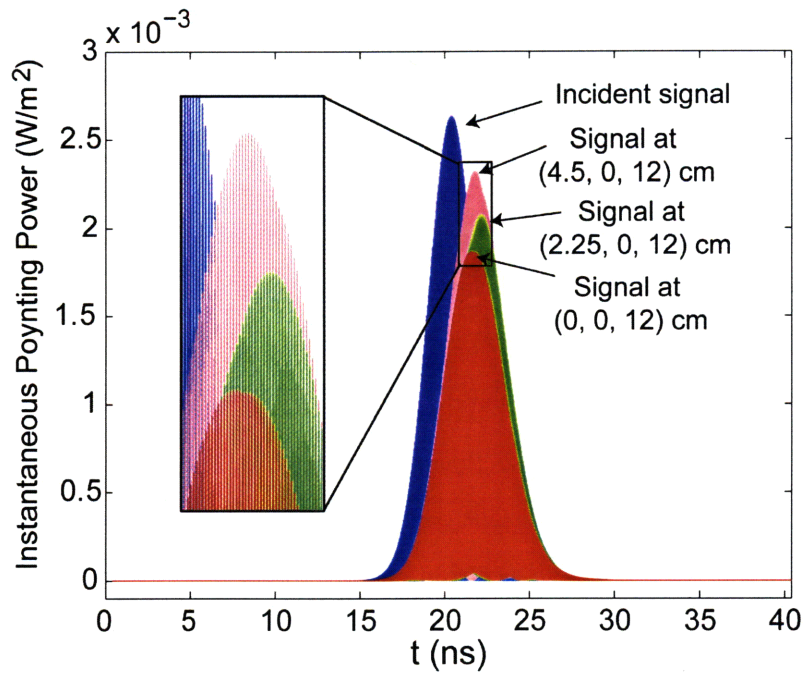
Figure 3-10: Instantaneous Poynting power S_z at $(4.5, 0, 12)$, $(2.25, 0, 12)$ and $(0, 0, 12)$ cm in the target plane compared to the incident signal in absence of the cloak as well as the PEC core.
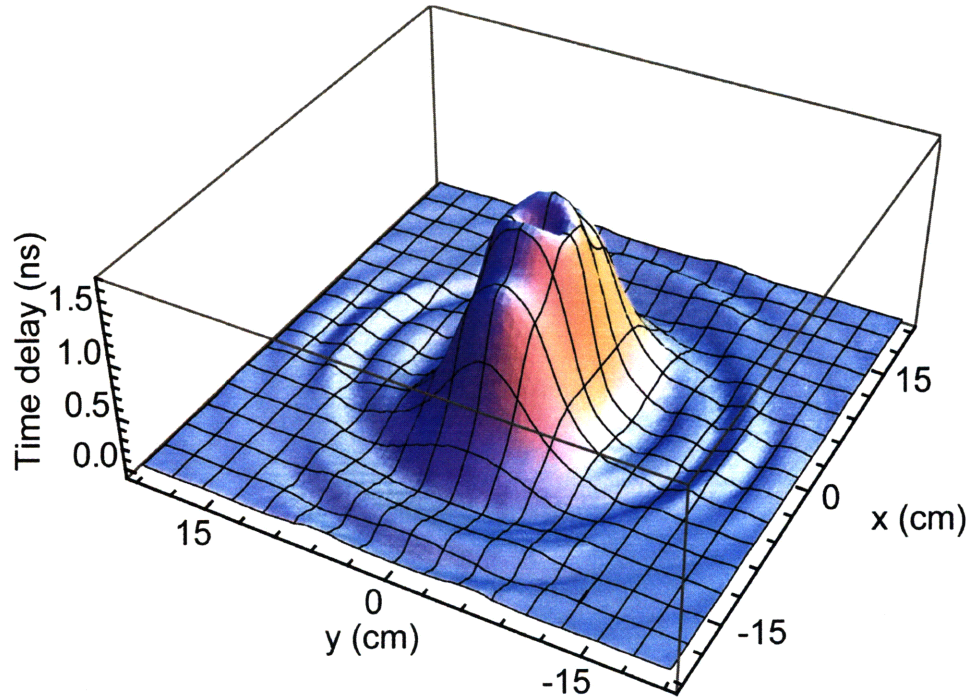
Figure 3-11: Time delay distribution of the signal arrived at the target plane after passing through a dispersive spherical invisibility cloak. Maximum delay is 1.755 ns while the delay at the center is 1.395 ns.

that the geometrical model of energy propagation is inadequate in certain cases, where a well-known example is the Poisson's spot [63]. Similarly, in the case of a dispersive spherical cloak, when the wave energy is approaching the inner boundary of the cloak, it cannot be approximated by a geometrical ray anymore. We have shown in last section that, for the dispersive model we are using, only the frequency components with frequencies above the cloaking frequency can reach the inner boundary, while all the other will be expelled completely. Therefore, no matter how narrow the bandwidth of the signal is, when it approaches the inner boundary, the signal will be seriously distorted and the precise location or arrival moment of the signal or energy is not well-defined in the regions near the inner boundary. Full-wave calculation strictly from Maxwell's equations is necessary in this case. In other words, there is no precise path for the "ray" traveling along the center of the cloak to follow.

Regarding the issue of the group velocity [20] and the energy transport velocity [21], it has been shown that they practically equal to the signal velocity except in anomalous dispersion with high absorption [62]. However, this conclusion has not taken into account the effect of anisotropy. The constitutive parameters ϵ_r and μ_r close to the inner boundary follow normal dispersions around their plasma frequencies. Yet the anisotropy causes the response of the material to be quite different even with an extremely small frequency change: an extremely small frequency change which causes the transition of ϵ_r and μ_r from positive to negative expels fields abruptly. Hence the response is strongly frequency sensitive but the material has normal dispersion. Therefore, besides anomalous dispersion with high absorption [62], in this particular case of a spherical dispersive cloak, the group velocity and the energy transport velocity are no longer equivalent to the signal velocity (the group velocity is infinity close to the inner boundary [20], the energy transport velocity is zero close to the inner boundary [21], while the signal velocity is finite and nonzero [62]). Even when the cloak is embedded in a medium with a large refractive index [2], it does not help to change this nonequivalence. As a result, the strong distortion still cannot be avoided.

In Fig. 3-12, we plot the accumulated energy transmission through each point of the target plane. It can be seen that the energy of the signal after traveling through the cloak is redistributed in the target plane due to diffraction, and the energy transported through the center in the target plane is neither the smallest nor the largest in this particular case. In other words, the cloak illuminated by the Gaussian pulse produces a distorted pattern over the target plane with the center being neither the darkest nor the brightest as shown in Fig. 3-12.

From the viewpoint of the ray model used in Refs. [2, 13, 17, 21], the problem we have is a symmetric one and thus any response of the cloak should be rotationally symmetric with respect to the z axis. However, it is interesting to see from Fig. 3-11 and Fig. 3-12 that neither the time-delay nor the redistributed energy at the target plane is rotationally symmetric. The variation along x axis is different from the variation along y axis. If the polarization of the incident light wave rotates by an angle, the time-delay and the energy redistribution patterns will be rotated by the same angle.
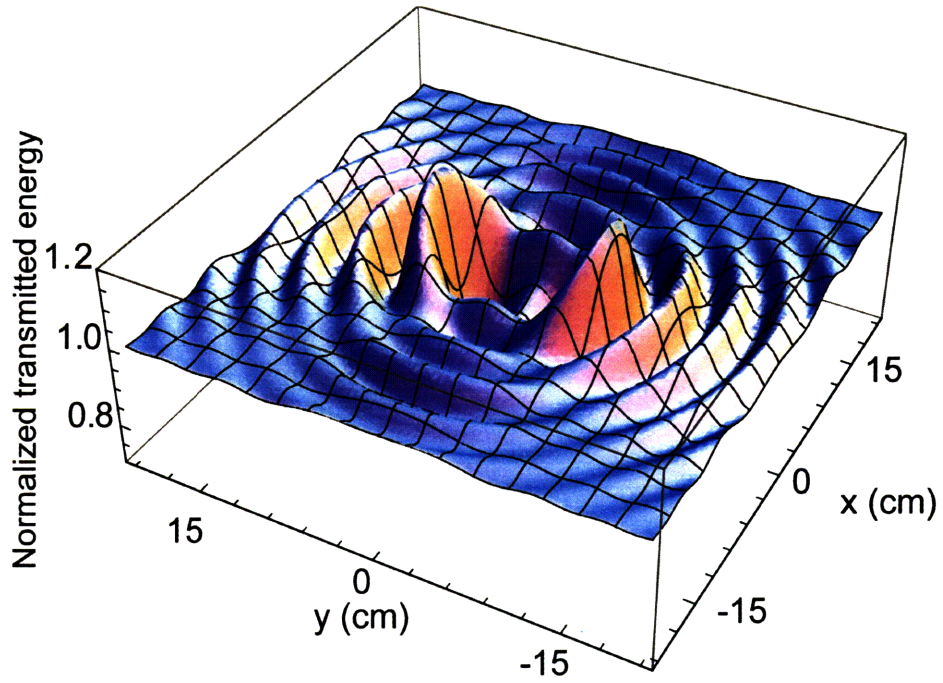
Figure 3-12: Normalized accumulated energy distribution of the signal arrived at the target plane after passing through a dispersive spherical invisibility cloak. The minimum is 0.7638 while it is 0.9075 at the center.

3.3 Summary

In this chapter, we studied more realistic situations of transformation-based invisibility cloaks. Influences from the imperfections due to loss and mismatches are analyzed. Dispersion effect in a spherical cloak is explored in details. The main conclusion are as follow.

- Under certain specific lossy conditions, the spherical cloak is still perfect for a backward scattering detector, while a cylindrical cloak with the same lossy conditions is visible.

- It is shown that electromagnetic waves with different frequencies have different depths of penetration and thus form a rainbow like field distribution inside the cloak whose radial permittivity and permeability are of Drude and Lorentz types. A quasi-monochromatic wave will gain a blue-shift of the frequency center in the forward propagating direction.

- The group velocity and energy transport velocity are not well-defined when the wave is approaching the inner boundary because the wave is seriously distorted. However, when the frequency band is narrow enough, we are still able to define the time-delay of the signal arriving at a target plane behind the cloak. A volcano-shaped spatial time-delay of the transmitted signal is demonstrated in a concrete example.

Chapter 4

Radiation by a Fast-moving Charged Particle through a Perfect Cloak

Physical laws that describe the nature govern the behavior of an object in space and time. For example, two sets of basic physical laws, Newton's laws of motion and Maxwell's equations, are both functions of space and time, while they apply to different physical objects—one is a concrete object with inertia, the other can be an electromagnetic wave, or a photon with zero stationary mass. In general, the space where theses physical laws apply is flat if gravity is ignored. In previous chapters, we have known that analogous to general relativity where time and space are curved, the space for light can also be bent, even in an almost arbitrary way [64]. The possibility of perfect invisibility cloaking [2, 13, 22, 59] was subsequently proposed, where metamaterials that construct the cloak mimic the coordinate transformation, squeezing the originally flat electromagnetic space and forcing light to follow curved trajectories [65]. The act of cloaking is commonly believed to be undetectable simply because the concealed region is not a part of the original electromagnetic space. Recent experimental progresses on cloaking are approaching this destination closer [6, 66]. Though the prediction of perfect invisibility is important, on the other hand, it is of the same importance to find a way to detect a perfect cloak no matter which frequency band it is working in and whether it is broad band or narrow band.

4.1 Motion in two spaces

The theoretical foundation behind transformation optics is the symmetry [67] of Maxwell's equations: the coordinate transformation does not change the form of Maxwell's equations but only change the permittivity and permeability tensors as well as the field values. An invisibility cloak, therefore, is like a "mirror" that images the the originally flat electromagnetic space into the physical space by squeezing the electromagnetic space. Looking at the "mirror" from outside, one can only see the illusion of a flat electromagnetic space. When a photon propagates through the bent electromagnetic space, it actually does not know the bending of the space, since it is completely located inside the electromagnetic space and there is no other reference for it to judge whether the space is bent or not. Therefore this photon will be cheated by the cloak as if it is passing a flat space. However, one should notice that when the space for Maxwell's equations (electromagnetic space) is squeezed, the space for Newton's laws of motion (mechanical space) is still flat. Before the coordinate transformation, they share the same physical space, but after transformation, they are separate. In other words, at the same physical location, a bent electromagnetic space and a flat mechanical space overlap. If one chooses the flat mechanical space as the reference, the bending of electromagnetic space is perceivable. This asymmetry can be utilized to detect a perfect cloak no matter which frequency band it is working in and whether it is broad band or narrow band.

In order to make a judgement whether the electromagnetic space is bent or flat, one must perceive both the electromagnetic space and the mechanical space at the same time, the latter of which will be chosen as the reference. Inside the cloak, all photons or electromagnetic waves propagate in the bent electromagnetic space, while an inertial particle moves in the flat mechanical space. Generally, these two spaces are not connected directly. The only bridge from the flat mechanical space to the bent electromagnetic space is the charge attached to a particle. A charged particle possesses both mechanical properties and electromagnetic properties, meaning that it is able to move inside these two spaces simultaneously. The charge, which goes together with the mass, moves uniformly in the flat mechanical space if the energy loss is negligible compared to the particle's kinetic energy.

96

At the same time, it is moving nonuniformly in the transformed electromagnetic space. This motion couples to photons and generates radiation.

Now we discuss the origin of this asymmetry. Though the transformation theory is strictly derived from Maxwell's equations, Maxwell's equations themselves do not govern the motion of charges directly, so the motion of the charged particle is determined in the flat space to be along a straight line. Once the charge of the mass couples to the photons, these photons' motion are governed by Maxwell equations and they propagate in the bent space. In short, this asymmetry of transformation theory stems from the inequality of positions between photons and charges in electromagnetic theory.

After understanding the difference of the appearance of electromagnetic space to charges and photons, we can study how much radiation the fast-moving charged particle will generate. From the transformation viewpoint, the charge is doing nonuniform motion in the virtual electromagnetic space and therefore it will generate radiation. We can also look at the same problem from the side of physical space.

In 1934, Cerenkov studied that liquids and solids emit visible radiation when bombarded by fast-moving electron beams [16]. Later, Frank and Tamm used the macroscopic theory and established that an electron moving uniformly in a medium radiates light when the electron velocity is greater than the velocity of light in the medium [16]. After that, a lot of studies has been carried out for the radiation generated by fast-moving charged particles through different kinds of media, homogeneous or heterogeneous, isotropic or anisotropic [68, 69]. However, most of these studies are only for simple geometries like planar plates or stratified layers, and for simple anisotropy like homogenous anisotropy. Few studies considered both anisotropy and inhomogeneity. Here we extend the Frank and Tamm's theory to a perfect spherical invisibility cloak with a fast-moving charged particle going through.

Figure 4-1 shows the geometry of a spherical cloak with a fast-moving charged particle going through with a uniform velocity. The spherical cloak is created by squeezing the virtual space such that a "hole" of $r < R_1$ in physical space is generated. In the physical space, the light ray is bent around the concealed region $r < R_1$ to make it "invisible", while the particle follows a straight line with a constant velocity. However, if we treat the

97
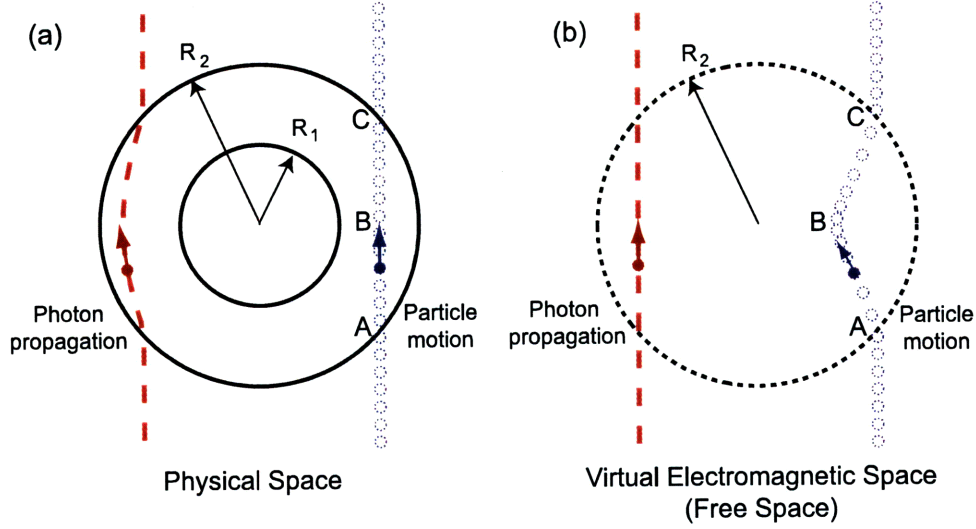
Figure 4-1: Trajectory of a fast-moving charged particle inside the cloak compared with the trajectory of the light ray in (a) the physical space and (b) the virtual electromagnetic space.

same problem in the virtual space as shown in Fig. 4-1(b), the particle's trajectory is bent. We can also see that the velocity of the particle is larger close to the outer boundary while smaller in the middle.

Suppose the attached charge to the particle is q and the velocity v is in $\hat{z}$ direction along the line $x = x_0$ and $y = y_0$. We can write down its current density as follows, $\overline{J}(\overline{r}, t) = \hat{z}qv\delta(x - x_0)\delta(y - y_0)\delta(z - vt)$. Since the cloak is created by the transformation $\overline{r} = \overline{f}(\overline{r}')$ characterized by the Jacobian $\Lambda^i_{i'}$, the corresponding current density in the virtual space can be obtained as [15]

$$\overline{J}'(\overline{r}', t) = |\Lambda|^{-1}\overline{\overline{\Lambda}} \cdot \overline{J}(\overline{r}, t) = q\overline{\overline{\Lambda}} \cdot \hat{z}v\delta(\overline{r}' - \overline{f}^{-1}(\hat{x}x_0 + \hat{y}y_0 + \hat{z}vt))$$

We can see that the charge is moving nonuniformly in the original flat electromagnetic space with the velocity $\overline{\overline{\Lambda}} \cdot \hat{z}v$, as shown in Fig. 4-1(b). It is well-known that a nonuniformly moving charge will generate radiation. In the following, we will demonstrate the radiation process in the physical space directly. The first step is to derive the dyadic Green function of an electric dipole within the cloak.

98

4.2 Dyadic Green function by vector eigenwave expansion

We start with studying the dyadic Green function $\overline{\overline{G}}_E^c$ when an electric dipole is put within the cloak. Since $\overline{\overline{G}}_E^c = \overline{\overline{G}}_E^o + \overline{\overline{G}}_E^r$, where $\overline{\overline{G}}_E^o$ is the dyadic Green function when there is no reflection from the boundaries $r = R_1$ and $r = R_2$, while $\overline{\overline{G}}_E^r$ represents the contribution of these reflections, we first derive $\overline{\overline{G}}_E^o$.

The expression for the scalar potentials inside a linearly transformed spherical cloak is shown in Section 2.1.1, which is $\Psi = k_t(r - R_1)j_n(k_t(r - R_1))P_n^m(\cos\theta)e^{im\phi}$, where $k_t = k_oR_2/(R_2 - R_1)$ and j_n is the spherical Bessel function of the nth order. By introducing an auxiliary tensor $\overline{\overline{T}} = \hat{r}\hat{r}(r - R_1)^2/r^2 + \hat{\theta}\hat{\theta} + \hat{\phi}\hat{\phi}$, we first define the vector eigenwaves inside the cloak,

$$\overline{M}_{n,m} = \nabla \times \hat{r}\Psi \tag{4.1}$$

$$\overline{N}_{n,m} = \tfrac{1}{k_t}\nabla \times (\overline{\overline{T}} \cdot \overline{M}_{n,m}) \tag{4.2}$$

Explicitly, they can be written as

$$
\begin{aligned}
\overline{M}_{n,m} &= \hat{\theta}\frac{1}{r\sin\theta}k_t(r - R_1)j_n(k_t(r - R_1))P_n^m(\cos\theta)ime^{im\phi} \\
&\quad -\hat{\phi}\frac{1}{r}k_t(r - R_1)j_n(k_t(r - R_1))\frac{\partial}{\partial\theta}P_n^m(\cos\theta)e^{im\phi} \tag{4.3} \\
\overline{N}_{n,m} &= \hat{r}\frac{(r - R_1)}{r^2}n(n + 1)j_n(k_t(r - R_1))P_n^m(\cos\theta)e^{im\phi} \\
&\quad +\hat{\theta}\frac{1}{r}\frac{\partial}{\partial r}(r - R_1)j_n(k_t(r - R_1))\frac{\partial}{\partial\theta}P_n^m(\cos\theta)e^{im\phi} \\
&\quad +\hat{\phi}\frac{1}{r\sin\theta}\frac{\partial}{\partial r}[(r - R_1)j_n(k_t(r - R_1))]P_n^m(\cos\theta)ime^{im\phi} \tag{4.4}
\end{aligned}
$$

It is easily seen that

$$\overline{M}_{n,m} = \frac{1}{k_t}\nabla \times (\overline{\overline{T}} \cdot \overline{N}_{n,m}) \tag{4.5}$$

So the vector eigenwaves $\overline{M}_{n,m}$ and $\overline{N}_{n,m}$ satisfy symmetric relationships of Eqs. (4.2) and (4.5).

99

We define an inner product between vetors $\overline{A}$ and $\overline{B}$ as

$$(\overline{A}, \overline{B}) = \int_{R_1}^{\infty} \int_0^{\pi} \int_0^{2\pi} (\overline{A} \cdot \overline{\overline{T}} \cdot \overline{B}) r^2 \sin\theta \mathrm{d}r \mathrm{d}\theta \mathrm{d}\phi \tag{4.6}$$

Under this definition, we can show the orthogonality between $\overline{M}_{n,m}$ and $\overline{N}_{n,m}$.

$$(\overline{M}_{n,m}(\omega), \overline{N}_{n',-m'}(\omega')) = 0$$

$$(\overline{N}_{n,m}(\omega), \overline{N}_{n',-m'}(\omega')) = \frac{2\pi^2 n(n+1)}{2n+1} (-1)^2 \delta_{nn'} \delta_{mm'} \delta(\omega - \omega')$$

$$(\overline{M}_{n,m}(\omega), \overline{M}_{n',-m'}(\omega')) = \frac{2\pi^2 n(n+1)}{2n+1} (-1)^m \delta_{nn'} \delta_{mm'} \delta(\omega - \omega') \tag{4.7}$$

The electric and magnetic dyadic Green funtions $\overline{\overline{G}}_E^o$ and $\overline{\overline{G}}_H^o$ satisfy the Maxwell equations as follows,

$$\nabla \times (\overline{\overline{T}}^{-1} \cdot \nabla \times \overline{\overline{G}}_E^o) - \overline{\overline{T}} \cdot k_t^2 \overline{\overline{G}}_E^o = \overline{\overline{I}} \delta(\overline{r} - \overline{r}') \tag{4.8}$$

$$\nabla \times (\overline{\overline{T}}^{-1} \cdot \nabla \times \overline{\overline{G}}_H^o) - \overline{\overline{T}} \cdot k_t^2 \overline{\overline{G}}_H^o = \nabla \times [\delta(\overline{r} - \overline{r}') \overline{\overline{T}}] \tag{4.9}$$

According to the Ohm-Rayleigh method [70], we can write the right part of Eq. (4.9) as

$$\nabla \times [\delta(\overline{r} - \overline{r}') \overline{\overline{T}}] = \int_0^{\infty} d\kappa \sum_{n,m} \left[\overline{N}_{n,m}(\kappa) \overline{A}_{n,m}(\kappa) + \overline{M}_{n,m}(\kappa) \overline{B}_{n,m}(\kappa) \right] \tag{4.10}$$

Utilizing the orthogonality between $\overline{M}_{n,m}$ and $\overline{N}_{n,m}$ and applying the inner product as defined above to Eq. (4.10) as

$$(\overline{N}_{n',-m'}(\kappa'), \nabla \times [\delta(\overline{r} - \overline{r}') \overline{\overline{T}}])$$

$$= (\overline{N}_{n',-m'}(\kappa'), \int_0^{\infty} d\kappa \sum_{n,m} \left[\overline{N}_{n,m}(\kappa) \overline{A}_{n,m}(\kappa) + \overline{M}_{n,m}(\kappa) \overline{B}_{n,m}(\kappa) \right]) \tag{4.11}$$

we are able to get

$$\overline{A}_{n,m}(\kappa) = \frac{2n+1}{2\pi^2 n(n+1)} (-1)^m \kappa \overline{M}'_{n,-m}(\kappa) \cdot \overline{\overline{T}}'^{-1} \tag{4.12}$$

100

where the prime means replacing $\bar{r}$ by $\bar{r}'$. Similarly,

$$\overline{B}_{n,m}(\kappa) = \frac{2n+1}{2\pi^2 n(n+1)}(-1)^m \kappa \overline{N}'_{n,-m}(\kappa) \cdot \overline{\overline{T}}'^{-1} \tag{4.13}$$

We can write $\overline{\overline{G}}^o_H$ in the similar expansion as Eq. (4.10) as follows,

$$\overline{\overline{G}}^o_H = \overline{\overline{T}}^{-1} \int_0^\infty d\kappa \sum_{n,m} \frac{2n+1}{2\pi^2 n(n+1)}(-1)^m \kappa$$
$$\cdot \left\{ a(\kappa)\overline{N}_{n,m}(\kappa)\overline{M}'_{n,-m}(\kappa) + b(\kappa)\overline{M}_{n,m}(\kappa)\overline{N}'_{n,-m}(\kappa) \right\} \cdot \overline{\overline{T}}'^{-1} \tag{4.14}$$

we can finally get that

$$\overline{\overline{G}}^o_H = \frac{i\pi}{2}\overline{\overline{T}}^{-1} \sum_{n,m} \frac{(2n+1)(-1)^m}{2\pi^2 n(n+1)}$$
$$\cdot \begin{cases} \left(\overline{N}^{(1)}_{n,m}\overline{M}'_{n,-m} + \overline{M}^{(1)}_{n,m}\overline{N}'_{n,-m} \right) \cdot \overline{\overline{T}}'^{-1}, & r > r' \\ \left(\overline{N}_{n,m}\overline{M}'^{(1)}_{n,-m} + \overline{M}_{n,m}\overline{N}'^{(1)}_{n,-m} \right) \cdot \overline{\overline{T}}'^{-1}, & r < r' \end{cases} \tag{4.15}$$

where the superscript $(\cdot)'$ means replacing (r,θ,ϕ) by (r',θ',ϕ') and $(\cdot)^{(1)}$ means replacing the spherical Bessel function j_n by the spherical Hankel function of the first kind $h_n^{(1)}$.

The electric dyadic Green function $\overline{\overline{G}}^o_E$ can be obtained similarly as follows,

$$\overline{\overline{G}}^o_E = -\delta(\bar{r}-\bar{r}')\overline{\overline{T}}'^{-1} + \frac{i\pi}{2k_t}\overline{\overline{T}}^{-1} \sum_{n,m} \frac{(2n+1)(-1)^m}{2\pi^2 n(n+1)} \cdot$$
$$\begin{cases} \left(\overline{M}^{(1)}_{n,m}\overline{M}'_{n,-m} + \overline{N}^{(1)}_{n,m}\overline{N}'_{n,-m} \right) \cdot \overline{\overline{T}}'^{-1}, & r > r' \\ \left(\overline{M}_{n,m}\overline{M}'^{(1)}_{n,-m} + \overline{N}_{n,m}\overline{N}'^{(1)}_{n,-m} \right) \cdot \overline{\overline{T}}'^{-1}, & r < r' \end{cases} \tag{4.16}$$

Then by matching the boundary conditions at $r = R_2$ and $r = R_1$, we can further get that $\overline{\overline{G}}^r_E = 0$. Therefore $\overline{\overline{G}}^{11}_E = \overline{\overline{G}}^o_E$. The transmitted field in the region of $r > R_2$ can be written by the dyadic Green function $\overline{\overline{G}}^{12}_E$

$$\overline{\overline{G}}^{12}_E = \frac{i\pi}{2k_t} \sum_{n,m} \frac{(2n+1)(-1)^m}{2\pi^2 n(n+1)} \cdot \left(\overline{M}^{out}_{n,m}\overline{M}'_{n,-m} + \overline{N}^{out}_{n,m}\overline{N}'_{n,-m} \right) \cdot \overline{\overline{T}}'^{-1} \tag{4.17}$$

where $\overline{M}^{out}$ and $\overline{N}^{out}$ are directly obtained from $\overline{M}$ and $\overline{N}$ by letting $R_1 = 0$.

The electric field generated by a dipole inside the cloak can thus be written as

$$\overline{E}(\overline{r}, t) = \begin{cases} i\omega\mu_t \iiint \overline{\overline{G}}_E^{12} \cdot \overline{J}(r')dV', & r > R_2 \\ i\omega\mu_t \iiint \overline{\overline{G}}_E^{11} \cdot \overline{J}(r')dV', & R_1 < r < R_2 \\ 0, & r < R_1 \end{cases} \qquad (4.18)$$

4.3   Instantaneous field evaluation

From above discussions, we have known that a uniformly moving charged particle though an invisibility cloak will generate radiation because the particle is moving nonuniformly in the virtual electromagnetic space. In this section we calculate the radiation directly in the physical space. For a fast-moving charge q with velocity v in $\hat{z}$ direction along the line of $x = x_0$ and $y = y_0$, we can write down the expression for its current as $\overline{J}(r) = \hat{z}qv\delta(x - x_0)\delta(y - y_0)\delta(z - vt)$, as we have shown at the end of Section 4.1.

In order to take into account of the dimension of the charge, we replace $\delta(z - vt)$ by a Gaussian function $\frac{1}{\sigma\sqrt{2\pi}}e^{-(z-vt)^2/(2\sigma^2)}$ while $\delta(x - x_0)\delta(y - y_0)$ is kept. Therefore the current now is

$$\overline{J}(\overline{r}, t) = \hat{z}qv\delta(x - x_0)\delta(y - y_0)\frac{1}{\sigma\sqrt{2\pi}}e^{-(z-vt)^2/(2\sigma^2)} \qquad (4.19)$$

It is similar to the case that a bunch of electrons are shot along the same line and are moving together. Or we can treat it as a small segment of an electron beam. In practice, this kind of electron bunching has been used in studying Cerenkov radiation [68]. When $\sigma = 0$, the Gaussian function returns to a delta function.

We first Fourier transform the time varing current into frequency domain, as follows

$$\begin{aligned} \overline{J}(\overline{r}) &= \frac{1}{2\pi}\int_{-\infty}^{\infty} \overline{J}(\overline{r}, t)e^{i\omega t}dt \qquad (4.20) \\ &= \hat{z}\frac{q}{2\pi}\delta(x - x_0)\delta(y - y_0)e^{-\sigma^2\omega^2/2v^2}e^{i\omega z/v} \end{aligned}$$

where we decompose the original time-varying current into a lot of time-harmonic current

line sources, each havings its own frequency. For each time-harmonic current line source, the field distribution can be solved utilizing the dyadic Green function derived in last section. Therefore, through inverse Fourier transformation, the response of the cloak due a fast-moving charged particle going through can be solved. In the following, the detailed calculation procedure will be shown.

We first perform a simple manipulation to the time-harmonic current source as follows,

$$
\begin{aligned}
\overline{J}(\overline{r}) = \ &\hat{z}\frac{q}{2\pi}\delta(x - x_0)\delta(y - y_0)e^{-\sigma^2\omega^2/2v^2}e^{i\omega z/v} \\
&-\hat{z}\frac{q}{2\pi}\delta(x - x_0)\delta(y - y_0)e^{-\sigma^2\omega^2/2v^2}e^{i\omega z/v}(u(z - z_1) - u(z - z_2)) \\
&+\hat{z}\frac{q}{2\pi}\delta(x - x_0)\delta(y - y_0)e^{-\sigma^2\omega^2/2v^2}e^{i\omega z/v}(u(z - z_1) - u(z - z_2)) \quad (4.21)
\end{aligned}
$$

where $u(z)$ is the step function and z_1 and z_2 correspond to the end points between which the segment of the line source complely lies inside the cloak. This seemingly trivial step is in fact very important to the calculation. The first two terms on the right side of the equal sign in the above equation corresponds to the current line source after cutting the segment inside the cloak. The last term is the true segment inside the cloak. The first two terms can be treated as they are in free space while the last term must involve the dyadic Green function we derived in last section.

Now we deal with the first source term at the right side of the equal sign in Eq. (4.21). The electric field in free space due to this source term satisfies the following equation,

$$
\nabla \times \nabla \times \overline{E}(\overline{r}) - k_0^2\overline{E}(\overline{r}) = \hat{z}\frac{q}{2\pi}\delta(x - x_0)\delta(y - y_0)e^{-\frac{\sigma^2\omega^2}{2v^2}}e^{i\frac{\omega}{v}z} \quad (4.22)
$$

By shifting the z axis to the line of $x = x_0$ and $y = y_0$ and establishing a new cylindrical coordinate system (ρ_p, ϕ_p, z), we can easily obtain the solution as

$$
\overline{E}(\overline{r}) = -\frac{q}{8\pi\omega\epsilon_0}e^{-\frac{\sigma^2\omega^2}{2v^2}}e^{i\frac{\omega}{v}z}\{\hat{z}(k_0^2 - (\frac{\omega}{v})^2)H_0^{(1)}(k_\rho\rho_p) - \hat{\rho}_p\frac{i\omega}{v}k_\rho H_1^{(1)}(k_\rho\rho_p)\} \quad (4.23)
$$

where $H_0^{(1)}$ and $H_1^{(1)}$ are Hankel functions of the first kind to the zeroth order and first order, respectively. The relation that $H_0^{(1)'}(x) = -H_1^{(1)}(x)$ is used in the derivation.

The second source term on the right side of the equal sign in Eq. (4.21) is a finite

segment. We use the well-known dyadic Green function in free space,

$$\overline{E}(\overline{r}) = i\omega\mu \left(\overline{\overline{I}} + \frac{1}{k_0^2}\nabla\nabla \right) \cdot \iiint dV' \frac{e^{ik_0|\overline{r}-\overline{r}'|}}{4\pi|\overline{r}-\overline{r}'|} \tag{4.24}$$

The integration can be done numerically. We cut the segment between z_1 and z_2 into N small pieces. By denoting $x_p = x - x_0$, $y_p = y - y_0$ and $r_p = |\overline{r} - \overline{r}'|$, we can evaluate the electric field as

$$\overline{E}(\overline{r}) = \sum_{n=1}^{N} \frac{i\omega\mu_0 I\ell(z_n)}{4\pi} \left[\hat{z} \left(\frac{1}{r_{pn}} + \frac{i}{k_0 r_{pn}^2} - \frac{1}{k_0^2 r_{pn}^3} \right) \right.$$
$$+ \hat{x} \frac{x_{pn}z_{pn}}{k_0^2} \left(-\frac{k_0^2}{r_{pn}^3} - \frac{3ik_0}{r_{pn}^4} + \frac{3}{r_{pn}^5} \right)$$
$$+ \hat{y} \frac{y_{pn}z_{pn}}{k_0^2} \left(-\frac{k_0^2}{r_{pn}^3} - \frac{3ik_0}{r_{pn}^4} + \frac{3}{r_{pn}^5} \right)$$
$$\left. + \hat{z} \frac{z_{pn}z_{pn}}{k_0^2} \left(-\frac{k_0^2}{r_{pn}^3} - \frac{3ik_0}{r_{pn}^4} + \frac{3}{r_{pn}^5} \right) \right] e^{ik_0 r_{pn}} \tag{4.25}$$

where

$$I\ell(z_{pn}) = \frac{q}{2\pi} e^{-\frac{\sigma^2\omega^2}{2v^2}} e^{i\frac{\omega}{v}z_n} \frac{z_2 - z_1}{N} \tag{4.26}$$

Subtracting Eq. (4.25) from Eq. (4.23), the electric fields due to the current line source after cutting the segment inside the cloak can be obtained. Here we need to mention that the fields we calculated are in free space. Since it has been proved that when the source is outside of a cloak, the electric field inside the cloak can be obtained by the coordinate transformation directly, the true fields inside the cloak layer due to the current line source after cutting the segment inside the cloak are obtained from transformation.

The last source term is dealt with by Eq. (4.18). Then the total fields generated by the complete time-harmonic line source are obtained by combining all the source terms' contributions. In order to get the fields in time domain, we still need to do the inverse Fourier transform.

104

According to the inverse Fourier transform, the fields in time domain are

$$\overline{E}(\overline{r}, t) = \int_{-\infty}^{\infty} d\omega \overline{E}(\overline{r}) e^{-i\omega t}$$

$$= 2\Re \left\{ \int_{0}^{\infty} d\omega \overline{E}(\overline{r}) e^{-i\omega t} \right\} \tag{4.27}$$

and

$$\overline{H}(\overline{r}, t) = 2\Re \left\{ \int_{0}^{\infty} d\omega \overline{H}(\overline{r}) e^{-i\omega t} \right\} \tag{4.28}$$

Therefore, the total energy radiated out through an imaginary sphere with radius r is

$$
\begin{aligned}
W &= \int_{0}^{2\pi} \int_{0}^{\pi} r^2 \sin\theta d\theta d\phi \cdot \int_{-\infty}^{\infty} dt \overline{E}(\overline{r}, t) \times \overline{H}(\overline{r}, t) \cdot \hat{r} \\
&= \int_{0}^{2\pi} \int_{0}^{\pi} r^2 \sin\theta d\theta d\phi \int_{-\infty}^{\infty} dt \\
&\quad \left\{ 2 \int_{0}^{\infty} d\omega \left[\overline{E}_{\text{Re}} \cos(\omega t) + \overline{E}_{\text{Im}} \sin(\omega t) \right] \right. \\
&\quad \left. \times 2 \int_{0}^{\infty} d\omega' \left[\overline{H}_{\text{Re}} \cos(\omega' t) + \overline{H}_{\text{Im}} \sin(\omega' t) \right] \right\} \cdot \hat{r} \\
&= \int_{0}^{2\pi} \int_{0}^{\pi} r^2 \sin\theta d\theta d\phi \cdot 4\pi \int_{0}^{\infty} d\omega \left(\overline{E}_{\text{Re}} \times \overline{H}_{\text{Re}} + \overline{E}_{\text{Im}} \times \overline{H}_{\text{Im}} \right) \cdot \hat{r} \quad (4.29)
\end{aligned}
$$

where the subscripts of Re and Im denote the real part and the imaginary part of corresponding vectors, respectively.

The energy radiated per unit frequency is

$$\frac{dW}{d\omega} = \int_{0}^{2\pi} \int_{0}^{\pi} r^2 \sin\theta d\theta d\phi \cdot 4\pi \left(\overline{E}_{\text{Re}} \times \overline{H}_{\text{Re}} + \overline{E}_{\text{Im}} \times \overline{H}_{\text{Im}} \right) \cdot \hat{r} \tag{4.30}$$

4.4 Radiation process

In this section we are concerned with demonstrating the physical radiation process. Before we start, we classify all kinds of possible radiations that will appear in our discussion. For a uniformly moving charged particle, Cerenkov radiation will occur if the velocity of

the particle is larger than the phase velocity of light inside the medium. In addition, if the particle is moving through inhomogeneous media, transition radiation will occur at the interface and inside the media, and there is no threshold for the particle's velocity. For a nonuniformly moving charged particle in isotropic media, there are some other kinds of radiation besides Cerenkov radiation. The Bremsstrahlung occurs when the particle's acceleration is parallel with its velocity. Synchrotron radiation occurs when the acceleration of the particle is perpendicular with its velocity.

The cloak we choose is a spherical cloak with inner radius $R_1 = 1\mu$m and outer radius $R_2 = 2\mu$m. The constitutive parameters inside the cloak layer satisfy the relations that $\bar{\bar{\epsilon}} = \epsilon_r \hat{r}\hat{r} + \epsilon_t \hat{\theta}\hat{\theta} + \epsilon_t \hat{\phi}\hat{\phi}$ and $\bar{\bar{\mu}} = \mu_r \hat{r}\hat{r} + \mu_t \hat{\theta}\hat{\theta} + \mu_t \hat{\phi}\hat{\phi}$, where $\epsilon_t = \epsilon_0 \frac{R_2}{R_2 - R_1}$, $\epsilon_r = \epsilon_t \frac{(r - R_1)^2}{r^2}$, $\mu_t = \mu_0 \frac{R_2}{R_2 - R_1}$, and $\mu_r = \mu_t \frac{(r - R_1)^2}{r^2}$. The particle's velocity is fixed at $v = 0.9c$, where c is the speed of light in free space. The parameter σ in the Gaussian distribution function of the current description is chosen to be $\sigma = 0.05\mu$m. The total charge q is set to be the equivalence of 1000 electrons.

In the physical space, the charged particle is moving uniformly. In the virtual space, as shown in Fig. 4-1(b), the charged particle is doing an nonuniform motion. We first plot the radiation process in the physical space as shown in Fig. 4-2. We can divide the radiation process into two stages, one for $t < 0$ and the other for $t > 0$, if we specify that when $t = 0$, the particle is located in the middle of its trajectory, i.e. at $((R_1 + R_2)/2, 0, 0)$ (point B in Fig. 4-1). We can see that in the beginning at $t = -7$ fs, the charged particle is approaching the cloak but is still outside. There is no radiation generated. As the particle enters into the cloak, some radiation is generated. At $t = 0$ fs, the charged particle is located at point B. It is interesting to see that the wave front has already passed the particle and is propagating away, meaning that the first stage of radiation generation has finished. At $t = 3$ fs, the radiation generated in the first stage has completely separated from the charged particle. However, the charged particle starts to generate another radiation, meaning the second stage of radiation generation has started. At $t = 7$ fs, the charged particle has come out from the cloak, so the second stage of radiation generation has finished too. It is seen that at $t = 7$ fs, the radiation from the second stage is composed of two particular shapes. One is a rough shape of a cone while the other is like a circle. At $t = 11$ fs, all radiations propagate

away from the cloak and are separated from the charged particle.

We can explain the above process by comparing the motion in the physical space and that in the virtual space. When the particle enters the cloak, its velocity in the virtual space in Fig. 4-1(b) has an abrupt change at point A, which will generate some radiation in virtual space. This radiation corresponds to the transition radiation occurs at the incident point at the outer boundary of the cloak in physical space (point A in Fig. 4-1(a)). Similarly, when the particle comes out at the other side of the cloak, another abrupt velocity change occurs in the virtual space (point C in Fig. 4-1(b)), which corresponds to the transition radiation occurred at the emitting point at the outer boundary of the cloak in physical space (point C in Fig. 4-1(a)). During the motion of the particle inside the cloak in the physical space (segment AC in Fig. 4-1(a)), it keeps on generating transition radiation due the inhomogeneity and anisotropy of the cloak materials. Regarding its motion in the virtual space (curved segment ABC in Fig. 4-1(b)), it can be mainly divided into two parts—motion along AB and motion AC, corresponding to the two radiation stages. During the motion process, the particle's velocity keeps on changing the direction as well as the absolute velocity value, which gives rise to Bremsstrahlung and synchrotron radiation due to the acceleration. Another kind of radiation that exists in the regions close to the outer boundary of the cloak in the model we use here (close to A or C in both Fig. 4-1(a) and (b)), is the Cerenkov radiation when the velocity of the particle is larger than the speed of light.

It is easier to examine the velocity difference between the light and the charged particle in the virtual space since in the virtual space, the light propagates with c everywhere and the particle's velocity is scaled accordingly. When the particle enters the cloak in the virtual space (point A in Fig. 4-1(b)), it actually generates two radiations, one due to abrupt velocity change at point A the other due to its motion within the cloak near point A. The corresponding radiations in the physical space are those as follows. One is the transition radiation due to the impinging of the particle on the outer boundary and the other is the transition radiation from the particle's motion inside the inhomogeneous medium near the outer boundary. In either physical or virtual space, it is difficult to distinguish these two radiations since they start at the same time when the particle enters the cloak. When the particle moves close to point B in the virtual space (Fig. 4-1(b)), its velocity in the virtual
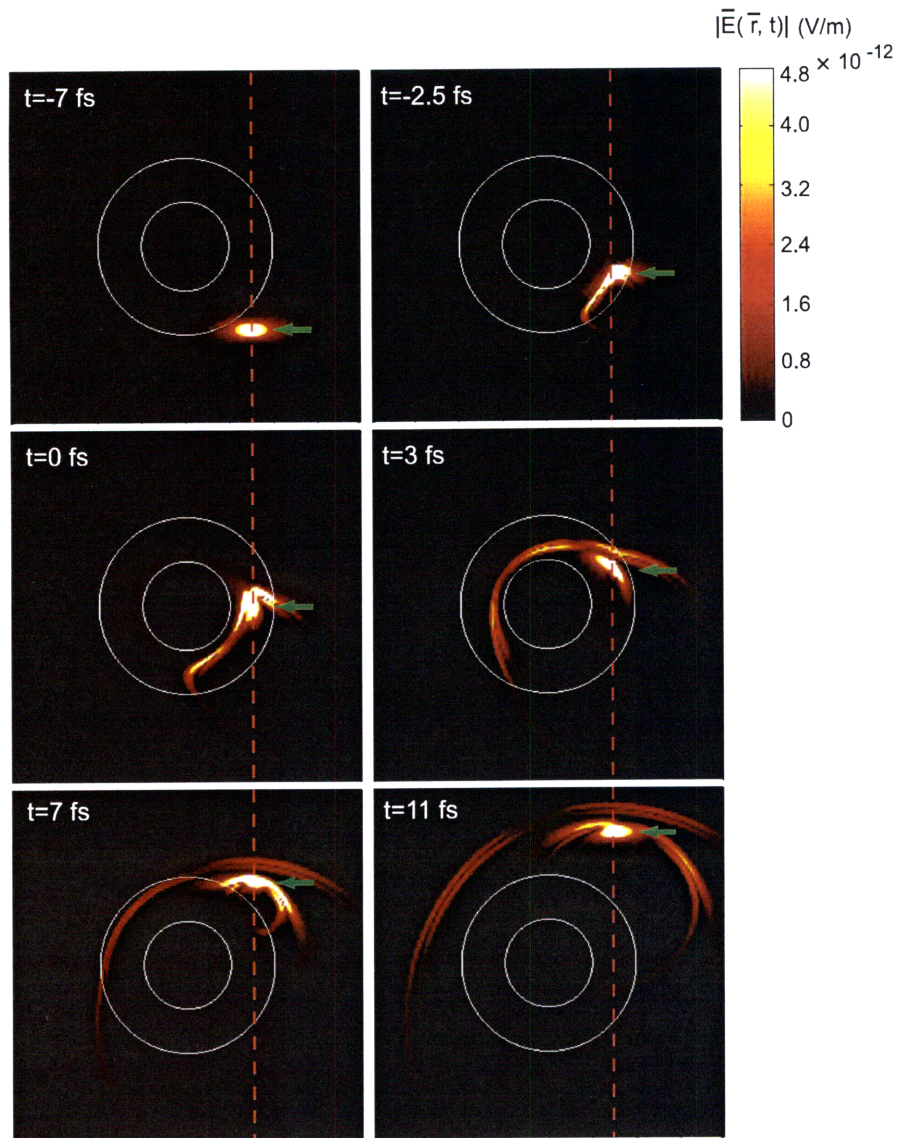
Figure 4-2: Intensity of $|E(\bar{r}, t)|$ during the radiation process of a charged particle going through a spherical invisibility cloak. The dotted line represents the trajectory of the particle. The small arrow indicates the exact position of the particle's center along its trajectory. The inner radius and outer radius of the cloak are 1μm and 2μm, respectively. Net charge amount is equal to 1000 electrons. $v = 0.9c$.

space slows down compared to the speed of light. Thus the light from the first radiation stage has chance to catch up and overtake the particle. In our calculated case, when the particle is close to point B, the radiation generated by this particle at this moment is quite small because of its small velocity in the virtual space. After the particle leaves point B, the particle in the virtual space is accelerating. When its velocity gets higher, it is able to generate obvious radiation, the radiation in the second stage. The radiation generated along the segment BC in virtual space is very similar to the previous studies on accelerating charges [71]. An important point is that when the velocity is increased to be large enough (in the regions close to point A in the model used here), the Cerenkov radiation will occur and contribute to the total radiation [71]. It is interesting to see that when the particle comes out, the radiation from the second stage exhibits two different shapes. The rough shape of a cone is the transmission of radiation generated along the segment BC in the virtual space before hitting point C. The circle-like shape is the radiation due to the abrupt velocity change at point C. Because this abrupt velocity change only occurs at one point, the radiation is basically a spherical wave, and thus form a circle-like wave front. The reason these two shapes of radiation are distinguishable is because they start at different times. The shape similar to a cone is formed earlier than the circle-like radiation. At the incident point A, two similar radiations exist too, but they start at the same time and their wave fronts are mixed together.

Since the impinging only happens at one point, the radiation it generated must similar to a spherical wave. However, the other branch of the second radiation is from the previous motions of the particle inside the cloak and it is just transmitted across the outer boundary. Therefore it still keeps that shape of a rough cone. Consequently, we see two branches in the second radiation while we did not see in the first radiation an obvious distinguishability between the radiation due to the impinging and the radiation due to the motion inside the cloak. This is because they start at the same time when the particle enters into the cloak, being mixed with each other.

The total radiated energy can be calculated to be 2.89×10^{-14} J. In Fig. 4-3, we plot the frequency spectrum of the radiated energy. It is shown that the bandwidth of the radiation is generally broad-band and can be further controlled by the parameter of Gaussian dis-
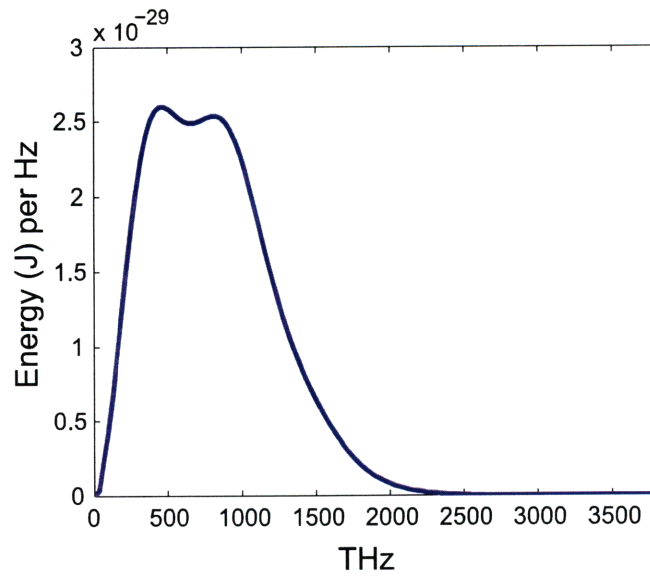
Figure 4-3: Frequency spectrum of the radiated energy from the fast-moving charged particle through the invisibility cloak. The inner radius and outer radius of the cloak are $1\mu m$ and $2\mu m$, respectively. Net charge amount is equal to 1000 electrons. $v = 0.9c$.
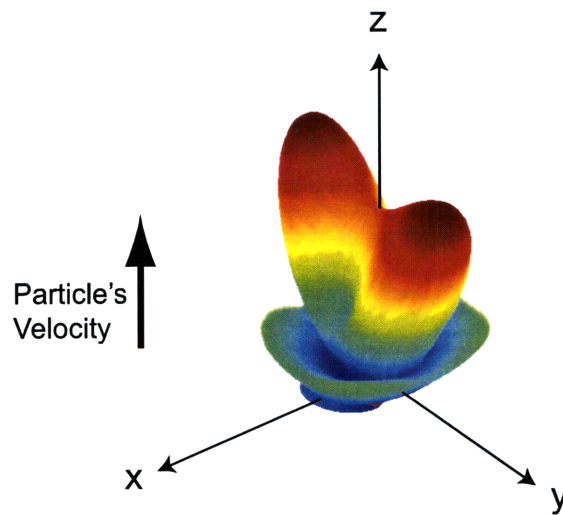
Figure 4-4: Spatial radiation pattern at 500 THz by the fast-moving charged particle through the invisibility cloak. The inner radius and outer radius of the cloak are $1\mu m$ and $2\mu m$, respectively. Net charge amount is equal to 1000 electrons. $v = 0.9c$.

tribution. The energy distribution in frequency domain increases in the beginning, which is similar to the radiation caused by a single electron going through a typical medium, while the energy distribution goes down when the frequency is high, which is because the Gaussian shape of the charge profile has determined the concentration of most frequency components over the low frequency part. It can be shown that, over the frequency range from 500 THz to 501 THz, each of this charge package of 1000 electrons will generate radiation energy equal to about 78 photons. The radiation pattern at 500 THz is shown in Fig. 4-4. So the radiation energy with amount of about 78 photons within 500 THz and 501 THz is distributed roughly according to the pattern in Fig. 4-4.

4.5 Summary

This chapter is devoted to the radiation generated by a fast-moving charged particle through a spherical invisibility cloak with uniform velocity. The reason of radiation is ascribed to the nonuniform motion in the virtual electromagnetic space. The transition radiations that occur at the incident spot and emitting spot when the particle enters and leaves the cloak correspond to the abrupt velocity changes at the corresponding points in the virtual space. The transition radiation during the piercing process corresponds to the deceleration and acceleration radiations (Bremsstrahlung) and synchrotron radiation in the virtual space. In addition, in regions where the particle's velocity is large enough, the Cerenkov radiation will also occur. The total radiated energy, the frequency spectrum and the radiation pattern at a particular frequency are provided. Based on the results in this chapter, we claim that an invisibility cloak can be detected by simply using an electron gun to shoot electrons through the invisibility cloak.

Chapter 5

Practical Implementation of Invisibility Cloaks

There have been a lot of practical designs of invisibility cloaks proposed to work at different frequencies [3, 4, 5, 27, 28, 32] and experiments using different metamaterial structures [6, 60, 72, 73]. However, due to the lack of appropriate methods to model and evaluate the performance of a practical cloak, the design procedures in previous studies were very inefficient.

This chapter is concerned with the practical implementations through accurate electromagnetic modeling. The inhomogeneous simplified cloaks are discussed. The focus is on the potential improvements and simplifications of constructing a metamaterial based invisibility cloak. Finally, we suggest to use only a few homogenous metamaterial layers to construct a practical cloak with satisfying performance at normal incidence and oblique incidence.

5.1   Inhomogeneous cloaks with simplified parameters

To construct a perfect cloak is very difficult due to its stringent conditions on constitutive parameters of tensor forms. In studies of the transformation-based invisibility cloaks, simplified cylindrical cloaks for normally incident waves with only one polarization are often used in experimental demonstration [6], simulations [3, 74], and other practical de-

signs [4, 5, 26, 27, 31, 75]. However, the scattering evaluation at normal incidence is not sufficient to describe the full performance of such simplified cloaks. Furthermore, scattering results for normal incidence were obtained only semi-analytically from simulation tools [25, 29] by coefficient fitting with simulated field patterns, being neither convenient nor strict. Therefore, a fully analytic method to evaluate the performance of simplified cylindrical cloaks at both normal and oblique incidences is needed in designing invisibility cloaks.

Overall, previous studies on simplified cloaks are not complete due to the lack of analytic tools. For example, the main reasons for scattering from a simplified cloak are the mismatches at the outer and inner boundaries. There were studies on the mismatch at the outer boundary that showed that impedance matching at the outer boundary applied by a high-order quadratic transformation in Refs. [4, 29] is able to decrease the scattering efficiently, while there is little study on the mismatch at the inner boundary.

5.1.1 Analytic scattering analysis using state-variable approach

The configuration of scattering from a cylindrical cloak with outer radius R_2 and inner radius R_1 follows that in Fig. 2-3 where a time harmonic plane wave $\overline{E}_i = (\hat{v}_i E_{vi} + \hat{h}_i E_{hi})e^{i\overline{k}_i \cdot \overline{r}}$ is incident with $\overline{k}_i = \hat{x}k_\rho + \hat{z}k_z$, $k_i^2 = \omega^2 \mu_0 \epsilon_0$, $\hat{h}_i = \frac{\hat{z} \times \hat{k}_i}{|\hat{z} \times \hat{k}_i|}$ and $\hat{v}_i = \hat{h}_i \times \hat{k}_i$. In this section we focus on incident waves with vertical polarization, i.e. $E_{hi} = 0$ while our method can also be applied to horizontal polarization. Another point here is that the cloak layer between R_1 and R_2 with permittivity tensor $\overline{\overline{\epsilon}} = \epsilon_\rho \hat{\rho}\hat{\rho} + \epsilon_\phi \hat{\phi}\hat{\phi} + \epsilon_z \hat{z}\hat{z}$ and permeability tensor $\overline{\overline{\mu}} = \mu_\rho \hat{\rho}\hat{\rho} + \mu_\phi \hat{\phi}\hat{\phi} + \mu_z \hat{z}\hat{z}$ is a simplified cylindrical cloak. Without loss of generality, we assume that the concealed region of $\rho < R_1$ is a PEC. We denote $\alpha = \pi/2 - \theta_i$ as the incident angle such that $\alpha = 0$ corresponds to the normal incidence.

In the region of $\rho > R_2$, we use scalar potentials ψ^z_{TM} and ψ^z_{TE} to describe the TE^z and TM^z harmonic cylindrical waves [23], as we did in Section 2.1.2. The difficulty of the current problem is that the wave function inside the cloak has no closed-form solution. Instead of resorting to commercial simulation softwares, we derive the state propagator matrix in the cloak shell using state-variable approach [41] in the following to handle this

difficulty. We denote $\overline{E} = \overline{E}_\rho + \overline{E}_s$ and $\overline{H} = \overline{H}_\rho + \overline{H}_s$, where $\overline{E}_\rho$ and $\overline{H}_\rho$ are components parallel to $\hat{\rho}$ while $\overline{E}_s$ and $\overline{H}_s$ are components perpendicular to $\hat{\rho}$, and $\nabla\times = \nabla_s\times + \nabla_\rho\times$, where

$$
\nabla_s\times = \begin{bmatrix} 0 & \frac{-\partial}{\partial z} & \frac{\partial}{\rho\partial\phi} \\ \frac{\partial}{\partial z} & 0 & 0 \\ \frac{-\partial}{\rho\partial\phi} & 0 & 0 \end{bmatrix} \text{ and } \nabla_\rho\times = \begin{bmatrix} 0 & 0 & 0 \\ 0 & 0 & \frac{-\partial}{\partial\rho} \\ 0 & \frac{\partial}{\rho\partial\rho}\rho & 0 \end{bmatrix} \tag{5.1}
$$

Faraday's law and Ampere's law can be written as

$$
\nabla_\rho \times \overline{E}_s + \nabla_s \times \overline{E}_\rho = i\omega(\mu_\phi\hat{\phi}\hat{\phi} + \mu_z\hat{z}\hat{z}) \cdot \overline{H}_s
$$
$$
\nabla_s \times \overline{E}_s = i\omega\mu_\rho\overline{H}_\rho \tag{5.2}
$$

$$
\nabla_\rho \times \overline{H}_s + \nabla_s \times \overline{H}_\rho = -i\omega(\epsilon_\phi\hat{\phi}\hat{\phi} + \epsilon_z\hat{z}\hat{z}) \cdot \overline{E}_s
$$
$$
\nabla_s \times \overline{H}_s = -i\omega\epsilon_\rho\overline{E}_\rho \tag{5.3}
$$

Noting that for harmonic cylindrical waves of order n, the field has $e^{in\phi}$ and $e^{ik_z z}$ dependencies, hence the state transfer equation can be deduced after eliminating E_ρ and H_ρ in Eqs. (5.2) and (5.3) as follows:

$$
\frac{\partial}{\partial\rho} \begin{bmatrix} E_z \\ E_\phi \\ H_z \\ H_\phi \end{bmatrix} =
$$

$$
\begin{bmatrix} 0 & 0 & -\frac{ink_z}{\omega\epsilon_\rho\rho} & -i\omega\mu_\phi + \frac{ik_z^2}{\omega\epsilon_\rho} \\ 0 & -\frac{1}{\rho} & i\omega\mu_z - \frac{in^2}{\omega\epsilon_\rho\rho^2} & \frac{ink_z}{\omega\epsilon_\rho\rho} \\ \frac{ink_z}{\omega\mu_\rho\rho} & i\omega\epsilon_\phi - \frac{ik_z^2}{\omega\mu_\rho} & 0 & 0 \\ -i\omega\epsilon_z + \frac{in^2}{\omega\mu_\rho\rho^2} & -\frac{ink_z}{\omega\mu_\rho\rho} & 0 & -\frac{1}{\rho} \end{bmatrix} \cdot \begin{bmatrix} E_z \\ E_\phi \\ H_z \\ H_\phi \end{bmatrix} \tag{5.4}
$$

Here another assumption that all the constitutive parameters are functions of only ρ is used.

We let the state function be the four-dimensional vector of $\overline{V} = [E_z\ E_\phi\ H_z\ H_\phi]^T$ and denote the matrix in Eq. (5.4) as $\overline{\overline{T}}$. We cut the cloak shell between $\rho = R_1$ and $\rho = R_2$

115
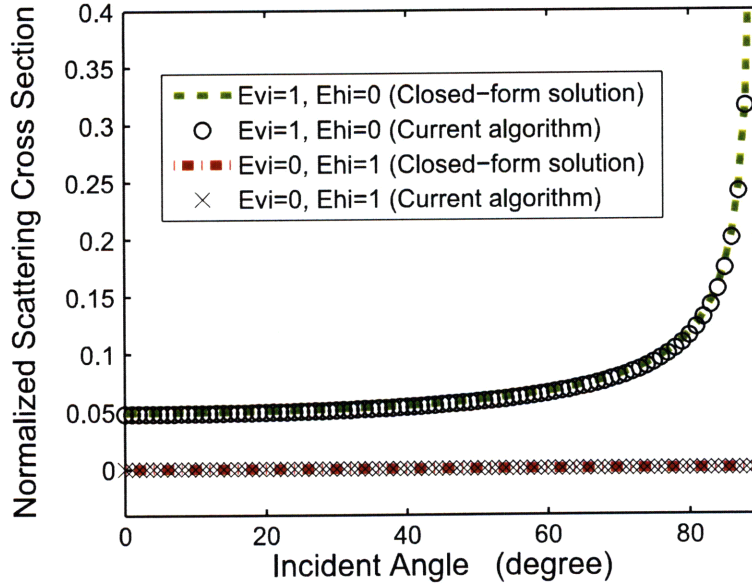
Figure 5-1: Normalized scattering cross section Q_{scat} (normalized to $2R_2$) from an ideal cylindrical invisibility cloak whose inner boundary is set at $R_1 + \delta$. $\delta = 0.01R_1$. $R_2 = 1.5\lambda_0 = 2.08R_1$.

into N layers, each of which has thickness of $\Delta\rho$. It follows from Eq. (5.4) that

$$\overline{V}(\rho_{j+1}) - \overline{V}(\rho_j) = \Delta\rho\overline{\overline{T}}(\rho_j) \cdot \overline{V}(\rho_j) \tag{5.5}$$

Subsequently,

$$\overline{V}(R_2) = \left[\prod_{j=1}^{N} (\overline{\overline{I}} + \Delta\rho\overline{\overline{T}}(\rho_j)) \right] \cdot \overline{V}(R_1) \tag{5.6}$$

By choosing a sufficiently large N and matching the boundary conditions at $\rho = R_1$ and $\rho = R_2$, we are able to solve the field solution for various cylindrical cloaks with continuously varying parameters.

In order to validate this algorithm, we first study the scattering from an ideal cylindrical cloak whose closed-form solution for arbitrary incident angle has been derived in Section 2.1.2. The constitutive parameters for an ideal 2D cylindrical cloak satisfy the relation that $\epsilon_\rho/\epsilon_0 = \mu_\rho/\mu_0 = (\rho - R_1)/\rho$, $\epsilon_\phi/\epsilon_0 = \mu_\phi/\mu_0 = \rho/(\rho - R_1)$, and $\epsilon_z/\epsilon_0 = \mu_z/\mu_0 =$

$[R_2/(R_2 - R_1)]^2(\rho - R_1)/\rho$ [3, 6]. Since constitutive parameters of infinite values at the inner boundary of $\rho = R_1$ are unachievable in practice, we peel a part of the cloak close to the inner boundary, i.e., to set the inner boundary at $\rho = R_1 + \delta$, where $\delta = 0.01R_1$, without changing constitutive parameters otherwhere. In Fig. 5-1 we plot the normalized scattering cross section $Q_{scat} = 2\omega\eta_o \cos\alpha/[(E_{vi}^2 + E_{hi}^2)R_2] \cdot \{1/\epsilon_1 \sum_{n=-\infty}^{\infty} |a_n^{(N)}|^2 + 1/\mu_1 \sum_{n=-\infty}^{\infty} |a_n^{(M)}|^2\}$ [23] of this ideal but perturbated cylindrical cloak. It can be seen that the current algorithm provides strict results. In addition, it is interesting to see that the horizontal polarization has almost zero scattering. As we have discussed in Section 2.1.2, the surface currents at the inner boundary of a perfect cylindrical cloak is important to prevent waves from coming into the concealed region and being scattered. Obviously, by peering a small part from the inner boundary, these surface currents do not exist any more. However, for horizontal polarization, the PEC core happens to provide the electric surface current which is necessary for the perfect cloaking. Therefore, little scattering is caused for horizontal polarization.

5.1.2 Influence of nonlinear transformation
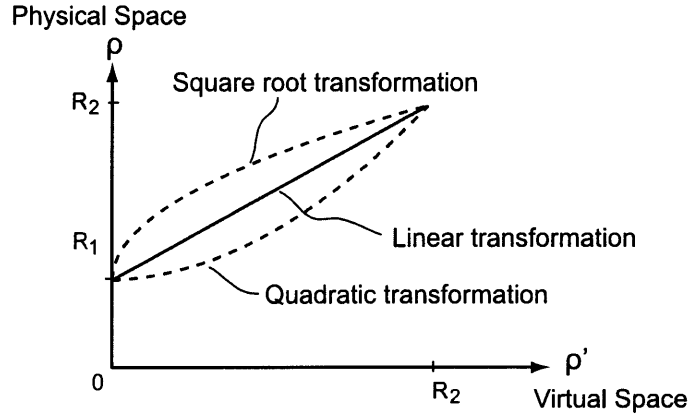
Figure 5-2: Different transformations in cylindrical coordinates to construct cylindrical cloaks. Linear transformation: $\rho = R_1 + (R_2 - R_1)\rho'/R_2$ [2, 3]. Quadratic transformation: $\rho = [1 - R_1/R_2 + (\rho' - R_2)R_1/R_2^2]\rho' + R_1$ [4, 5]. Square root transformation: $\rho = R_1 + (R_2 - R_1)\sqrt{\rho'/R_2}$.

The original model proposed in Ref. [2] and implemented in Ref. [6] were gener-

ated from linear transformation. Yet we can use different kinds of transformations to construct cloaks and compare their performances using our analytic algorithm. Now we consider different transformations from virtual space ρ' to physical space ρ as follows: linear transformation as $\rho = R_1 + (R_2 - R_1)\rho'/R_2$ [2, 3]; quadratic transformation as $\rho = [1 - R_1/R_2 + (\rho' - R_2)R_1/R_2^2]\rho' + R_1$ [4, 5]; and square root transformation as $\rho = R_1 + (R_2 - R_1)\sqrt{\rho'/R_2}$. The linear transformation allows the formation of virtual space within physical space, which is compressed linearly in the radial direction during the process. In the quadratic transformation, such compression is denser near the inner boundary. In the square root transformation, such compression is denser near the outer boundary. They can form different simplified cylindrical cloaks: (a) Linear simplified cloak [3, 6, 25] with $\epsilon_z = \epsilon_0[R_2/(R_2 - R_1)]^2$, $\mu_\rho = \mu_0[(\rho - R_1)/\rho]^2$ and $\mu_\phi = \mu_0$; (b) Impedance matched linear simplified cloak [29] with $\epsilon_z = \epsilon_0 R_2/(R_2 - R_1)$, $\mu_\rho = \mu_0 R_2/(R_2 - R_1)[(\rho - R_1)/\rho]^2$ and $\mu_\phi = \mu_0 R_2/(R_2 - R_1)$; (c) Impedance matched quadratic simplified cloak [4, 5] with $\epsilon_z = \epsilon_0/[2R_1\rho'/R_2^2 - 2R_1/R_2 + 1]^2$, $\mu_\rho = \mu_0(\rho'/\rho)^2[2R_1\rho'/R_2^2 - 2R_1/R_2 + 1]^2$ and $\mu_\phi = \mu_0$; and (d) Impedance matched square root simplified cloak with $\epsilon_z = \epsilon_0 2R_2(\rho - R_1)^2/(R_2 - R_1)^3$, $\mu_\rho = \mu_0 R_2(\rho - R_1)^2/[2(R_2 - R_1)\rho^2]$ and $\mu_\phi = \mu_0 2R_2/(R_2 - R_1)$. Note that (a) and (b) are both from linear transformation and (b), (c) and (d) have matched impedance at the outer boundary [4, 5, 29].

Figure 5-3 shows the electric field distribution in xy plane of different simplified cylindrical cloaks illuminated by a normally incident plane wave with vertical polarization. In the region of $\rho > R_2$, only the scattered field is plotted. In Fig. 5-3(a), the linear simplified cloak has some intrinsic scattering [25], especially in the backward direction due to the impedance mismatch at the outer boundary. From Fig. 5-3(a) to Fig. 5-3(b), the field pattern inside the cloak shell (the bending effect of waves) does not change much, since these two cases are both from linear transformation. However, the scattered field (normalized scattering cross section Q_{scat} [23]) is reduced significantly because the impedance at the outer boundary has been matched. The ring-like scattered field pattern is mainly from the zeroth order scattering [23, 25], which is impossible to be completely eliminated by simplified cloaks due to the lack of surface magnetic current in this case [23, 45]. When the waves reach the inner boundary, instead of inducing magnetic current along $\hat{\phi}$ direction in
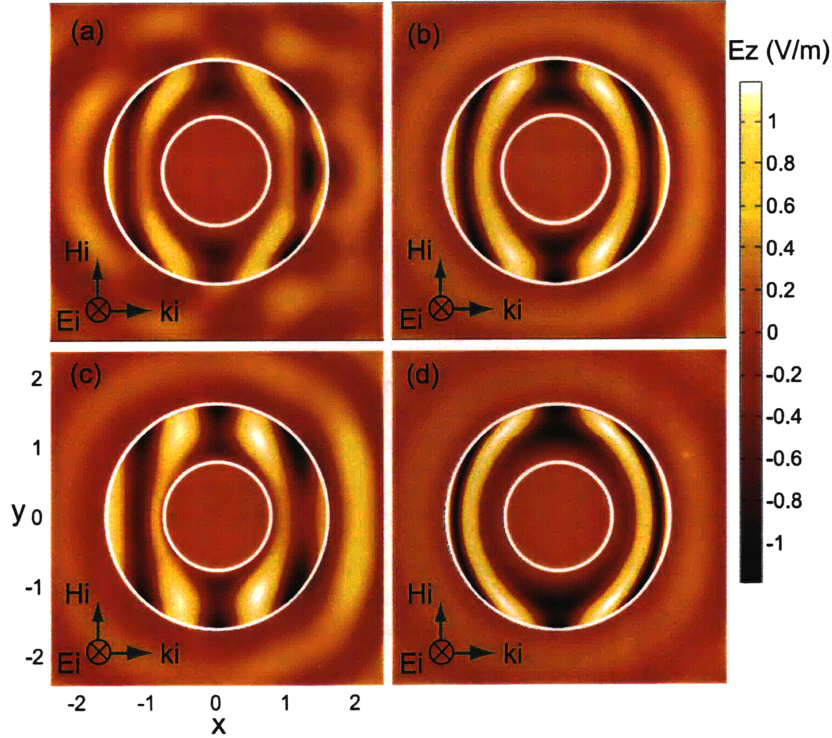
Figure 5-3: Electric field distribution of different simplified cylindrical cloaks illuminated by a vertically polarized and normally incident plane wave. Only scattered field is plotted outside of the cloak. $R_2 = 1.5\lambda_0 = 2.08R_1$. (a) Linear simplified cloak; (b) Impedance matched linear simplified cloak; (c) Impedance matched quadratic simplified cloak; (d) Impedance matched square root simplified cloak. From (a) to (d), the normalized scattering cross section (normalized to $2R_2$) is 0.299, 0.125, 0.360 and 0.034, respectively.

the case of an ideal cylindrical cloak [23, 45], they induce electric current along $\hat{z}$ direction on the surface of PEC core which reradiates and contributes to scattering. From Fig. 5-3(b) to Fig. 5-3(c), the impedance at the outer boundary stays matched, but the quadratic transformation in Fig. 5-3(c) forces most waves to be bent close to the inner boundary. Thus, more energy of the incident waves is blocked by the PEC core in Fig. 5-3(c) than in Fig. 5-3(b), forming a shadow behind the cloak characterized by a strong forward scattering as shown in Fig. 5-3(c). It is worth noting that the normalized scattering cross section in Fig. 5-3(c) is even larger than that in Fig. 5-3(a). This result does not contradict with that in Ref. [4], since in the case studied in Ref. [4], the surface electric current on the PEC core happens to be helpful for complete cloaking [23, 45]. In Fig. 5-3(d), the square

root transformation forces most waves to be bent away from the inner boundary and thus produces a very small scattering cross section. Figure 5-4 shows the far-field differential normalized scattering cross section [23] of cases (a) to (d) in Fig. 5-3. It can be seen that all the simplified cloaks having matched impedance at the outer boundary are able to suppress the backward scattering efficiently. But the impedance matched quadratic simplified cloak has so large forward scattering which leads to an even larger total scattering cross section, while the impedance matched square root simplified cloak is able to suppress both backward and forward scattering, which therefore results in the smallest total scattering cross section.
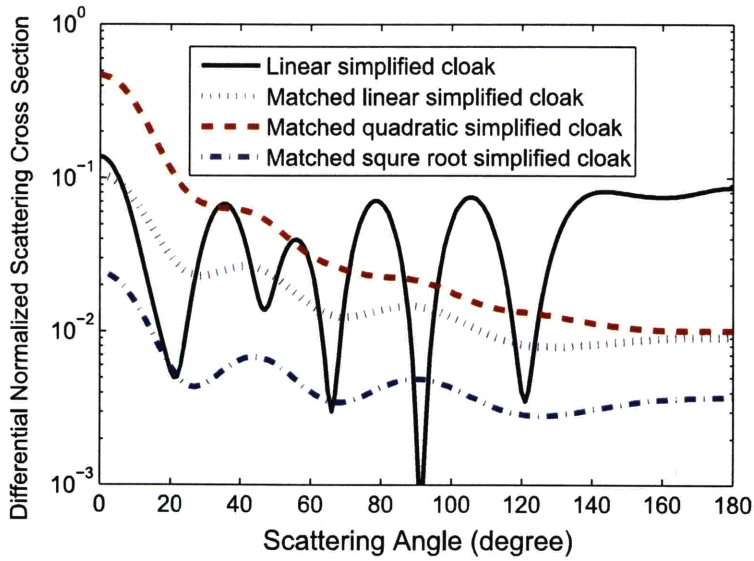
Figure 5-4: Comparison of the far-field differential normalized scattering cross sections of different simplified cylindrical cloaks illuminated by a vertically polarized and normally incident plane wave. $R_2 = 1.5\lambda_0 = 2.08R_1$.

5.1.3 Performance with oblique incidence

We can further calculate the scattering at nonnormal incidences. For each simplified cloak, since only ϵ_z, μ_ρ and μ_ϕ are specified, we require that $\mu_z/\mu_0 = \epsilon_z/\epsilon_0$, $\epsilon_\rho/\epsilon_0 = \mu_\rho/\mu_0$ and $\epsilon_\phi/\epsilon_0 = \mu_\phi/\mu_0$ for the purpose of demonstration. As shown in Fig. 5-5, the reduced scattering cross section can only be achieved within a limited range of incident angles, be-

yond which the scattering is even larger than a bare PEC without any cloak. This result is reasonable since the simplified cloaks are all designed for only normal incidence while the scattering performance at other incident angles has not been considered. Therefore it can be expected that as the incident angle increases, the scattering will increase. But an important question is what is the critical incident angle beyond which a simplified invisibility cloak no longer makes an object "invisible" but makes it even more "visible". Obviously, this critical incident angle is of great importance in practical applications of simplified invisibility cloaks.
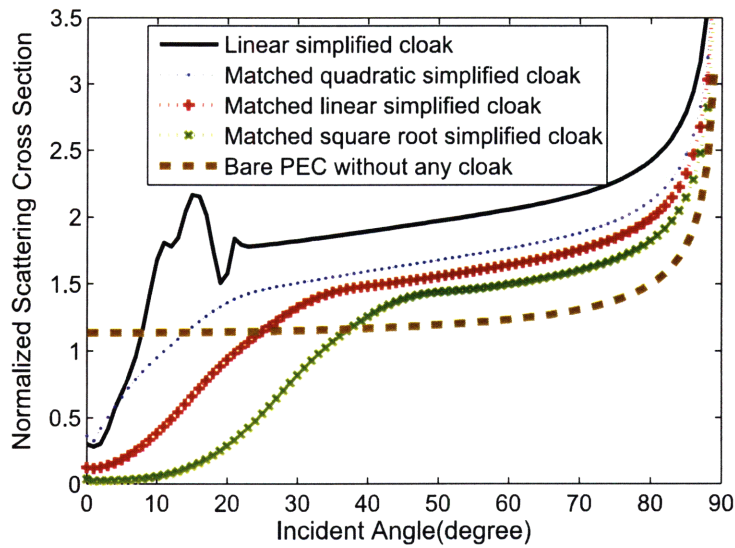
Figure 5-5: Dependance of normalized scattering cross sectioin (normalized to $2R_2$) on incident angles for different simplified cloaks. $R_2 = 1.5\lambda_0 = 2.08R_1$.

5.2 Multi-layered cloaks with homogeneous anisotropic layers

The difficulty in constructing a perfect invisibility cloak is the requirement of continuously varying inhomogeneity and high anisotropy with extreme constitutive parameters. We have known from last section that simplified parameters based on the coordinate transformation can be utilized to facilitate the physical realization [3, 6, 27], in expense of the inherent

121

scattering [25]. However this simplification still has not brought much convenience to practical construction using metamaterial structures. A feasible way to construct a cloak in reality is to use multi-layered structures to approximate the spatially changing constitutive parameters. The first sample of cylindrical cloak was created using multi-layered meta-materials [6]. Bi-layered isotropic media was also proposed for achieving the effective anisotropy [26], but a lot of thin layers are needed which increases the construction complexity. Moreover, the transformation theory did not predict the performance of a practical construction composed of discontinuous layers of homogeneous anisotropic metamaterials. Therefore, it is very necessary to provide a better way to design a practical cloak with satisfying performance.

Here by utilizing the analytic scattering model of a multi-layered cylindrical cloak and utilizing genetic optimization, we are able to show that, although only a few layers of anisotropic materials are used, an optimized multi-layered invisibility cloak with almost zero scattering can still be achieved

5.2.1 Analytic formalism at normal incidence

In order to get the exact behavior of a multi-layered cloak, the analytical model of a cylindrical cloak created with multi-layered anisotropic materials needs to be studied. We use a cylindrical cloak as an example. Without loss of generality, the case of a vertically polarized (E field parallel with z axis) plane wave with unit magnitude normally incident onto an M-layer cylindrical cloak (from region 1 to M) is considered, as shown in Fig. 5-6. The case of horizontal polarization can be analyzed similarly. The radii of the boundaries of different layers within the cloak are denoted by $R^{(m)}$ ($m = 0, 1, \cdots, M$). The relative constitutive parameters in region m are assumed to be constants denoted by $\mu_{\rho m}$, $\mu_{\phi m}$ and ϵ_{zm} while the region $m = 0$ is assumed to be free space and there is a thin PEC coating on the boundary between region M and region $M + 1$. Any object inside region $M + 1$ is guaranteed to be untouched from external electromagnetic waves due to the PEC coating. The remaining task is to minimize the scattering from the whole structure.

122
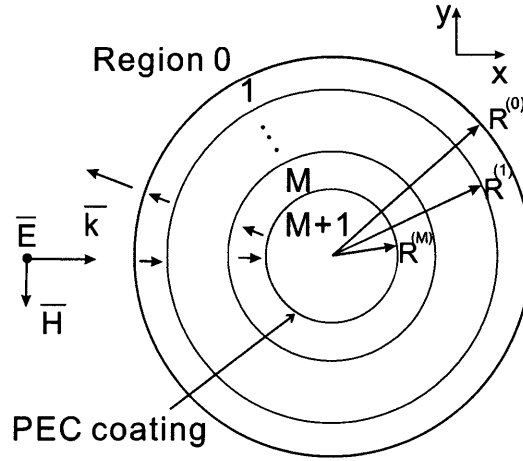
Figure 5-6: Configuration of a multi-layered cylindrical cloak with each layer being anisotropic and homogeneous.

The electric fields E_{zm} in the region m satisfy the following equation,

$$\frac{1}{\rho}\frac{\partial}{\partial\rho}\left(\frac{\rho}{\mu_{\phi m}}\frac{\partial E_{zm}}{\partial\rho}\right) + \frac{1}{\rho^2}\frac{\partial}{\partial\phi}\left(\frac{1}{\mu_{\rho m}}\frac{\partial E_{zm}}{\partial\phi}\right) + k_0^2\epsilon_{zm}E_{zm} = 0 \tag{5.7}$$

By applying the method of separation of variables, the general expression for the electric fields in region m can be expressed as

$$E_{zm} = \sum_{n=-\infty}^{\infty} a_{mn}\left(J_{\nu_{mn}}(k_m\rho) + \tilde{r}_{m(m+1)n}H_{\nu_{mn}}^{(1)}(k_m\rho)\right)e^{in\phi} \tag{5.8}$$

where $\nu_{mn} = n\sqrt{\mu_{\phi m}/\mu_{\rho m}}$ and the wave number in region m is $k_m = k_0\sqrt{\epsilon_{zm}\mu_{\phi m}}$. Different from the isotropic layered case, here ν_{mn} is a fraction. Symbols of $J_{\nu_{mn}}$ and $H_{\nu_{mn}}^{(1)}$ represent the ν_{mn}th order Bessel function and the ν_{mn}th order Hankel function of the first kind, respectively. Besides, a_{mn} is the unknown coefficient and $\tilde{r}_{m(m+1)n}$ is the general scattering coefficient from the boundary R_m if we treat the Bessel function as the incident wave and the Hankel function as the reflected wave. When a wave is incident from region m onto the the boundary R_m, the direct reflection coefficient is $r_{m(m+1)n} = (j'j_1 - \eta_m/\eta_{m+1}jj_1')/(-h'j_1 + \eta_m/\eta_{m+1}hj_1')$, and the direct transmission coefficient is $t_{m(m+1)n} = -2i/(\pi k_m R_m)/(-h'j_1 + \eta_m/\eta_{m+1}hj_1')$. Here $j = J_{\nu_{mn}}(k_m R_m)$, $j' = J'_{\nu_{mn}}(k_m R_m)$,

123

$j_1 = J_{v_{(m+1)n}}(k_{m+1}R_m)$, $j_1' = J'_{v_{(m+1)n}}(k_{m+1}R_m)$, $h = H_{v_{mn}}(k_m R_m)$, $h' = H'_{v_{mn}}(k_m R_m)$,

$h_1 = H_{v_{(m+1)n}}(k_{m+1}R_m)$, $h_1' = H'_{v_{(m+1)n}}(k_{m+1}R_m)$, and $\eta_m = \sqrt{\mu_{\phi m}/\epsilon_{zm}}$. Similarly, for

an outgoing wave the direct reflection and transmission coefficients on $R^{(m)}$ are $r_{(m+1)mn} = (h_1'h - \eta_{m+1}/\eta_m h_1 h')/(-j_1'h + \eta_{m+1}/\eta_m j_1 h')$ and $t_{(m+1)mn} = 2i/(\pi k_{m+1}R_m)/(-j_1'h + \eta_{m+1}/\eta_m j_1 h')$. Therefore, the scattering coefficient in layer m (m=0, 1, ..., M-1) can be

written as [41]

$$\tilde{r}_{m(m+1)n} = r_{m(m+1)n} + \tilde{t}_{(m+1)mn} \tag{5.9}$$

where $\tilde{t}_{(m+1)mn} = t_{m(m+1)n}t_{(m+1)mn}\tilde{r}_{(m+1)(m+2)n}/(1 - r_{(m+1)mn}\tilde{r}_{(m+1)(m+2)n})$ represents

the wave coming out from R_m due to the multiple reflections and transmissions on the

boundaries inside $R^{(m)}$. At $R^{(M)}$ (i.e. R_1), $\tilde{r}_{M(M+1)n} = -J_{v_{Mn}}(k_M R_M)/H_{v_{Mn}}(k_M R_M)$,

therefore all the $\tilde{r}_{m(m+1)n}$ can be derived using Eq. (5.9), and a_{mn} can also be derived

by matching the boundary conditions. The coefficients of the scattering fields in region 0

are $b_{0n} = a_{0n}\tilde{r}_{01n}$. Based on the cylindrical scattering model, the far-field total scattering

efficiency or the scattering cross section normalized by the geometrical cross section for

the multilayered cylindrical cloak is obtained as

$$Q_{scat} = \frac{2}{kR_1} \sum_{n=-\infty}^{\infty} |b_{0n}|^2 \tag{5.10}$$

In practice, the ideal parameters obtained from the transformation method need to be

discretized for realization, which will destroy the perfect invisibility of the cloak. Using the

proposed method, such effects of descretization and simplification of the transformation-

based cloak can be quantitatively analyzed. For example, Schurig et al. proposed a 10-

layer simplified cloak with $\mu_\phi = 1$ for the experiment [6], in which the copper cylinder

core with radius $0.709\lambda_0$ is coated by a multilayered cloak with inner radius $0.768\lambda_0$ and

outer radius $1.670\lambda_0$. Utilizing the parameters including the losses in the metamaterials in

Ref. [6], and assuming the core to be PEC for convenience, for the normal incidence of

a vertically polarized plane wave, the near field distributions can be calculated using our

method. For example, Fig. 5-7 shows the electric field distribution of the case studied in

124
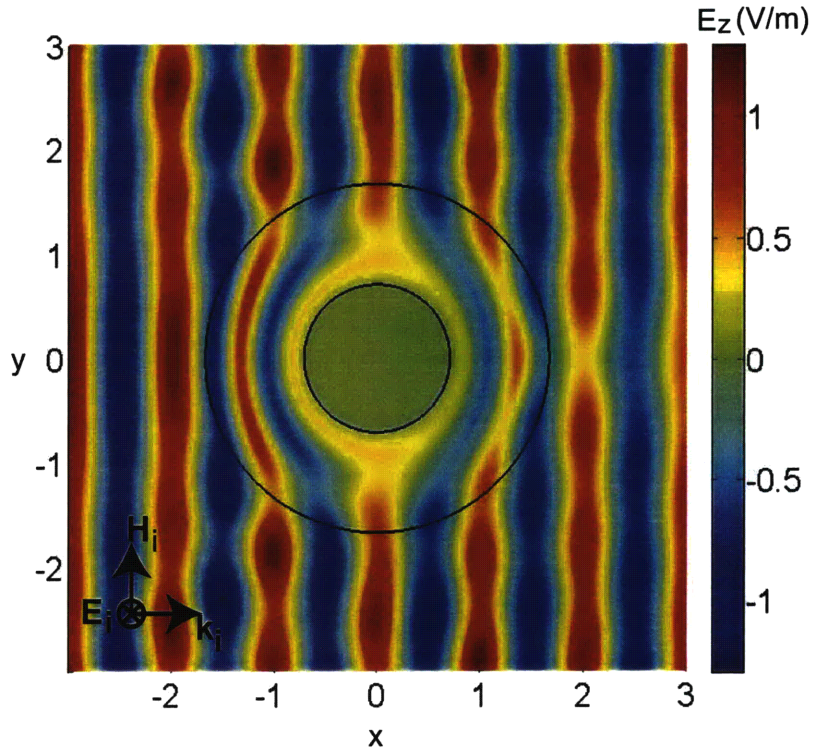
Figure 5-7: E_z field distribution for a vertically polarized (electric field perpendicular with the xy plane) plane wave incident from left to right onto the 10-layer cloak proposed in Ref. [6].

the previous experiment. Our analytical model shows some qualitative agreement with the experimental field distribution shown in [6], where both reduced forward scattering and reduced backward scattering can be observed.

5.2.2   Genetic optimization of a cloak at normal incidence

Genetic algorithm is a widely used optimization method in engineering and science that enables the individuals of candidate solutions to an optimization problem evolve to better solutions [76]. In genetic algorithm, all input variables are encoded as chromosomes. A population of chromosomes of candidate solutions are generated in the beginning and then evolve from generation to generation. In each generation, the fitness of every individual in the population is evaluated, based on which better individuals are selected from the current

125
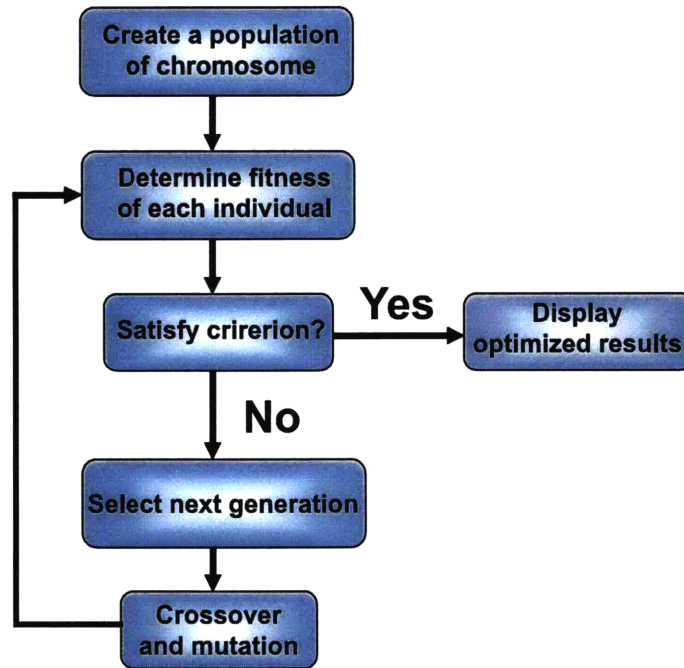
Figure 5-8: Flow chart of genetic algorithm.

population, and modified (crossover and mutation) to form a new population. The new
population is then used in the next iteration of the algorithm. The whole procedure is as
shown in Fig. 5-8. Commonly, the algorithm terminates when either a maximum number
of generations has been produced, or a satisfactory fitness level has been reached for the
population. Here our criterion of terminating the algorithm is that the best fitness of the
population doe not change in a round of 30 generations.

In this section we will show that our proposed method can realize a general multi-
layered cloak without following the ideal transformation parameters, but still possess-
ing a satisfying performance. Meanwhile, the extreme values exist in a conventional
transformation-based cloak can be avoided. In applying the genetic algorithms, the in-
ner radius of the cloak is fixed and the chromosome is a string of 0s and 1s represent-
ing a set of constitutive parameters of each layer and the outer radius in the form of
$\{\epsilon_{z1}, \mu_{\rho 1}, \mu_{\phi 1}, ..., \epsilon_{zM}, \mu_{\rho M}, \mu_{\phi M}, R^{(0)}\}$. The value of each parameter is determined by a
linear mapping from the integer denoted by the binary number to the search space. The

126

	Optimized cloak				TB full parameter cloak			
layer	μ_ρ	μ_ϕ	ϵ_z	η/η_0	μ_ρ	μ_ϕ	ϵ_z	η/η_0
1	0.674	2.002	3.384	0.769	0.186	5.391	4.349	1.113
2	0.057	5.001	7.258	0.830	0.140	7.147	3.280	1.476
3	0.151	6.836	3.532	1.391	0.089	11.245	2.085	2.322
4	0.010	7.508	7.008	1.035	0.032	31.735	0.739	6.551

Table 5.1: The relative constitutive parameters for the optimized 4-layer cloak and the transformation-based (TB) full parameter 4-layer cloak.

thickness of each layer is set to be identical and can also be considered as an optimization input. The fitness of an individual is chosen to be $1/Q_{scat}$, where Q_{scat} is the total scattering of this individual shown by Eq. (5.10). After making use of the roulette wheel selection, in which individuals with larger fitness have larger chance of going forward to the next generation, setting the single point crossover probability and the mutation probability to be 0.6 and 0.05, respectively, and ensuring that the fittest individual is able to propagate to the next generation, evolution is carried out and optimization is obtained finally.

Since it is much easier to create a cloak with only a few layers of matematerials, we consider the 4-layer cloak as an example. The inner radius of the cloak is $R^{(4)} = 0.709\lambda_0$, the same as the size of the copper cylinder used in previous experiment [6]. Taking into account the practical constraints on the constitutive parameters of the metamaterials, the search space of all the relative constitutive parameters is between 0.01 and 8. The outer radius $R^{(0)}$ is set between $0.8\lambda_0$ and $1.67\lambda_0$. Using our proposed method, we design a 4-layer optimized cloak with outer radius $0.894\lambda_0$ and with the parameters shown in Table 5.1. Figure 5-9 shows the calculated electric field distribution when a vertically polarized plane wave normally incident from left to right onto the optimized cloak. It is shown that in the near-field region of the cloak, the incident electric fields remain almost unperturbed.

Figure 5-10 shows the far-field differential normalized scattering cross sections when a vertically polarized plane wave normally incident onto different types of cloaks. When there is only a bared PEC cylinder with radius $0.709\lambda_0$, the differential scattering cross section is shown by the solid line in Fig. 5-10, and the total scattering Q_{scat} (normalized to $2R_1$) is found to be 2.19. For Schurig's cloak (dashed line), the forward and backward scattering have been reduced by about 4.8dB and 4.1dB, respectively, and its Q_{scat} is 0.49.

127
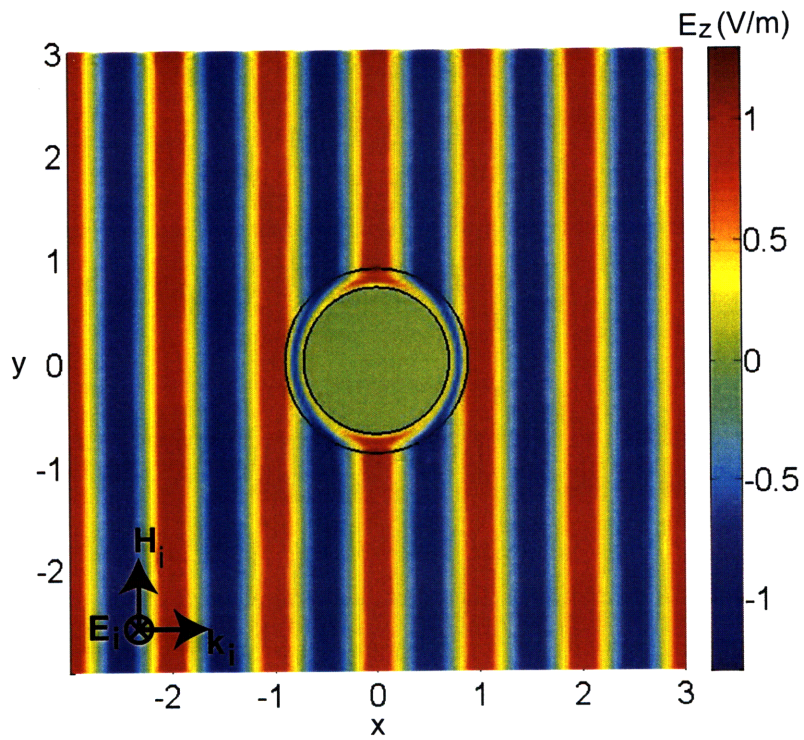
Figure 5-9: Electric field distributions for a plane wave incident from left to right onto the optimized 4-layer cylindrical cloak. The total normalized scattering cross section (normalized to $2R_1$) is 0.0039.
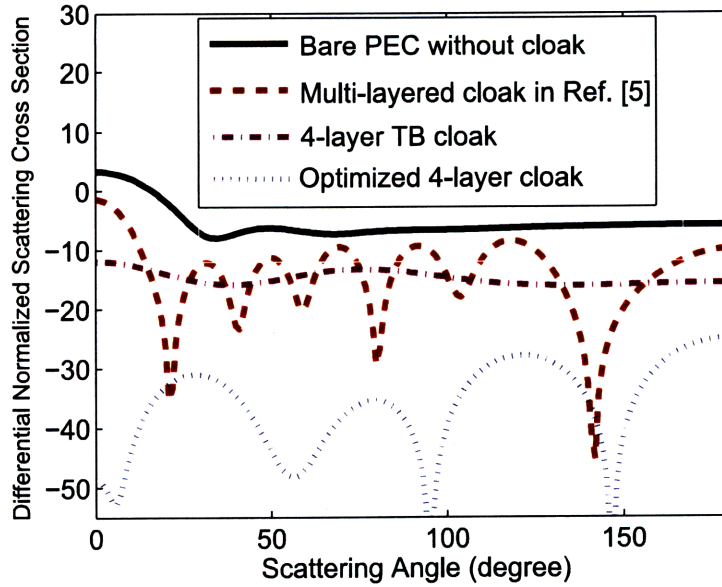
Figure 5-10: Comparison of the differential normalized cross sections when a vertically polarized plane wave normally incident on to the PEC cylinder without cloak (solid), the PEC cylinder with the cloak proposed in Ref. [6] (dash), a 4-layer transformation-based (TB) full parameter cloak (dash dot), and the optimized 4-layer cloak (dot).

For comparison, we use a transformation-based full parameter cloak, whose dimensions are the same as the optimized cloak but with parameters of each layer obtained from sampling the ideal inhomogeneous parameters at the center of each layer, as indicated in Table 5.1. Its differential normalized scattering cross section (dash doted line) is shown and its Q_{scat} is 0.11. When the optimized cloak is used (dotted line), more than 20dB improvement is achieved in all different angles and Q_{scat} is greatly reduced to be 0.0039.

It is interesting to see from Table 5.1 that the optimized parameters are quite different from the parameters obtained by the coordinate transformation theory. Taking the ϕ component as an example, as shown in Table 5.1, the value of relative permeability in the most inner layer is optimized to be 7.508, instead of the value 31.735 as suggested by the transformation method. The parameters achieved here are relatively small and within the limit of metamaterials, which will increase the possibility of realizing such an optimized cloak. This is very important to the implementation of a cloak in practice. As we have known, for an ideal cylindrical cloak, the ϕ component of constitutive parameters need to approach

129

infinity at the inner boundary to support the surface currents. Such an extreme value near the inner boundary is nearly impossible to realize. Though a truncation method [23, 42, 45] at the inner boundary can be used to avoid this extreme value, however, scattering will be aroused and it has been shown that the performance of such a truncated cloak is sensitive to the perturbations near the inner boundary [23, 42]. In order to get a performance as good as our proposed cloak, here Q_{scat} is 0.0039, only about $7 \times 10^{-6}\lambda_0$ truncation is allowed near the inner boundary, which means extremely large values of permeability about $10^5\mu_0$ is needed in the ϕ direction near the inner boundary. This is a disadvantage of the transformation-based cloak in practical implementation.

The reason why nearly perfect invisibility can still be achieved in a cloak with only a few layers can be physically explained as follows. The scattering of such kinds of multi-layered cloaks is determined by the recurrence equation of Eq. (5.9). When $m = 0$, Eq. (5.9) indicates that the nth order scattering is the sum of the direct scattering at $R^{(0)}$ denoted by r_{01n} and the wave coming out from $R^{(0)}$ caused by the multiple reflections and transmissions at the inner boundaries, denoted by $\tilde{t}_{10n}$. In order to minimize the total scattering, the parameters of the cloak should be chosen so that r_{01n} and $\tilde{t}_{10n}$ cancel each other. As denoted by Eq. (5.9), $\tilde{r}_{01n}$ are determined simultaneously by ν_{mn}, k_m and η_m in all the layers. Thus the matching of impedances between adjacent layers does not assure a small total scattering. For example, the extreme case of filling all 4 layers with air (perfect match) will result in a large scattering corresponding to the solid line in Fig. 5-10. On the contrary, the mismatch of the impedances, as shown in Table 5.1, can be utilized to form multiple reflections and transmissions among the inner layers, which eventually produces a transmission to the free space being able to destructively interfere with the direct reflection occurs at the outer boundary. In our proposed optimized cloak, the 0th direct reflection coefficient at $R^{(0)}$ is $r_{010} = -0.1135 - 0.3172i$, while the 0th transmission coefficient from $R^{(0)}$ is $\tilde{t}_{010} = 0.1130 + 0.2947i$, therefore, the 0th scattering coefficient is $\tilde{r}_{010} = -0.0005 - 0.0225i$ which is very small, due to the destructive interference. This is also similar to the one-dimensional multi-layered case of the Fabry-Perot etalon filter, where the impedances of each layer are not necessary to be matched in order to get zero reflection.

5.2.3 Optimized cloak at oblique incidence

In Section 5.1.3, we have shown that the performance of certain simplified cloaks deteriorates quickly with the increase of incident angle, because these simplified cloaks are designed only for normal incidence. It is desirable to have some other method to construct a more easily realizable cloak working for even oblique incidence. Here we will demonstrate the multi-layered cloak working for oblique incidence after the optimization.

For oblique incidence, the difficulty here is that there is no closed-form solution to the wave equation inside each layer. We have provided a method to calculate the scattering from a general cloak under oblique incidence in Section 5.1.1 based on the state-variable approach [41]. Therefore, for each layer, we can apply this method to calculating each state propagator matrix and their product will be the final state propagator matrix. Taking a 4-layer cloak as an example, the state propagator equation will be

$$
\overline{V}(R_2) = \left[\prod_{j=3N+1}^{4N} (\overline{\overline{I}} + \Delta\rho\overline{\overline{T}}(\rho_j)) \right] \cdot \left[\prod_{j=2N+1}^{3N} (\overline{\overline{I}} + \Delta\rho\overline{\overline{T}}(\rho_j)) \right]
$$
$$
\cdot \left[\prod_{j=N+1}^{2N} (\overline{\overline{I}} + \Delta\rho\overline{\overline{T}}(\rho_j)) \right] \cdot \left[\prod_{j=1}^{N} (\overline{\overline{I}} + \Delta\rho\overline{\overline{T}}(\rho_j)) \right] \cdot \overline{V}(R_1) \qquad (5.11)
$$

After obtaining the state propagator matrix, we can solve the field distribution over the entire space, as we have done in Section 5.1. Now by applying the genetic optimization, we are able to get a multi-layered cloak to work with oblique incidence.

For comparison with the performance of simplified cloaks at oblique incidence, we consider a cylindrical structure with the same size as in Section 5.1, where the inner radius $R_2 = 1.5\lambda_0 = 2.08R_1$. We set the number of layers to be 4. Each layer has the same thickness. Another condition is that we force all relative parameters in each layer to be less than 10. The geometry is as shown in Fig. 5-11. The incident wave is vertically polarized, i.e. only electric field has z component. The incident angle is chosen to be $30°$. We fist choose the scattering from the bare PEC core with radius $R_1 = 0.721\lambda_0$ as the reference, whose E_z field distribution in the xy plane is shown in Fig. 5-12. It can be seen that the scattering is quite large. The normalized scattering cross section (normalized to $2R_2$) is 1.175 in this case.

131

Figure 5-11: Configuration of a 4-layer cloak when a vertically polarized plane wave is obliquely incident with the incident angle of $30°$.

Figure 5-12: E_z field distribution in xy plane due to scattering from a bare PEC cylinder when a vertically polarized plane wave is obliquely incident with the incident angle of $30°$. The normalized scattering cross section (normalized to $2R_2$) is 1.175.

I	Optimizing three parameters					
layer	μ_ρ	μ_ϕ	ϵ_z	ϵ_ρ	ϵ_ϕ	μ_z
1	0.962	1.423	1	1.154	1	1
2	1.128	0.160	1	0.598	1	1
3	0.792	2.754	1	1.321	1	1
4	0.665	1.025	1	2.625	1	1
II	Optimizing six parameters					
layer	μ_ρ	μ_ϕ	ϵ_z	ϵ_ρ	ϵ_ϕ	μ_z
1	0.550	2.320	1.725	0.438	1.781	3.409
2	0.283	3.584	1.657	0.262	3.953	0.037
3	0.224	8.204	0.614	0.189	8.674	1.754
4	0.057	9.994	0.015	1.540	9.069	0.030

Table 5.2: The relative constitutive parameters for the optimized 4-layer cloak by (I) optimizing three parameters each layer and (II) optimizing six parameters each layer.

We have two sets of optimizations. One is to control ϵ_z, μ_ρ and μ_ϕ for each layer (the simplified cloaks only need these three parameters), while keeping relative ϵ_ρ, ϵ_ϕ and μ_z as constant of 1. The other is to control all these six parameters for each layer. The performances of these two optimized 4-layer cloaks are shown in Fig. 5-13 and Fig. 5-14. Their relative constitutive parameters are shown in Table 5.2. It is seen in Fig. 5-13 that by controlling only three parameters each layer, the total scattering has reduced much when compared to the bare PEC core in Fig. 5-12. The normalized scattering cross section (normalized to $2R_2$) is reduced from 1.175 to 0.498. After optimizing all six parameters for each layer of the cloak, the normalized scattering cross section (normalized to $2R_2$) is 0.013, close to "invisibility" as shown in Fig. 5-14. It is worth mentioning that the 4-layer cloak in Fig. 5-14 that is optimized at the single incident angle of 30° is still valid for other incident angles. In Fig. 5-15, we can see that this cloak has good performance over a large range of incident angles.

We can generally ascribe this low scattering phenomenon to the cancelation of the first reflection on the outer boundary and the total transmission from inside the cloak to outside the cloak, similar to the reason described in last section. However, with oblique incidence, the description of the wave behavior is much more complicated. For normal incidence, since vertically polarized waves and horizontally polarized waves are decoupled, only vertically polarized scattering will be generated in response to the vertical incidence. When
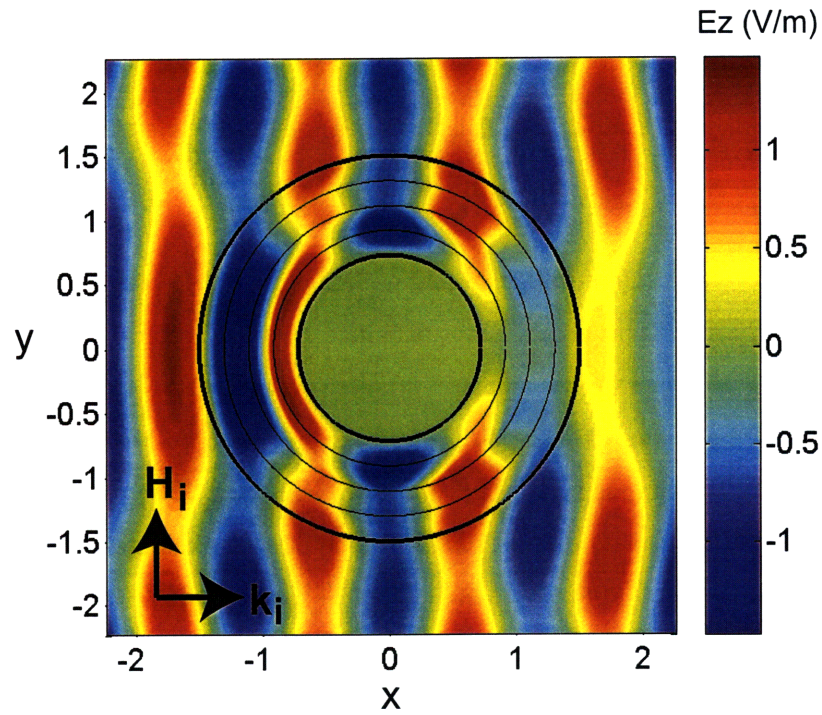
Figure 5-13: E_z field distribution in the xy plane due to scattering from a 4-layer cloak when a vertically polarized plane wave is obliquely incident with the incident angle of $30°$. The cloak's ϵ_z, μ_ρ and μ_ϕ in each layer are optimized while the relative ϵ_ρ, ϵ_ϕ and μ_z are kept as constant of 1. The normalized scattering cross section (normalized to $2R_2$) is 0.498.
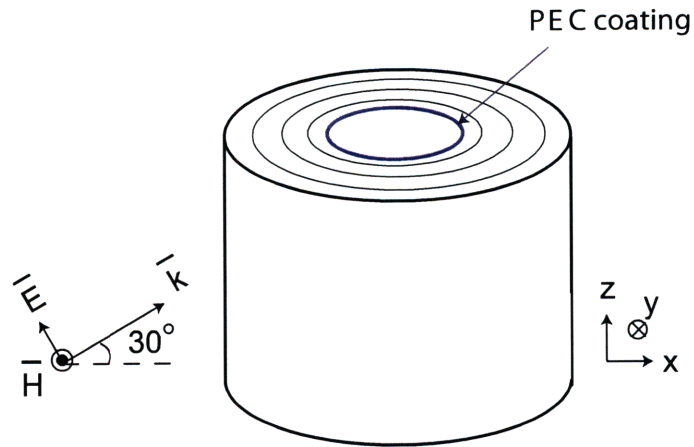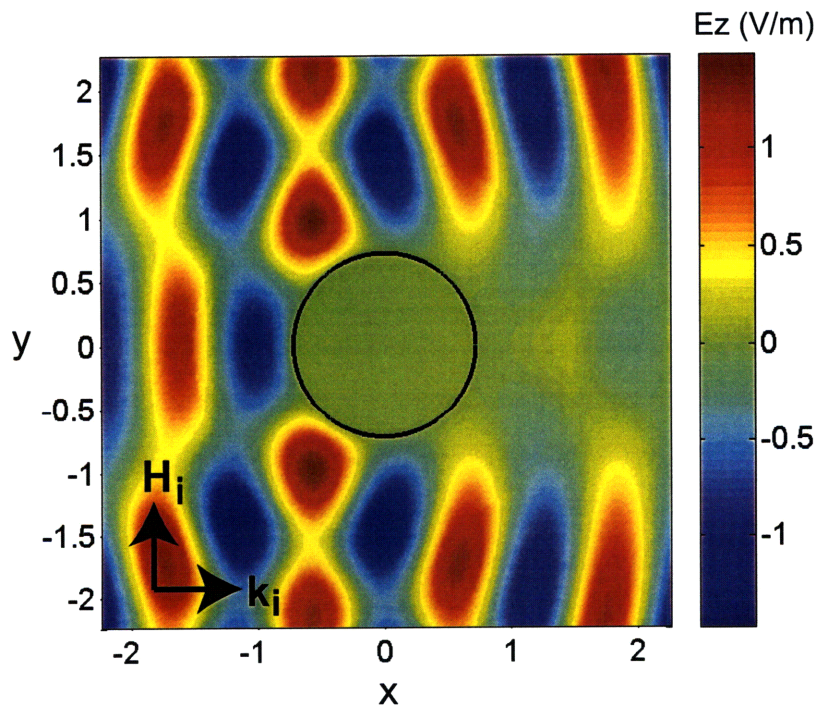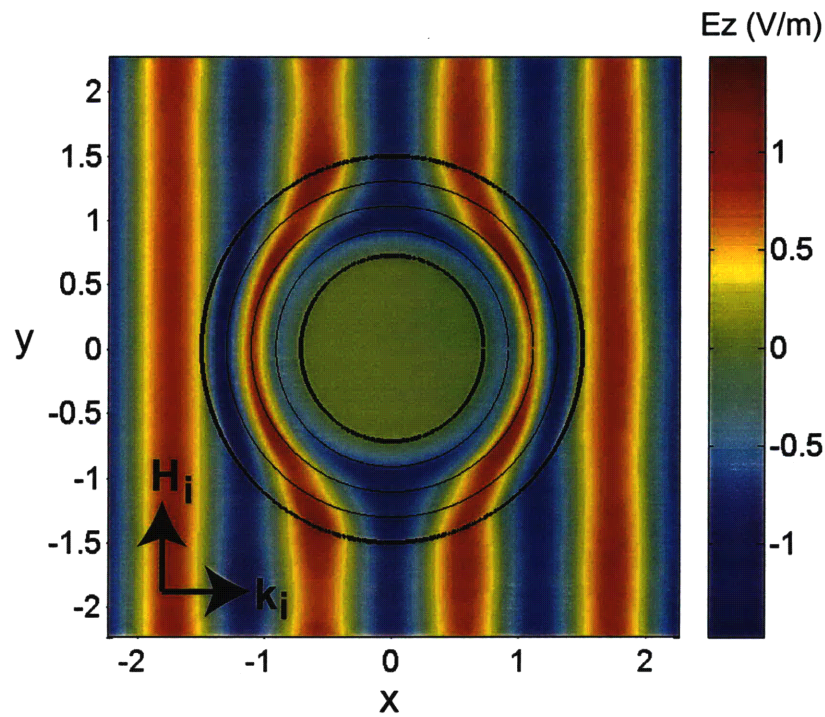
Figure 5-14: E_z field distribution in the xy plane due to scattering from a 4-layer cloak when a vertically polarized plane wave is obliquely incident with the incident angle of 30°. All six parameters of each layer within the cloak are optimized. The normalized scattering cross section (normalized to $2R_2$) is 0.013.
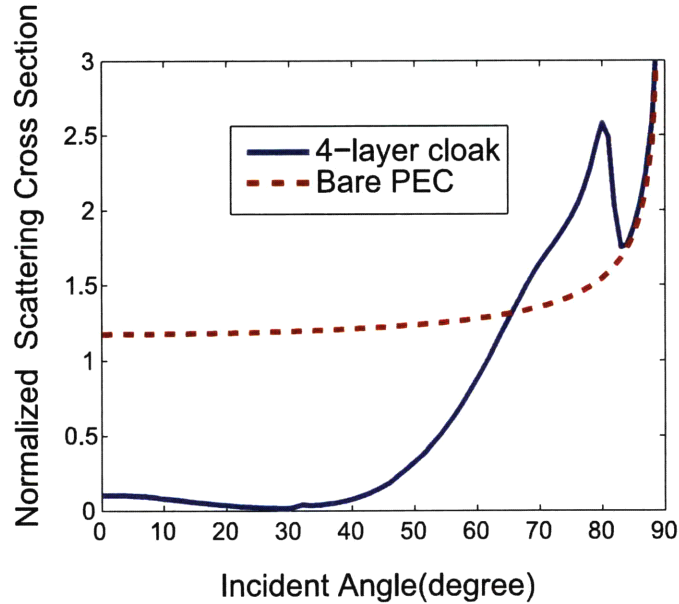
Figure 5-15: Dependence of normalized scattering cross section (normalized to $2R_2$) on the incident angle for the 4-layer cloak created by optimizing all six parameters of each layer within the cloak. The dotted line corresponding to the normalized scattering cross section (normalized to $2R_2$) of the bare PEC core is shown for comparison.

the incident angle is tilted, vertically polarized and horizontally polarized waves become coupled to each other. So both vertically polarized and horizontally polarized waves will be generated even when the incident polarization is only singly polarized.

From above discussion, we can see that the combination of analytic formalism and genetic algorithm is a powerful tool which may find more applications in the practical implementation of invisibility cloaks in the future.

5.3 Practical limitations on invisibility cloaks

To evaluate the applicability of transformation theory to invisibility cloaks, it is necessary to discuss the practical limitations on invisibility cloaks, like how large an object can be concealed with the current technology of metamaterial fabrication, and how many layers we need to approximate a transformation-based cloak. In this section, we compare the performance of spherical cloaks with different sizes and different losses, and we also study

136

the influence of the number of layers.

Loss is an important issue in the application of metamaterials. Table 5.3 shows the scattering from spherical cloaks with different inner radius and different thickness when the loss tangent of 0.01 is applied to all constitutive parameters. The concealed object within $r < R_1$ is PEC. The thickness of the cloak is $d = R_2 - R_1$. It can be seen that, when the size of the object to be concealed increases, the scattering generally increases as well. For a given size of the object to be concealed, using a thin cloak is helpful for reducing the scattering. However, a very small thickness of the cloak will challenge the fabrication, since the constitutive parameters need to vary sharply within this small thickness. In addition, it can be seen that the larger the object, the more difficult it is to cloak it using lossy metamaterials with the same loss tangent. Generally speaking, in order to achieve obvious cloaking effect, as shown in Table 5.3, the sizes of the cloak and the object to be concealed need to be in the same order of a wavelength within the extent of current metamaterial technologies.

It is also important to study how much loss is allowed to achieve a required scattering cross section for a particular object to be concealed. Table 5.4 shows the maximum loss tangent allowed for all constitutive parameters if the required normalized scattering cross section (normalized to πR_1^2) is fixed to be 0.01. It can be seen that generally, to achieve the normalized scattering cross section of 0.01, the loss needs to be very small. The larger the cloak and the object to be concealed, the smaller loss is required. Typically, the loss tangent of the cloak is larger than 0.01 for microwave frequencies [6], which means that using current metamaterial technology, it is very difficulty to achieve small scattering (reduced by 2 orders) for the transformation-based invisibility cloaks.

In practice, the continuously inhomogeneous cloak is of ten approximated layers of metamaterials [6]. Figure 5-16 shows the dependence of normalized scattering cross section (normalized to πR_1^2) on the number of layers. It can be seen that cloaking an object with the radius of 4λ needs more layers to reach a stable scattering than that with the radius of 1λ. A little loss will expedite the converging of scattering as the number of layers increases, because loss makes the discretization of the cloak more homogeneous. However, as we can see, the scattering from a lossy cloak that converges fast has a larger scattering

d/R_1	Radius of PEC sphere R_1							
	1λ	2λ	4λ	6λ	8λ	10λ	100λ	1000λ
1/1000	0.0067	0.0254	0.0856	0.1613	0.2417	0.3206	0.9811	1.0073
1/100	0.0068	0.0263	0.0884	0.1664	0.2491	0.3299	0.9992	1.0255
1/10	0.0097	0.0365	0.1205	0.1847	0.3301	0.4322	1.1896	1.2165
1/8	0.0106	0.0398	0.1306	0.2414	0.3553	0.4636	1.2454	1.2724
1/6	0.0123	0.0457	0.1489	0.2732	0.3998	0.5192	1.3412	1.3685
1/4	0.0162	0.0594	0.1905	0.3451	0.4993	0.6418	1.5432	1.5710
1/2	0.0332	0.1179	0.3617	0.6316	0.8849	1.1065	2.2330	2.2624
1	0.1013	0.3410	0.9638	1.5732	2.0846	2.4888	3.9901	4.0222

Table 5.3: Normalized scattering cross section (normalized to πR_1^2) from spherical cloaks with different sizes. R_1 is the radius of PEC sphere to be concealed and d is the thickness of the cloak. The loss tangent for all constitutive parameters is set to be 0.01.

d/R_1	Radius of PEC sphere R_1							
	1λ	2λ	4λ	6λ	8λ	10λ	100λ	1000λ
1/1000	1.24E-2	6.04E-3	3.00E-3	1.99E-3	1.49E-3	1.19E-3	1.19E-4	1.20E-5
1/100	1.21E-2	5.93E-3	2.94E-3	1.96E-3	1.47E-3	1.17E-3	1.17E-4	1.17E-5
1/10	1.01E-2	4.96E-3	2.46E-3	1.64E-3	1.23E-3	9.82E-4	9.85E-5	9.87E-6
1/8	9.66E-2	4.74E-3	2.35E-3	1.56E-3	1.18E-3	9.38E-4	9.37E-5	9.39E-6
1/6	8.90E-3	4.39E-3	2.18E-3	1.45E-3	1.09E-3	8.71E-4	8.69E-5	8.70E-6
1/4	7.75E-3	3.81E-3	1.89E-3	1.26E-3	9.49E-4	7.58E-4	7.55E-5	7.55E-6
1/2	5.30E-3	2.62E-3	1.30E-3	8.67E-4	6.51E-4	5.20E-4	5.21E-5	5.21E-6
1	2.93E-3	1.45E-3	7.25E-4	4.83E-4	3.63E-4	2.90E-4	2.89E-5	2.89E-6

Table 5.4: The maximum loss tangent that can be applied to all constitutive parameters of a spherical cloak with different sizes when the normalized scattering cross section (normalized to πR_1^2) is fixed to be 0.01. R_1 is the radius of PEC sphere to be concealed and d is the thickness of the cloak.
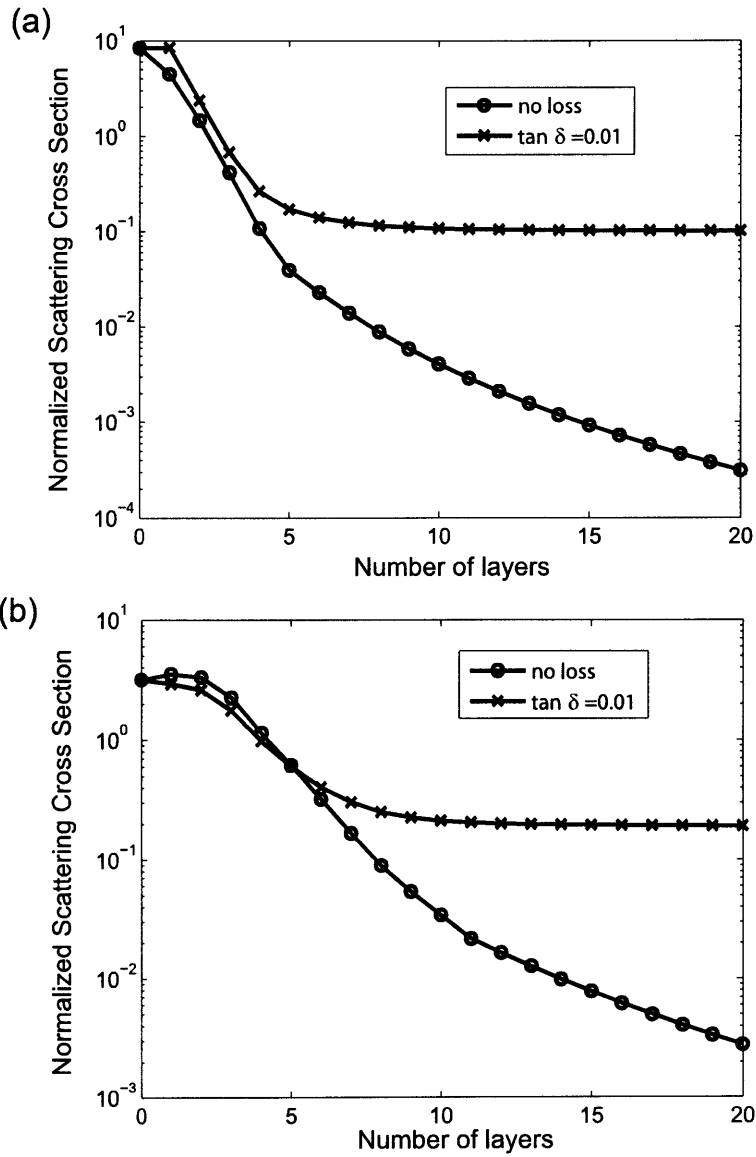
Figure 5-16: Dependence of normalized scattering cross section (normalized to πR_1^2) on the number of layers. The concealed object is PEC. The two curves correspond to lossless case and lossy case where a loss tangent of 0.01 is applied to all constitutive parameters. (a) Both the radius of PEC and the thickness of the cloak are 1λ. (b) The radius of PEC is 4λ while the thickness of the cloak is 1λ.

than a lossless cloak with the same number of layers.

Another question is whether we can use isotropic dielectrics to construct a cloak instead of anisotropic metamaterials. Here we emphasize that anisotropy is of key importance in the cloaking phenomenon and thus cannot be eliminated. We can use Fig. 1-2 to explain our arguments. In Fig. 1-2(a), the horizontal lines can be treated as phase fronts propagating upwards and the vertical lines are the corresponding power propagation directions. After transformation, as shown in Fig. 1-2(b), the mesh is distorted. As long as this transformation is not a conformal mapping, the angles between horizontal lines and vertical lines are no longer conserved, meaning the phase propagation direction and the power propagation direction will not be in the same direction. Anisotropy is necessary in this case. Therefore, using isotropic dielectrics to construct a transformation-based invisibility cloak is generally impossible.[1]

5.4 Summary

In this chapter, two parts of practical implementations are considered. The first part is for inhomogeneous simplified cloaks that are often used in experiments. The effects of nonlinear transformation and incident angle are studied. The second part is for optimized multi-layered cloaks whose layers are homogeneous and anisotropic. Genetic algorithm is adopted to optimize the practical multi-layer structures. For both parts, analytic treatments are developed. Finally, practical imitations of size, loss and anisotropy are discussed. Main conclusions are as follows.

- Simplified cylindrical cloaks may produce a larger scattering at nonnormal incidences than that from an object without any cloak, making this object more "visible".

- The impedance-matched high-order transformation forces waves to be bent closer to the inner boundary and thus may produce stronger scattering than the simplified

---

[1]For example, in Fig. 1-2, the segment of the originally vertical red line in the first quadrant is bent counterclockwise due to the squeezing from the "hole", while an originally horizontal line in the same quadrant is bent clockwise under similar squeezing effect to avoid the "hole". Therefore the angle between these two lines is no longer right angle, meaning that the power direction and phase propagation direction are not the same. As long as the "hole" creation is necessary in the transformation, anisotropy is generated during the squeezing process.

linear one without impedance matched at the outer boundary. A square root transformation can improve scattering by guiding waves away from the inner boundary.

- Utilizing genetic algorithm, a multi-layered cloak can be optimized using homogeneous and anisotropic layers to be close to invisible at normal incidence.

- It is demonstrated that by optimizing the performance of the cloak at 30° incidence, the multi-layered cloak provides low bistatic scattering over a wide range of incident angles.

- In order to reduce the scattering from a PEC object by 2 orders, the loss tangent of the cloak generally cannot be larger than 0.01. This has implied important limitations on the applicability of transformation theory to invisibility cloaks.

Chapter 6

Conclusions

This thesis presents a systematic electromagnetic study of transformation-based invisibility cloaks. The theoretical analysis is based on macroscopic electromagnetic wave theory. The emphasis has been placed on the physical interpretation of the phenomenon of transformation-based invisibility with a better fundamental understanding. The results presented here solved some key problems in invisibility cloaking on both the theoretical and practical levels.

6.1 Conclusion of theoretical analysis

On the theoretical part, the work in this thesis studied three main aspects.

1. Interaction of a perfect invisibility cloak with electromagnetic waves

Firstly, the effectiveness of transformation-based invisibility cloaks are confirmed. By establishing the scattering models for the spherical and cylindrical cloaks, we are able to calculate the electromagnetic fields analytically over the whole space, based on which a better understanding can be obtained. It is shown that the spherical cloak proposed in Pendry *et al.*'s original work is indeed perfect for a monochromatic incident wave. This conclusion helps to resolve the disagreement between Pendry *et al.*'s paper and Leonhardt's paper on the point that whether perfect invisibility is theoretically achievable or not. For a cylindrical cloak, our full-wave results show that it is perfect not only for normal inci-

dence but also for oblique incidence. It is emphasized that at the inner boundary of an ideal cylindrical cloak, the external incident wave will induce electric and magnetic surface currents. These surface currents introduced here are formed by polarized currents and have no counterparts in the original virtual space. Therefore they cannot be predicted directly by the transformation theory.

Secondly, an invisibility cloak is able to cloak active sources. The principle of the transformation theory is to guide waves around the object to be concealed. Though the transformation theory demonstrated the effect of cloaking a passive object, it did not provide information on whether electromagnetic radiation originating from inside the concealed region can be kept from getting out or not. This means that anything emitting electromagnetic radiation might be instantly detectable. Our study shows that the invisibility cloak created by the transformation theory is still perfect for cloaking an object emitting electromagnetic radiation. We demonstrate that this phenomenon is due to the surface voltage effect at the inner boundary of the cloak.

Thirdly, mechanical response of an invisibility cloak is studied. Though the wave passes through the cloak as if nothing is there, the cloak is in fact subject to some local forces. We show that the outer boundary of the cloak withstands pressure forces from the incoming wave, while the bulk and the inner boundary withstand the forces attempting to extend the volume. Since the force are mainly in radial direction, we can roughly treat the recoil forces exerted to the electromagnetic wave as the centripetal forces under which the photons are able to do the circulating motion within the cloak.

2. Electromagnetic waves in an imperfect invisibility cloak

Firstly, by introducing perturbations to constitutive parameters, we show that under certain lossy conditions, the spherical cloak is still perfect for a back-scattering detector, while a cylindrical cloak with the same lossy conditions will still be visible. The scattering model we developed is useful for evaluating the effectiveness of an invisibility cloak.

Secondly, the dispersion effect is analyzed in details. A multi-layer algorithm able to describe the performance of a dispersive and lossy spherical cloak is developed. By applying the dispersions of Drude and Lorentz types to the constitutive parameters, it is

144

shown that electromagnetic waves with different frequencies have different depths of penetration in the cloak and thus form a rainbow like field distribution inside the cloak. A quasi-monochromatic wave will experience a blue-shift in the forward propagating direction. Based on the dispersion model, group velocity, energy transport velocity and signal time-delay are discussed. It is shown that group velocity and energy transport velocity are not well-defined when the wave is approaching the inner boundary because the wave is seriously distorted. However, when the frequency band is narrow enough, we are still able to define the time-delay of the signal arriving at a target plane behind the cloak. A volcano-shaped time-delay spatial distribution is demonstrated as a concrete example in our physical model.

3. Radiation caused by a fast-moving charged particle through an invisibility cloak

While photons can be guided by the cloak along curved trajectories, however, a moving charged particle will still follow a straight trajectory due to its inertia. This charged particle that is moving in the heterogenous and anisotropic cloak will induce electromagnetic radiation. The reason of radiation is also ascribed to the nonuniform motion in the virtual electromagnetic space.

We extend Frank and Tamm's theory of Cerenkov radiation due to a uniformly moving charged particle in homogenous and isotropic medium to the case of a uniformly moving charged particle through a perfect spherical invisibility cloak that is both inhomogeneous and anisotropic. The dyadic Green function of an electric dipole inside the cloak is derived. Based on that, the instantaneous field distribution is evaluated during the whole process of the charged particle passing through the cloak.

Our results show that the transition radiations that occur at the incident point and emitting point when the particle enters and leaves the cloak in the physical space correspond to the abrupt velocity changes at the corresponding points in the virtual space. The transition radiation during the piercing process corresponds to the deceleration and acceleration radiations (Bremsstrahlung and synchrotron radiation) in virtual space. Cerenkov radiation will also occur in certain regions close to the outer boundary when the particle's velocity is sufficiently large.

145

A concrete example of a spherical cloak with outer radius of $2\mu m$ and inner radius of $1\mu m$ with a Gaussian charge distribution of 1000 electrons going through is demonstrated. It is shown that the bandwidth of the radiation is generally broad-band and can be controlled by the parameter of Gaussian distribution. The radiated energy distribution in frequency domain increases in the beginning, which is similar to the radiation caused by a single electron going through a typical medium, while the radiated energy distribution goes down when the frequency is high, which is because the Gaussian shape of the charge profile has determined the concentration of most frequency components over the low frequency part. It is estimated that a charge package of 1000 electrons will generate about 78 photons over the frequency range 500 THz to 501 THz, that will distribute roughly according to the radiation pattern at 500 THz.

6.2 Conclusion of practical analysis

In this thesis, the practical studies are divided into two parts.

First, the simplified cloaks which are often used in experiments are studied. The analytic scattering calculation based on the state-variable method is carried out for both normal incidence and oblique incidence, being more efficient and accurate than the semi-analytic method often used in published literatures. It is found that the simplified cylindrical cloaks may produce a larger scattering at oblique incidence than that from an object without any cloak, making this object even more "visible". At normal incidence, the high-order transformation with impedance matched at the outer boundary, which was supposed to reduce the scattering in previous studies, can produce stronger scattering than the linear simplified one without matched impedance. This is due to the inefficiency of guiding waves close to the inner boundary. Therefore, a square root transformation can improve scattering by guiding waves away from the inner boundary.

Second, a multi-layered cloak using anisotropic and homogenous layers is proposed based on the genetic optimization for normal incidence and oblique incidence respectively. In order to get the exact behavior of a multi-layered cloak at normal incidence which is commonly used in practice, the analytical model of a cylindrical cloak created with multi-

layered anisotropic materials is firstly established based on the full-wave scattering theory. By the optimization with genetic algorithm, we show that, although only a few layers of anisotropic materials are used, an optimized multi-layered cloak with nearly zero scattering can still be achieved. The parameters obtained are relatively small and easier to be realized by metamaterials. The impedances between the adjoined layers do not necessarily match each other but can still produce extremely low scattering. For the oblique incidence, the results from the state-variable approach is chosen as the input of the optimization. It is demonstrated that using only a few layers, the optimized cloak can work over a large range of incident angles.

6.3 Suggested future work

In this section, I suggest some of the potential problems for future work.

1. Special relativity consistent cloaking of a moving object

We have analyzed a number of limitations that an invisibility cloak has, such as the loss, frequency dispersion, extreme values of constitutive parameters and continuously varying anisotropy. There is at least one more limitation which is important but has not been studied. All current studies on invisibility cloaking are limited to stationary state where the cloak as well as the concealed object cannot move. If we want to cloak an object which is moving fast, we must consider the relativistic effect of electromagnetic waves. We can divide this problem into two parts. One is the Doppler shift effect of the frequency of electromagnetic waves when the object is moving. Since the metamaterial constructing the cloak is dispersive, this Doppler shift will deteriorate the invisibility performance. The other part is the change of the background. In relativistic motion, Lorentz transformation is applied and the background becomes bianisotropic medium with respect to the object in motion. It is difficult to get the analytic scattering solution in this case, but we are able to use numerical simulation methods to get the scattering in the moving frame and then transform it back to the stationary frame.

2. Momentum of electromagnetic waves inside the cloak

The coordinate transformation theory shows how to transform electromagnetic space. However, the electromagnetic waves have both wave properties and particle properties—electromagnetic momemtum. Since the cloak does not produce any scattering, the net momentum transfer of electromagnetic waves to the cloak is zero. However, how do the momenta go through the cloak is not know yet. We have studied the Lorentz force distribution inside the cloak and shown that the recoil force might be the reason of turning the momenta around. In electromagnetics, the Lorentz force law is another basic law besides Maxwell's equations. The effect of coordinate transformation on Lorentz force law need to be considered. Based on the momentum conservation law as well as the Lorentz force analysis, the momentum of electromagnetic waves inside a transformation-based cloak can be studied. Because the cloak is anisotropic and inhomogeneous, the form of momentum in this case is expected to be complicated.

4. Non-reciprocal cloaks

A shortcoming of the perfect invisibility cloaks is that the wearer of these cloaks cannot perceive the external information when the outside observer cannot see the wearer at the same time. It will be very interesting to study how to cloak an object while still keeping it be able to receive the external signals. This is possible by using non-reciprocal materials. Recently, many structures of non-reciprocal metamaterials have been proposed and studied, which further increases the possibility of non-reciprocal cloaks. The problem is that in order to let the signal get into the concealed object, electromagnetic waves must penetrate into the concealed region. Therefore, the concealed object cannot be very lossy, otherwise the energy dissipation will make the object visible. Another possibility is to utilize active sources to compensate the energy dissipation

Appendix A

Wave Functions inside a Spherical Cloak Generated by Arbitrary Coordinate Transformations

A general derivation of the wave functions inside a spherical cloak generated by an arbitrary coordinate transformation is published in Ref. [77]. We list the main conclusions here.

Consider a general coordinate transformation between two spherical coordinate systems (r', θ', ϕ') and (r, θ, ϕ) that is described by

$$r' = f(r,\theta,\phi), \quad \theta' = g(r,\theta,\phi), \quad \phi' = h(r,\theta,\phi) \tag{A.1}$$

where r', θ' and ϕ' represent the coordinates in the original coordinate system and $f(\cdot)$, $g(\cdot)$ and $h(\cdot)$ can be arbitrary monotonic differentiable functions. Following the transformation theory based on the form-invariance of Maxwell's equations under space-time transformation, the constitutive parameters can be obtained as follows,

$$\bar{\bar{\epsilon}} = \epsilon_0 \bar{\bar{T}}^{-1}, \quad \bar{\bar{\mu}} = \mu_0 \bar{\bar{T}}^{-1} \tag{A.2}$$

where ϵ_0 and μ_0 represents the scalar permittivity and permeability of free space in the original space before transformation. The matrix T is defined by $T = \bar{\bar{J}}^T \bar{\bar{J}} / \det(\bar{\bar{J}})$, where

$\bar{\bar{J}} = \partial(f, g, h)/\partial(r, \theta, \phi)$ is the Jacobian matrix. According to the fields into TE and TM modes by introducing the vector potentials $\overline{A}_{\text{TE}}$ and $\overline{A}_{\text{TM}}$ in the new space and express the fields as

$$\begin{aligned}
\overline{B}_{\text{TM}} &= \nabla \times \overline{A}_{\text{TM}} \\
\overline{D}_{\text{TM}} &= \tfrac{i}{\omega}\{\nabla \times [\bar{\bar{\mu}}^{-1} \cdot \nabla \times \overline{A}_{\text{TM}}]\} \\
\overline{D}_{\text{TE}} &= -\nabla \times \overline{A}_{\text{TE}} \\
\overline{B}_{\text{TE}} &= \tfrac{i}{\omega}\{\nabla \times [\bar{\bar{\mu}}^{-1} \cdot \nabla \times \overline{A}_{\text{TM}}]\}
\end{aligned} \tag{A.3}$$

Since the media described by $\bar{\bar{\epsilon}}$ and $\bar{\bar{\mu}}$ is no longer isotropic, the directions of $\overline{A}_{\text{TE}}$ and $\overline{A}_{\text{TM}}$ are not necessary to be along the $\hat{r}$ direction. For mathematical convenience, we let

$$\begin{aligned}
\overline{A}_{\text{TM}} &= \left(\tfrac{\partial f}{\partial r}\hat{r} + \tfrac{\partial f}{r\partial\theta}\hat{\theta} + \tfrac{\partial f}{r\sin\theta\partial\phi}\hat{\phi}\right)\Phi_{\text{TM}} \\
\overline{A}_{\text{TE}} &= \left(\tfrac{\partial f}{\partial r}\hat{r} + \tfrac{\partial f}{r\partial\theta}\hat{\theta} + \tfrac{\partial f}{r\sin\theta\partial\phi}\hat{\phi}\right)\Phi_{\text{TE}}
\end{aligned} \tag{A.4}$$

where Φ_{TM} and Φ_{TE} are scalar potentials for TE and TM cases, respectively. Substituting Eq. (A.4) into Eq. (A.3), we obtain the partial differential equation for Φ_{TE} and Φ_{TM},

$$\left[\frac{\partial^2}{\partial f^2} + \frac{1}{f^2\sin g}\frac{\partial}{\partial g}\left(\sin g\frac{\partial}{\partial g}\right) + \frac{1}{f^2\sin^2 g}\frac{\partial^2}{\partial h^2} + k_0^2\right]\Phi = 0 \tag{A.5}$$

The solution for this equation is

$$\Phi = \hat{B}_n(k_0 f)P_n^m(\cos g)e^{imh} \tag{A.6}$$

where $\hat{B}_n(\cdot)$ is the Riccati-Bessel function, P_n^m is the associated Legendre polynomials of the nth order with degree m. Using Eq. A.4 we can obtain the vector potentials $\overline{A}_{\text{TE}}$ and $\overline{A}_{\text{TM}}$ as follows:

$$\overline{A}_{\text{TM}} = \sum_{m,n} a_{m,n}^{\text{TM}}\left(\frac{\partial f}{\partial r}\hat{r} + \frac{\partial f}{r\partial\theta}\hat{\theta} + \frac{\partial f}{r\sin\theta\partial\phi}\hat{\phi}\right)\hat{B}_n(k_0 f)P_n^m(\cos g)e^{imh} \tag{A.7}$$

$$\overline{A}_{\text{TE}} = \sum_{m,n} a_{m,n}^{\text{TE}}\left(\frac{\partial f}{\partial r}\hat{r} + \frac{\partial f}{r\partial\theta}\hat{\theta} + \frac{\partial f}{r\sin\theta\partial\phi}\hat{\phi}\right)\hat{B}_n(k_0 f)P_n^m(\cos g)e^{imh} \tag{A.8}$$

Thus all the components of the total fields can be obtained by substituting Eq. (A.7) and Eq. (A.8) into Eq. (A.3) and the results are as follows:

$$E_r = \frac{i}{\omega\mu_0\epsilon_0}\left[\frac{\partial f}{\partial r}\left(\frac{\partial^2}{\partial f^2}+k_0^2\right)+\frac{\partial g}{\partial r}\frac{\partial^2}{\partial f\partial g}+\frac{\partial h}{\partial r}\frac{\partial^2}{\partial f\partial h}\right]\Phi_{\mathrm{TM}}$$
$$+\frac{1}{\partial\epsilon_0}\left(\sin g\frac{\partial h}{\partial r}\frac{\partial}{\partial g}-\frac{1}{\sin g}\frac{\partial g}{\partial r}\frac{\partial}{\partial h}\Phi_{\mathrm{TE}}\right) \tag{A.9}$$

$$E_\theta = \frac{i}{\omega\mu_0\epsilon_0 r}\left[\frac{\partial f}{\partial\theta}\left(\frac{\partial^2}{\partial f^2}+k_0^2\right)+\frac{\partial g}{\partial\theta}\frac{\partial^2}{\partial f\partial g}+\frac{\partial h}{\partial\theta}\frac{\partial^2}{\partial f\partial h}\right]\Phi_{\mathrm{TM}}$$
$$+\frac{1}{\epsilon_0 r}\left(\sin g\frac{\partial h}{\partial\theta}\frac{\partial}{\partial g}-\frac{1}{\sin g}\frac{\partial g}{\partial\theta}\frac{\partial}{\partial h}\right)\Phi_{\mathrm{TE}} \tag{A.10}$$

$$E_\phi = \frac{i}{\omega\mu_0\epsilon_0 r\sin\theta}\left[\frac{\partial f}{\partial\phi}\left(\frac{\partial^2}{\partial f^2}+k_0^2\right)+\frac{\partial g}{\partial\phi}\frac{\partial^2}{\partial f\partial g}+\frac{\partial h}{\partial\phi}\frac{\partial^2}{\partial f\partial h}\right]\Phi_{\mathrm{TM}} \tag{A.11}$$
$$+\frac{1}{\epsilon_0 r\sin\theta}\left(\sin g\frac{\partial h}{\partial\phi}\frac{\partial}{\partial g}-\frac{1}{\sin g}\frac{\partial g}{\partial\phi}\frac{\partial}{partialh}\right)\Phi_{\mathrm{TE}} \tag{A.12}$$

$$H_r = \frac{1}{\partial\mu_0}\left(\frac{1}{\sin g}\frac{\partial g}{\partial r}\frac{\partial}{\partial h}-\sin g\frac{\partial h}{\partial r}\frac{\partial}{\partial g}\Phi_{\mathrm{TM}}\right)$$
$$+\frac{i}{\omega\mu_0\epsilon_0}\left[\frac{\partial f}{\partial r}\left(\frac{\partial^2}{\partial f^2}+k_0^2\right)+\frac{\partial g}{\partial r}\frac{\partial^2}{\partial f\partial g}+\frac{\partial h}{\partial r}\frac{\partial^2}{\partial f\partial h}\right]\Phi_{\mathrm{TE}} \tag{A.13}$$

$$H_\theta = \frac{1}{\mu_0 r}\left(\frac{1}{\sin g}\frac{\partial g}{\partial\theta}\frac{\partial}{\partial h}-\sin g\frac{\partial h}{\partial\theta}\frac{\partial}{\partial g}\right)\Phi_{\mathrm{TM}}$$
$$+\frac{i}{\omega\mu_0\epsilon_0 r}\left[\frac{\partial f}{\partial\theta}\left(\frac{\partial^2}{\partial f^2}+k_0^2\right)+\frac{\partial g}{\partial\theta}\frac{\partial^2}{\partial f\partial g}+\frac{\partial h}{\partial\theta}\frac{\partial^2}{\partial f\partial h}\right]\Phi_{\mathrm{TE}} \tag{A.14}$$

$$H_\phi = \frac{1}{\mu_0 r\sin\theta}\left(\sin g\frac{\partial h}{\partial\phi}\frac{\partial}{\partial g}-\frac{1}{\sin g}\frac{\partial g}{\partial\phi}\frac{\partial}{partialh}\right)\Phi_{\mathrm{TM}} \tag{A.15}$$
$$+\frac{i}{\omega\mu_0\epsilon_0 r\sin\theta}\left[\frac{\partial f}{\partial\phi}\left(\frac{\partial^2}{\partial f^2}+k_0^2\right)+\frac{\partial g}{\partial\phi}\frac{\partial^2}{\partial f\partial g}+\frac{\partial h}{\partial\phi}\frac{\partial^2}{\partial f\partial h}\right]\Phi_{\mathrm{TE}} \tag{A.16}$$

Appendix B

Wave Functions inside a Cylindrical Cloak Generated by Arbitrary Coordinate Transformations

Consider a general coordinate transformation between two cylindrical coordinate systems (ρ', ϕ', z') and (ρ, ϕ, z) that is described by

$$\rho' = f(\rho, \phi, z), \quad \phi' = g(\rho, \phi, z), \quad z' = z \tag{B.1}$$

where ρ', ϕ' and z' represent the coordinates in the original coordinate system and $f(\cdot)$, $g(\cdot)$ can be arbitrary monotonic differentiable functions. Using Eq. (A.2) in Appendix A, the constitutive parameters can be obtained similarly while the Jacobian matrix is $\overline{\overline{J}} = \partial(f, g, z')/\partial(\rho, \phi, z)$. Similar to Appendix A, we are able to introduce

$$\begin{aligned} \overline{A}_{\text{TM}} &= \hat{z}\Phi_{\text{TM}} \\ \overline{A}_{\text{TE}} &= \hat{z}\Phi_{\text{TE}} \end{aligned} \tag{B.2}$$

where Φ_{TM} and Φ_{TE} are scalar potentials for TE and TM cases, respectively. Substituting Eq. (B.2) into Eq. (A.3), we obtain the partial differential equation for Φ_{TE} and Φ_{TM},

$$\left[\frac{1}{f}\frac{\partial}{\partial f}f\frac{\partial}{\partial f} + \frac{1}{f^2}\frac{\partial^2}{\partial g^2} + \frac{\partial^2}{\partial z^2} + k_0^2 \right] \Phi = 0 \tag{B.3}$$

153

The solution for this equation is

$$\Phi = B_n(k_\rho f)e^{img}e^{ik_z z} \tag{B.4}$$

where $k_\rho = \sqrt{k_0^2 - k_z^2}$ and $B_n(\cdot)$ is the solution to Bessel equation. Using Eq. (A.4) we can obtain the vector potentials $\overline{A}_{TE}$ and $\overline{A}_{TM}$ as follows:

$$\overline{A}_{TM} = \sum_{m,n} a_{m,n}^{TM} \hat{z} B_n(k_\rho f)e^{imh}e^{ik_z z} \tag{B.5}$$

$$\overline{A}_{TE} = \sum_{m,n} a_{m,n}^{TE} \hat{z} B_n(k_\rho f)e^{imh}e^{ik_z z} \tag{B.6}$$

Thus all the components of the total fields can be obtained by substituting Eq. (B.5) and Eq. (B.6) into Eq. (A.3) and the results are as follows:

$$E_\rho = \frac{ik_z}{\mu_0\epsilon_0}\frac{\partial}{\partial\rho}\Phi_{TM} + \frac{[\frac{\partial f}{\partial\rho}\frac{\partial f}{\partial\phi} + f^2\frac{\partial g}{\partial\rho}\frac{\partial g}{\partial\phi}]\frac{\partial}{\partial\rho} - [(\frac{\partial f}{\partial\rho})^2 + f^2(\frac{\partial g}{\partial\rho})^2]\frac{\partial}{\partial\phi}}{[\frac{\partial f}{\partial\rho}\frac{\partial g}{\partial\phi} - \frac{\partial f}{\partial\phi}\frac{\partial g}{\partial\rho}]f\epsilon_0}\Phi_{TE} \tag{B.7}$$

$$E_\phi = \frac{ik_z}{\mu_0\epsilon_0\rho}\frac{\partial}{\partial\phi}\Phi_{TM} + \frac{[(\frac{\partial f}{\partial\phi})^2 + f^2(\frac{\partial g}{\partial\phi})^2]\frac{\partial}{\partial\rho} - [\frac{\partial f}{\partial\rho}\frac{\partial f}{\partial\phi} + f^2\frac{\partial g}{\partial\rho}\frac{\partial g}{\partial\phi}]\frac{\partial}{\partial\phi}}{[\frac{\partial f}{\partial\rho}\frac{\partial g}{\partial\phi} - \frac{\partial f}{\partial\phi}\frac{\partial g}{\partial\rho}]f\rho\epsilon_0}\Phi_{TE} \tag{B.8}$$

$$E_z = (\omega^2 - \frac{k_z^2}{\mu_0\epsilon_0\rho})\Phi_{TM} \tag{B.9}$$

$$H_\rho = \frac{ik_z}{\mu_0\epsilon_0}\frac{\partial}{\partial\rho}\Phi_{TE} + \frac{[(\frac{\partial f}{\partial\rho})^2 + f^2(\frac{\partial g}{\partial\rho})^2]\frac{\partial}{\partial\phi} - [\frac{\partial f}{\partial\rho}\frac{\partial f}{\partial\phi} + f^2\frac{\partial g}{\partial\rho}\frac{\partial g}{\partial\phi}]\frac{\partial}{\partial\rho}}{[\frac{\partial f}{\partial\rho}\frac{\partial g}{\partial\phi} - \frac{\partial f}{\partial\phi}\frac{\partial g}{\partial\rho}]f\mu_0}\Phi_{TE} \tag{B.10}$$

$$H_\phi = \frac{ik_z}{\mu_0\epsilon_0\rho}\frac{\partial}{\partial\phi}\Phi_{TE} + \frac{[\frac{\partial f}{\partial\rho}\frac{\partial f}{\partial\phi} + f^2\frac{\partial g}{\partial\rho}\frac{\partial g}{\partial\phi}]\frac{\partial}{\partial\phi} - [(\frac{\partial f}{\partial\phi})^2 + f^2(\frac{\partial g}{\partial\phi})^2]\frac{\partial}{\partial\rho}}{[\frac{\partial f}{\partial\rho}\frac{\partial g}{\partial\phi} - \frac{\partial f}{\partial\phi}\frac{\partial g}{\partial\rho}]f\rho\mu_0}\Phi_{TM} \tag{B.11}$$

$$H_z = (\omega^2 - \frac{k_z^2}{\mu_0\epsilon_0\rho})\Phi_{TM} \tag{B.12}$$

Bibliography

[1] L. Tsang, J. A. Kong, and K. H. Ding, *Scattering of Electromagnetic Waves:Volume I*, Wiley, 2000.

[2] J. B. Pendry, D. Schurig, and D. R. Smith, "Controlling electromagnetic fields," *Science*, vol. 312, pp. 1780–1782, 2006.

[3] S. A. Cummer, B.-I. Popa, D. Schurig, D. R. Smith, and J. B. Pendry, "Full-wave simulations of electromagnetic cloaking structure," *Phys. Rev. E*, vol. 74, pp. 036621, 2006.

[4] W. Cai, U. K. Chettiar, A. V. Kildishev, V. M. Shalaev, and G. W. Milton, "Non-magnetic cloak with minimized scattering," *Appl. Phys. Lett.*, vol. 91, pp. 111105, 2007.

[5] W. Cai, U. K. Chettiar, A. V. Kildishev, V. M. Shalaev, and G. W. Milton, ," *Opt. Express*, vol. 16, pp. 5444–5452, 2008.

[6] D. Schurig, J. J. Mock, B. J. Justice, S. A. Cummer, J. B. Pendry, A. F. Starr, and D. R. Smith, "Metamaterial electromagnetic cloak at microwave frequencies," *Science*, vol. 314, no. 7, pp. 977–980, 2006.

[7] H. C. Strifors and G. C. Gaunaurd, "Scattering of electromagnetic pulses by simple-shaped targets with radar cross section modified by a dielectric coating," *IEEE Trans. Antennas Propagat.*, vol. 46, pp. 1252–1262, 1998.

[8] B. Chambers and A. Tennant, "Optimized design of gaumann radar absorbing materials using a genetic algorithm," *Proc. Inst. Elect. Eng. Radar; Sonar; Navigat.*, vol. 143, pp. 23–30, 1996.

[9] A. Alu and N. Engheta, "Achieving transparency with plasmonic and metamaterial coatings," *Phys. Rev. E*, vol. 72, pp. 016623, 2005.

[10] A. H. Sihvola, "Peculiarities in the dielectric response of negative-permittivity scatterers," *Prog. Electromagn. Res.*, vol. pier-66, pp. 191–198, 2006.

[11] G. W. Milton and N. A. P. Nicorovici, "On the cloaking effects associated with anomalous localized resonance," *Proc. R. Soc. London A*, vol. 462, pp. 3027, 2006.

[12] D. A. B. Miller, "On perfect cloaking," *Opt. Express*, vol. 14, pp. 12457–12466, 2006.

[13] U. Leonhardt, "Optical conformal mapping," *Science*, vol. 312, pp. 1778–1780, 2006.

[14] U. Leonhardt and T. G. Philbin, *Transformation Optics and the Geometry of Light,*, to appear in Progress in Optics (edited by Emil Wolf), 2008.

[15] E. J. Post, *Formal structure of electromagnetics: general covariance and electromagnetics*, Interscience Publishers, 1962.

[16] J. A. Kong, *Electromagnetic Wave Theory*, EMW Publishing, 2008.

[17] D. Schurig, J. B. Pendry, and D. R. Smith, "Calculation of material properties and ray tracing in transformation media," *Opt. Express*, vol. 99, pp. 9794–9894, 2006.

[18] F. Zolla, S. Guenneau, A. Nicolet, and J. B. Pendry, "Electromagnetic analysis of cylindrical invisibility cloaks and the mirage effect," *Opt. Lett.*, vol. 32, pp. 1069–1071, 2007.

[19] A. Greenleaf, Y. Kurylev, M. Lassa, and G. Uhlmann, "Full-wave invisibility of active devices at all frequencies," *Commun. In Math. Phys.*, vol. 275, pp. 749–789, 2007.

[20] P. Yao, Z. Liang, and X. Jiang, "Limitation of the electromagnetic cloak with dispersive material," *Appl. Phys. Lett.*, vol. 92, pp. 031111, 2008.

[21] H. Chen and C. T. Chan, "Time delays and energy transport velocities in three dimensional ideal cloaking devices," *J. Appl. Phys.*, vol. 104, pp. 033113, 2008.

[22] H. Chen, B.-I. Wu, B. Zhang, and J. A. Kong, "Electromagnetic wave interactions with a metamaterial cloak," *Phys. Rev. Lett.*, vol. 99, pp. 063903, 2007.

[23] B. Zhang, H. Chen, B.-I. Wu, Y. Luo, L. Ran, and J. A. Kong, "Response of a cylindrical invisibility cloak to eletromagnetic waves," *Phys. Rev. B*, vol. 76, pp. 121101(R), 2007.

[24] B. Zhang, H. Chen, B.-I. Wu, and J. A. Kong, "Rainbow and blueshift effect of a dispersive spherical invisibility cloak impinged on by a nonmonochromatic plane wave," *Phys. Rev. Lett.*, vol. 101, pp. 063902, 2008.

[25] M. Yan, Z. Ruan, and M. Qiu, "Cylindrical invisibility cloak with simplified material parameters is inherently visible," *Phys. Rev. Lett.*, vol. 314, pp. 977–980, 2006.

[26] Y. Huang, Y. Feng, and T. Jiang, "Electromagnetic cloaking by layered structure of homogeneous isotropic materials," *Opt. Express*, vol. 15, pp. 11133–11141, 2007.

[27] W. Cai, U. K. Chettiar, A. V. Kildishev, and V. M. Shalaev, "Optical cloaking with metamaterials," *Nature Phot.*, vol. 1, pp. 224–227, 2007.

[28] B. Kante, A. Lustrac, J.-M. Lourtioz, and S. N. Burokur, "Infrared cloaking based on the electric response of split ring resonators," *Opt. Express*, vol. 16, pp. 9191–9198, 2008.

[29] M. Yan, Z. Ruan, and M. Qiu, "Scattering characteristics of simplified cylindrical invisibility cloaks," *Opt. Express*, vol. 15, pp. 17772–17782, 2007.

[30] W. Yan, M. Yan, and M. Qiu, "Non-magnetic simplified cylindrical cloak with suppressed zeroth order scattering," *Appl. Phys. Lett.*, vol. 93, pp. 021909, 2008.

157

[31] H. Chen, Z. Liang, P. Yao, X. Jiang, H. Ma, and C. T. Chan, "Extending the bandwidth of electromagnetic cloaks," *Phys. Rev. B*, vol. 76, pp. 241104, 2007.

[32] D. Wang, H. Chen, L. Ran, J. Huangfu, J. A. Kong, and B.-I. Wu, "Reconfigurable cloak for multiple operating frequencies," *Appl. Phys. Lett.*, vol. 93, pp. 043515, 2008.

[33] J. Zhang, J. Huangfu, Y. Luo, H. Chen, J. A. Kong, and B.-I. Wu, "Cloak for multi-layered and gradually changing media," *Phys. Rev. B*, vol. 77, pp. 035116, 2008.

[34] X. Cheng, H. Chen, B.-I. Wu, L. Ran, and J. A. Kong, "Cloak for multilayered and gradually changing media," *Progress In Electromagnetics Research Symposium(PIERS)*, vol. 2009, 2009.

[35] H. Ma, S. Qu, Z. Xu, and J. Wang, "Approximation approach of designing practical cloaks with arbitrary shapes," *Opt. Express*, vol. 16, pp. 15449–15454, 2007.

[36] C. Li and F. Li, "Two-dimensional electromagnetic cloaks with arbitrary geometries," *Opt. Express*, vol. 16, pp. 13414–13420, 2008.

[37] A. Nicolet F. Zolla and S. Guenneau, "Electromagnetic analysis of cylindrical cloaks of an arbitrary cross section," *Opt. Lett.*, vol. 33, pp. 1584–1586, 2008.

[38] H. C. Hulst, *Light scattering by small particles*, Dover Publishing, 1981.

[39] A. I. Nachman, "Reconstructions from boundary measurements," *Ann. Math.*, vol. 128, pp. 531–576, 1988.

[40] E. Wolf and T. Habashy, "Invisible bodies and uniqueness of the inverse scattering problem," *J. Mod. Opt.*, vol. 40, pp. 785–792, 1993.

[41] W. C. Chew, *Waves and Fields in inhomogeneous Media*, New York:IEEE Press, 1995.

[42] Z. Ruan, M. Yan, C. W. Neff, and M. Qiu, "Ideal cylindrical cloak: Perfect but sensitive to tiny perturbations," *Phys. Rev. Lett.*, vol. 99, pp. 113903, 2007.

[43] A. J. Ward and J. B. Pendry, "Refraction and geometry in maxwell's equations," *J. Mod. Opt.*, vol. 43, pp. 773–793, 1996.

[44] P. Sheng, "Waves on the horizon," *Science*, vol. 313, pp. 1399–1400, 2006.

[45] A. Greenleaf, Y. Kurylev, M. Lassa, and G. Uhlmann, "Improvement of cylindrical cloaking with the shs lining," *Opt. Express*, vol. 15, pp. 12717–12734, 2007.

[46] I. V. Lindell and P.P. Puska, "Reflection dyadic for the soft and hard surface with application tothe depolarising corner reflector," *IEE Proc.-Microw. Antennas Propag.*, vol. 143, pp. 417, 1996.

[47] R. Weder, "A rigorous time-domain analysis of full wave electromagnetic cloaking," *J. Phys. A: Mathematical and Theoretical*, vol. 41, pp. 065207, 2008.

[48] B. Wood and J. B. Pendry, "Metamaterials at zero frequency," *J. Phys.: Condens. Matter*, vol. 19, pp. 076208, 2007.

[49] C. A. Balanis, *Advanced Engineering Electromagnetics*, John Wiley&Sons, 1989.

[50] B. A. Kemp, T. M. Grzegorczyk, and J. A. Kong, "Optical momentum transfer to absorbing mie particles," *Phys. Rev. Lett.*, vol. 97, pp. 133902, 2006.

[51] P. Penfield and H. A. Haus, *Electromagnetics of Moving Media*, MIT Press, 1967.

[52] B. A. Kemp, *Optical Momentum Transfer to Macroscopic Media*, MIT PhD Thesis, 2007.

[53] D. R. Smith, W. J. Padilla, D. C. Vier, S. C. Nemat-Nasser, and S. Schultz, "Composite medium with simultaneously negative permeability and permittivity," *Phys. Rev. Lett.*, vol. 84, pp. 4184–4187, May 2000.

[54] R. A. Shelby, D. R. Smith, and S. Schultz, "Experimental verification of a negative index of refraction," *Science*, vol. 292, pp. 77–79, 2001.

[55] J. B. Pendry, "Negative refraction makes a perfect lens," *Phys. Rev. Lett.*, vol. 85, pp. 3966–3969, 2000.

[56] M. I. Tribelsky and B. S. Luk'yanchuk, "Anomalous light scattering by small particles," *Phys. Rev. Lett.*, vol. 97, pp. 263902, 2006.

[57] J. B. Pendry, A. Holden, W. Stewart, and I. Youngs, "Extremely low frequency plasmons in metallic mesostructures," *Phys. Rev. Lett.*, vol. 76, pp. 4773–4776, 1996.

[58] J. B. Pendry, A. J. Holden, D. Robbins, and W. Stewart, "Magnetism from conductors and enhanced nonlinear phenomena," *IEEE Trans. Microwave Theory Tech.*, vol. 47, pp. 2075–2084, 1999.

[59] B. Zhang, H. Chen, B.-I. Wu, and J. A. Kong, "Extraordinary surface voltage effect in the invisibility cloak with an active device inside," *Phys. Rev. Lett.*, vol. 100, pp. 063904, 2008.

[60] I. I. Smolyaninov, Y. J. Hung, and C. C. Davis, "Two-dimensional metamaterial structure exhibiting reduced visibility at 500 nm," *Opt. Lett.*, vol. 33, pp. 1342–1344, 2008.

[61] Z. Liang, P. Yao, X. Sun, and X. Jiang, "The physical picture and the essential elements of the dynamical process for dispersive cloaking structures," *Appl. Phys. Lett.*, vol. 92, pp. 131118, 2008.

[62] L. Brillouin, *Wave Propagation and Group Velocity*, Academic Press, New York and London, 1960.

[63] M. Born and E. Wolf, *Principles of Optics*, Pergamon Press, Oxford and New York, 1964.

[64] V. M. Shalaev, "Transforming light," *Science*, vol. 322, pp. 384–386, 2008.

[65] U. Leonhardt and T. Tyc, "Broadband invisibility by non-euclidean cloaking," *Science*, vol. 323, pp. 110–112, 2009.

[66] R. Liu, C. Ji, J. J. Mock, J. Y. Chin, T. J. Cui, and D. R. Smith, "Broadband ground-plane cloak," *Science*, vol. 323, pp. 366–369, 2009.

[67] R. P. Feynman, R. B. Leighton, and M. Sands, *The Feynman Lectures on Physics*, Addison-Wesley, 1989.

[68] J. V. Jelly, *Cerenkov Radiation and Its Applications*, Pergamon, London, 1958.

[69] M. L. Ter-Mikaelian, *High-Energy Electromagnetic Processes in Condensed Media,*, Wiley-Interscience, 1976.

[70] C. T. Tai, *Dyadic Green Functions in Electromagnetic Theory*, IEEE Press, 1994.

[71] G. N. Afanasiev, S. M. Eliseev, and Y. P. Stepanovsky, "Transition of the light velocity in the vavilov-cerenkov effect," *Proc. R. Soc. Lond. A*, vol. 454, pp. 1049–1072, 1998.

[72] P. Alitalo and S. Tretyakov, "Cylindrical transmission-line cloak for microwave," *Proceedings of iWAT2008, Antenna Technology: Small Antennas and Novel Metamaterials*, p. P104, 2008, Chiba, Japan.

[73] P. Alitalo, O. Luukkonen, L. Jylha, J. Venermo, and S. Tretyakov, "Transmission-line networks cloaking objects from electromagnetic fields," *IEEE Trans. Antennas and Propagat.*, vol. 56, pp. 416–424, 2008.

[74] C. Blanchard, J. Porti, B.-I. Wu, J. A. Morente, A. Salinas, and J. A. Kong, "Time domain simulation of electromagnetic cloaking structures with tlm method," *Opt. Express*, vol. 16, pp. 6461–6470, 2008.

[75] M. Farhat, S. Enoch, S. Guenneau, and A. B. Movchan, "Broadband cylindrical acoustic cloaking for linear surface waves in a fluid," *Phys. Rev. Lett.*, vol. 101, pp. 134501, 2008.

[76] D. A. Coley, *An introduction to genetic algorithms for scientists and engineers*, World Scientific Publishing Co., 1999.

[77] Y. Luo, H. Chen, J. Zhang, L. Ran, and J. A. Kong, "Design and analytical full-wave validation of the invisibility cloaks, concentrators, and field rotators created with a general class of transformations," *Phys. Rev. B*, vol. 77, pp. 125127, 2008.